Frictional Behavior of Polymers:

the Transition from Static to Kinetic Conditions

by

Robert S. Molique

Thesis submitted to the Faculty of the

Virginia Polytechnic Institute and State University

in partial fulfillment of the requirements for the degree of

MASTER OF SCIENCE

in

Mechanical Engineering

N. S. Eiss Jr.

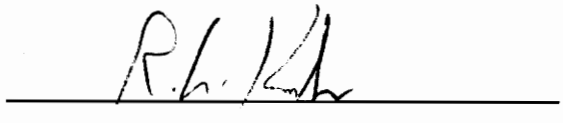

R. G. Kander

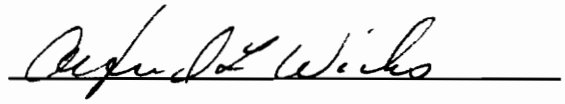

A. L. Wicks

February 1994

Blacksburg, Virginia

Frictional Behavior of Polymers:

the Transition from Static to Kinetic Conditions

by

Robert S. Molique

Norman S Eiss, Jr., Chairman

Mechanical Engineering

ABSTRACT

It is believed that the noise produced in squeaking dashboards is caused by the drop in friction force during the transition from static to kinetic conditions between the mating plastic components of the dashboard. The frictional behavior of a polymer determines whether there is a drop in friction force during this transition. This study investigates the frictional behavior of polymers under dry sliding conditions. Various compositions of ABS plastic along with Polypropylene were tested in a flat-on-flat configuration. There appears to be no consistent evidence of surface roughness effects on the magnitude of the drop in friction force. The surface roughness did have an effect on the frictional behavior of the polymers as did the material composition. A new test apparatus was designed to study the transition from static to kinetic conditions more closely. A computer model was developed to simulate this transition. The computer model was used to illustrate the effect of the friction-velocity curve on the frictional behavior of a surface interaction. A few conclusions are made about which friction mechanisms are in control of the polymer-on-polymer tribological system.

Acknowledgements

First, I would like to thank Dr. N. S. Eiss, Jr. for his patience and guidance which he has provided over much of my college career. He has taught me so much over the past couple of years and helped me to accomplish my goals. I would also like to thank him for his efforts in finding the financial support necessary to complete this project. I would like to thank the members of my committee, Dr. R. G. Kander and Dr. A. L. Wicks, for their time and for everything they have taught me over the past year and a half.

I am thankful to the Mechanical Engineering Department and Ford Motor company for sponsoring the project. I am also thankful to the Chemical Engineering Department for use of their lab in the processing of some of the materials used in the project. I would like to thank the Mechanical Engineering machine shop crew and electrical shop personnel for their assistance and guidance on the modification and fabrication of the testing equipment.

I would like to thank Alan Arkus and Ed Lee for working with me on the design of the new test apparatus. I would also like to thank everyone else in the Tribology Lab who helped me in so many different ways.

Finally, I would like to thank God, my Mom, my Dad, my brother (Rick), my sister (Julie), and my fiancée (Cathy) for their love and encouragement which they have provided throughout my life.

"The area of analysis of transitions is one of the most difficult in the whole of tribology; I take my hat off to ... anyone else who is able to do this."

Dr. E. Rabinowicz, M.I.T.

"Ditto."

R. Molique, V.P.I. & S.U.

Table of Contents

List of Figures

List of Tables

1.0 Introduction

It has been found that the instrument panel (IP) components of Ford Motor vehicles make a noise or squeak when subjected to vibrations caused by the engine or the road. Research has shown that the plastic parts of the IP, which are in dry contact, exhibit stick-slip frictional behavior. Consequently, when the plastic parts are forced to move relative to one another they release energy during every slip. The slip excites the IP and some of the energy is transformed to sound. The lubrication or separation of these components is either not possible or very costly. It is believed that a material combination which does not exhibit stick-slip frictional behavior will not produce squeaks.

B. P. McCann [1] studied the frictional behavior of several material combinations under dry sliding conditions. He was able to make several conclusions about how frictional behavior is related to system parameters such as surface roughness, normal load, material, and system stiffness. The surface roughness tests were run with four different materials. Unfortunately, only two different surface roughnesses were available for testing. The normal load tests were run with nine different materials. He concluded

that unstable frictional behavior is less likely to occur with rougher surfaces. He also concluded that unstable frictional behavior is less likely to occur at lower normal loads. Some questions arose from these conclusions. Will the surface roughness dependence be found in other materials? Which surface roughness parameters are important in determining unstable frictional behavior? And will the normal load dependence apply for other materials?

The project had two objectives: 1) to answer the questions which arose from McCann's work and 2) to gain a better understanding of why some material combinations exhibit stick-slip behavior and some do not. For the first objective, experiments were run on a pin-on-disk apparatus. Testing conditions were similar to those experiments run by Mr. McCann with some modifications. For the second objective, one has to take a closer look at the transition from static conditions to kinetic conditions. The existing test apparatus was originally designed to measure wear and steady state friction force values. The need for valid friction force values during the transition from static to kinetic conditions prompted the design of a new test apparatus which could measure dynamic friction forces. The limitations of the existing apparatus were used to assist in the design of the new test apparatus. Also, computer models of the existing and new test apparatus were developed to obtain a better understanding of the dynamics of the friction interface.

This paper will discuss several aspects of the frictional behavior of polymers under dry sliding conditions. In Chapter 2, friction in general is discussed, including friction mechanisms and frictional behavior. Previous tribological research performed

on polymers is reviewed. Chapter 3 describes the details of the experimental apparatus and procedures used in this study. In Chapter 4, the results of all experiments are presented. Chapter 5 discusses the experimental results. The computer models are presented and the analytical results are used to interpret some of the experimental results. Conclusions drawn from the discussion are listed in Chapter 6. In Chapter 7, recommendations are made for the direction of future research pertaining to this subject.

2.0 Literature Review

When discussing polymer friction, it is easiest to first talk about metal friction. Metal-on-metal systems are usually simpler and tribologists have a better understanding of the friction mechanisms involved. The first section of this literature review introduces the basic friction mechanisms as they apply to metals. The second section discusses polymer friction mechanisms and presents what has been found by investigators concerning polymer friction. Because stick-slip motion is considered to be so important in the generation of unwanted sound in IP's, the basics of stick-slip motion are included in section 2.3. Previous research on the effect of surface roughness on friction in dry sliding contacts is summarized is section 2.4. The last section reviews the literature pertaining to the processing and aging of ABS, Poly(Acrylonitrile-Butadiene-Styrene) materials. This section is germane to the processes used to modify the materials utilized in this study.

The basic understanding of metal friction was developed in the early 1900's long before polymers were in widespread use. When polymer friction was studied, it was found that some of the same concepts could be transferred directly from metals to

polymers. The two tribological systems are similar with the notable exceptions of the polymers' viscoelastic nature and its greater sensitivity to temperature and strain rate.

2.1 Metal Friction

When two surfaces are put together with a normal force, W, and forced in the tangential direction with a force, F, the surfaces can be modeled as individual asperities in contact as shown in Figure 2.1. An equilibrium of forces must exist.

$$\sum F_x = F - s(a'' \cos\theta) - p(a'' \sin\theta) = 0$$

$$F = s(a'' \cos\theta) + p(a'' \sin\theta) \qquad (1)$$

$$F = sA + pA'$$

$$\sum F_y = -W + p(a'' \cos\theta) - s(a'' \sin\theta)$$

$$W = p(a'' \cos\theta) - s(a'' \sin\theta) \qquad (2)$$

$$W = pA - sA'$$

And the friction coefficient, μ, is given by:

$$\mu = F/W = (p \sin\theta + s \cos\theta)/(p \cos\theta - s \sin\theta)$$

where p is the normal stress, s is the shear stress, and θ is the average slope of the asperities. It has been generally accepted that there are two main components of friction force, the adhesive component and the plastic deformation component [2, 3]. The total friction force is found by calculating the two components of friction separately and adding them together. The adhesion friction can be found by setting $\theta=0$ in equation (1). The force due to adhesion, F_{adh}, is equal to the real area of contact, A, times the

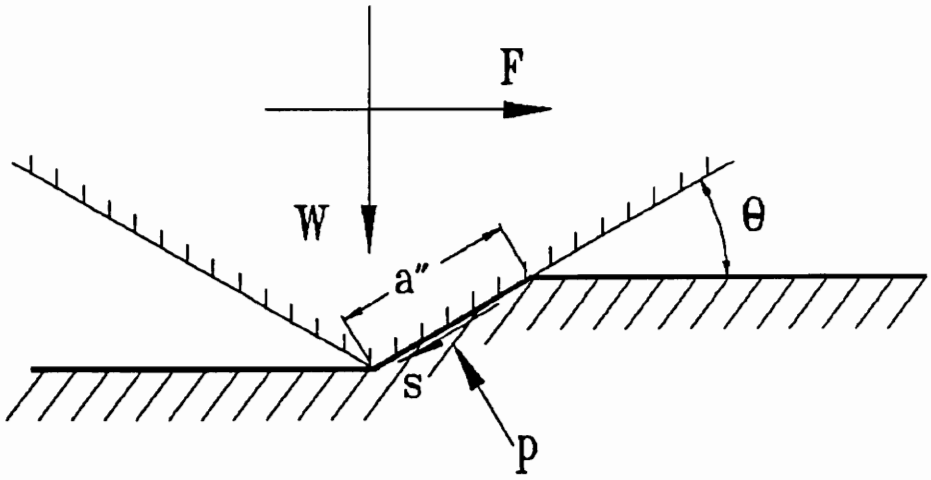

Figure 2.1 - Theoretical surface contact of a typical asperity.

shear stress on the interface, s.

$$F_{adh} = As \qquad (3)$$

The plastic deformation or plowing component of friction, F_p, is the force required to plow the asperities by simple plastic deformation and is found by setting s=0.

$$F_p = p(a'' \sin\theta)$$

and $$\mu_p = F_p/W = \tan\theta$$

There are a few complications that arise when predicting the friction force using the above equations. Some of these parameters are hard to find and some are changing during a friction test. For example, the friction force due to adhesion can be found from A and s, equation (3). Due to surface irregularities, the real area of contact is difficult to find exactly. The real area of contact, A, is some fraction of the apparent area of contact. Some investigators have found A experimentally by measuring the electrical resistance of the two metal surfaces in contact [2].

2.2 Polymer Friction

For polymers, it has been generally accepted that the same two components are responsible for the coefficient of friction [4, 5, 6]. However, there are a few additional complications. The polymer material below the surface may undergo viscoelastic deformation which may affect the friction force; therefore, the volume of material involved in the friction process is greater for polymers than for metals. This realization led to the definition of two zones, called the interfacial zone and the deformation zone

[4, 7]. For metals and polymers the adhesion and plowing components of friction occur in the interfacial zone. For polymers the viscoelastic deformation below the surface in the deformation zone also contributes to the friction force because of hysteresis losses.

Another complication is that polymers are much more sensitive than metals to velocity and temperature. When these conditions change during a friction test, the friction force may also change. Also, polymers have a lower thermal conductivity than metals. Thus, larger temperature differences between the surface and the bulk material are required to conduct the heat away from the surface. Because the surface temperatures are higher, frictional heat generation is more of a concern in a polymer contact than in a metal contact.

Further discussion of the two components of friction and how they relate to polymers follows.

2.2.1 Deformation

The deformation portion of friction for polymers is particularly evident in rolling friction [8]. In rolling friction, the friction force is related to the amount of energy dissipated in the material. For a hard sphere rolling on a polymer sample, the friction force times the distance per unit time equals the amount of energy used to deform the polymer minus the energy recovered from the polymer pushing up on the rear of the roller. The amount of energy recovered is related to the loss properties of the polymer ($E^{-1/3}\tan\delta$) or viscoelastic response. An equation for the coefficient of rolling friction

is: $\mu_r \approx (\pi/2)W^{1/3}R^{-2/3}(1-\nu^2)^{1/3}E^{-1/3}\tan\delta$ [9]

where W is the normal force, R is the radius of the roller, E and ν are the modulus and Poisson's ratio of the polymer flat, and tan δ is the loss tangent of the polymer. The loss tangent is equal to E″/E′, the ratio of the Young's loss modulus to the Young's storage modulus. Figure 2.2 [10] shows the measured coefficient of rolling friction (μ_r) of a rigid sphere on a specimen of PTFE as a function of temperature at constant rolling velocity. One can see how this relationship closely resembles that of the relationship between $E^{-1/3}\tan\delta$, the viscoelastic response, and temperature.

It is known that the mechanical properties of a polymer are dependent on the testing conditions, specifically the rate of deformation. Similarly, the loss tangent is dependent on rolling velocity. Increasing the velocity (rate of deformation) is the same as decreasing the temperature. Hence, the W.L.F. (Williams-Landel-Ferry) transform can be used effectively to form a friction force vs. velocity curve. The W.L.F. equation is a theoretical relationship between temperature and a time variable and is of the form:

$$\log a_T = \frac{B\,(T-T_0)}{A + (T-T_0)}$$

where A and B are constants and a_T is a shift factor equal to a ratio of time variables. This transform is useful when a particular apparatus is limited in the range of velocities over which it can be run. A friction-velocity curve can be generated, which covers a much larger range of velocities than the apparatus is capable of covering, by running the tests at different temperatures. The W.L.F. transform has been used to show how sliding

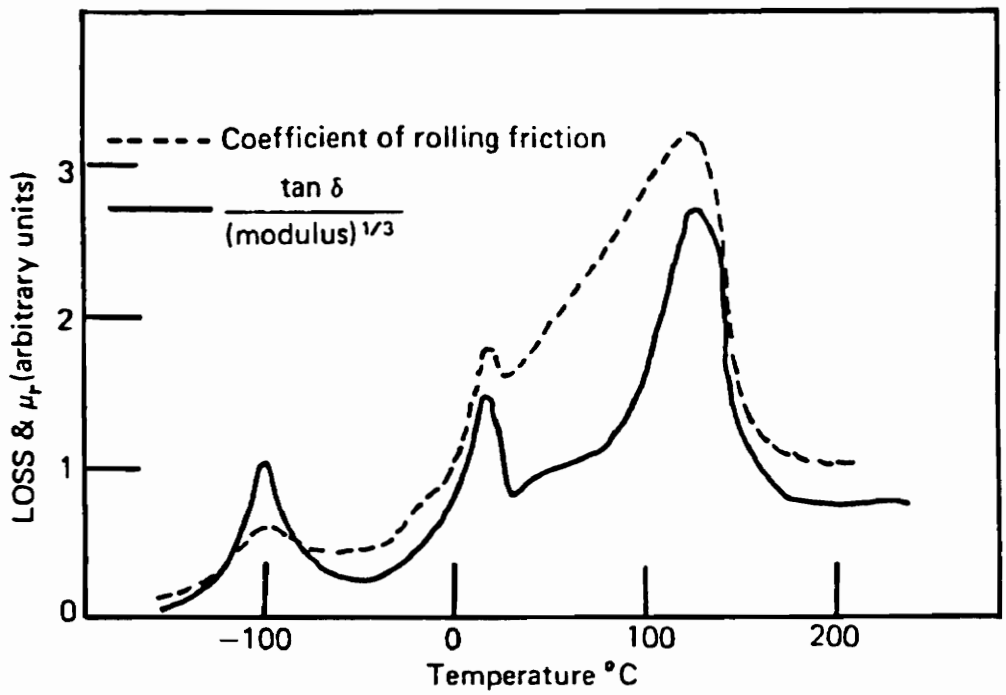

Figure 2.2 - Comparison of viscoelastic deformation friction (in the rolling of a sphere) with the hysteresis loss property for PTFE. [10]

friction is similar to rolling friction and is discussed in the next paragraph.

For a slider sliding over a flat, the viscoelastic deformation component of friction has the same relationship as a roller rolling over a flat [7, 10]. In sliding, the friction force is due to adhesion and deformation, but the deformation component of friction is related (as in rolling friction) to the amount of energy required to deform the polymer minus the energy recovered from the polymer pushing up on the rear of the slider. The friction due to the deformation below the surface can be found experimentally if the adhesion component and the plowing component are small. Lubricating the surfaces usually does a good job of minimizing the adhesion component of friction (See section 2.2.2). Experiments were done with a hard smooth sphere on a lubricated rubber. Figure 2.3 shows how the sliding coefficient of friction varies with velocity and temperature. Also shown is the master curve for this system formed by using the W.L.F. transform.

Other examples of friction force due to deformation include plastic grooving, tearing and transverse cracking [4, 7, 12]. These friction mechanisms could contribute to the friction force if significant plastic deformation is present.

2.2.2 Adhesion

As seen from equation (3), the adhesion component is dependent on the real area of contact and the shear strength of the interface.

Area

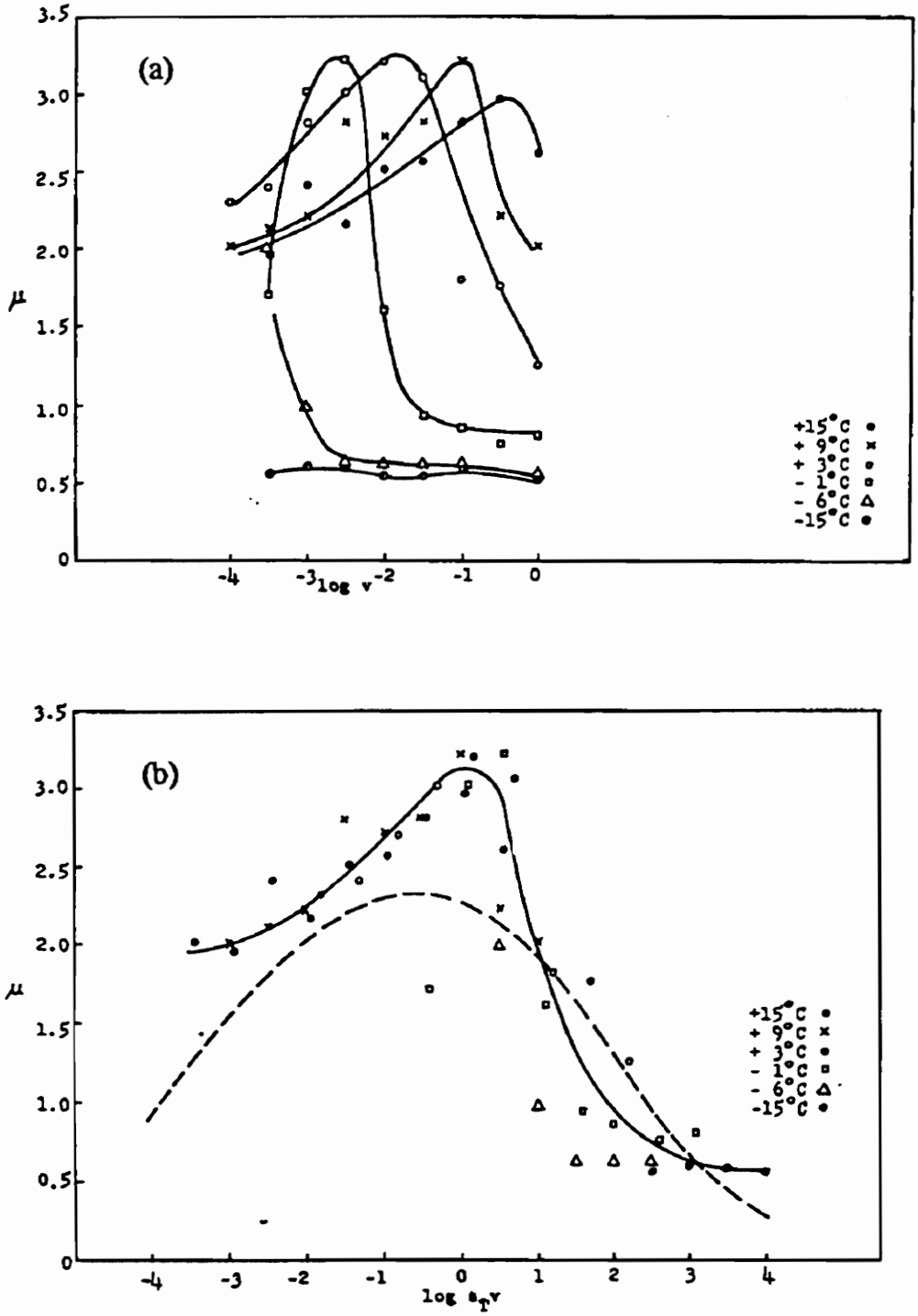

Figure 2.3 - (a) Coefficient of friction vs. log velocity at various temperatures for acrylonitrile-butadiene rubber. (b) Master curve at 20°C for acrylonitrile-butadiene rubber, - - - - Grosch [11], ____ Ludema [10].

Many investigators have tried to determine the real area of contact between two surfaces [2]. For metals, the area was estimated by assuming plastic deformation and using Amonton's law: $A=W/H$, where H is the hardness of the metal. This could be applied to polymers assuming plastic deformation. Hertzian equations assume elastic contact of a perfectly smooth sphere of radius R on a perfectly flat smooth surface: $A=\pi(\frac{3}{4}(WR/E^*))^{2/3}$, where $1/E^* = (1-\nu_1^2)/E_1 + (1-\nu_2^2)/E_2$ and E and ν are the modulus and Poisson's ratio of the materials. In real situations the surfaces are not perfectly smooth. The area of contact is dependent on the surface characteristics of the samples. Greenwood and Williamson [13] modeled a rough surface as a surface made up of many smooth spherical asperities of varying height which deform elastically. They used the Hertzian contact equations to derive an equation for the area of contact between two rough surfaces: $A=(W/(E^*(\sigma_s\kappa_s)^{1/2})$, where σ_s and κ_s are the surface peak height standard deviation and mean curvature of the surface, respectively. This equation was used to develop the plasticity index which is a measure of the extent of plastic deformation of a surface. The plasticity index is defined as $\Phi = E^*(\sigma_s\kappa_s)^{1/2}/H$, where H is the hardness of the material [3].

Obviously, the real area of contact in elastic contact is dependent on the Young's modulus of the material. For polymers, the Young's modulus is a function of temperature and deformation rate. Here, just as in the deformation component of friction, the velocity and temperature and how much they change throughout the friction process become important in estimating the area of contact.

Shear strength

When two polymer surfaces are in contact, Van der Waals forces form the bond between the surfaces that determines the shear strength of the interface [14]. For clean surfaces, this is approximately equal to the bulk shear strength of the polymer, τ. For contaminated surfaces, the interfacial shear strength will be less than τ. Some investigators [15] report that if A and τ are known for a given polymer then

$$F_{adh} = kA\tau \qquad (4)$$

where k is a factor less than 1 which is determined by the surface contamination. If the shear strength of the material is equal to the shear strength of the interface then k = 1. But if the surfaces are contaminated, then the shear strength of the interface is less than the shear strength of the bulk polymer, $k < 1$. For well lubricated surfaces, k is approximately equal to zero. Sometimes F_{adh} is found by running lubricated and unlubricated tests. For the lubricated tests, if the force required to shear the lubricant is small then k is small and the difference in the measured friction force between the two tests (lubricated and unlubricated) is equal to F_{adh}.

The shear strength of the interface could also be different from the bulk shear strength if there is a morphological or chemical composition difference at the surface. For example, the molding process can create a morphology at the surface which is different than the morphology of the bulk material. The difference in morphology results in a difference in mechanical properties [16]. The shear stress in equation (3) is limited by the interfacial shear strength, which may or may not be the same as the bulk shear

strength.

B. Briscoe has worked extensively in making predictions of the shear strength of polymers using empirical formulas [7, 17, 18, 19]. Experiments were done using a smooth hard sphere on a thin polymeric film which reduced the effects of the deformation component of friction. The materials and contact geometry were chosen so that Hertz elastic equations could be used to estimate the real area of contact. Since the friction force was due almost entirely to adhesion and the real area of contact could be estimated, then τ could be found by measuring the friction force and using equation (4), assuming k=1.

It was found that for a wide variety of polymers the friction force varied with the mean contact pressure, P, or W/A. As it turned out, the shear strength, τ, varied linearly with the mean contact pressure [17, 20]. Figure 2.4 shows the variation of shear strength with contact pressure for a variety of polymers. All the functions can be written as $\tau = \tau_o + \alpha P$, where τ_o and α are constants for a given polymer, temperature and sliding velocity.

The effect of temperature on τ depends on the polymer. For most polymers τ_o is independent of temperature up to a certain point then it follows the Arrhenius relation: $\tau_o = \tau'_o \exp\{-Q/RT\}$, where τ'_o is an intrinsic shear stress related to the value of τ at which the transition from temperature independence to temperature dependence occurs. This transition usually occurs around T_g, the glass transition temperature of the polymer [17].

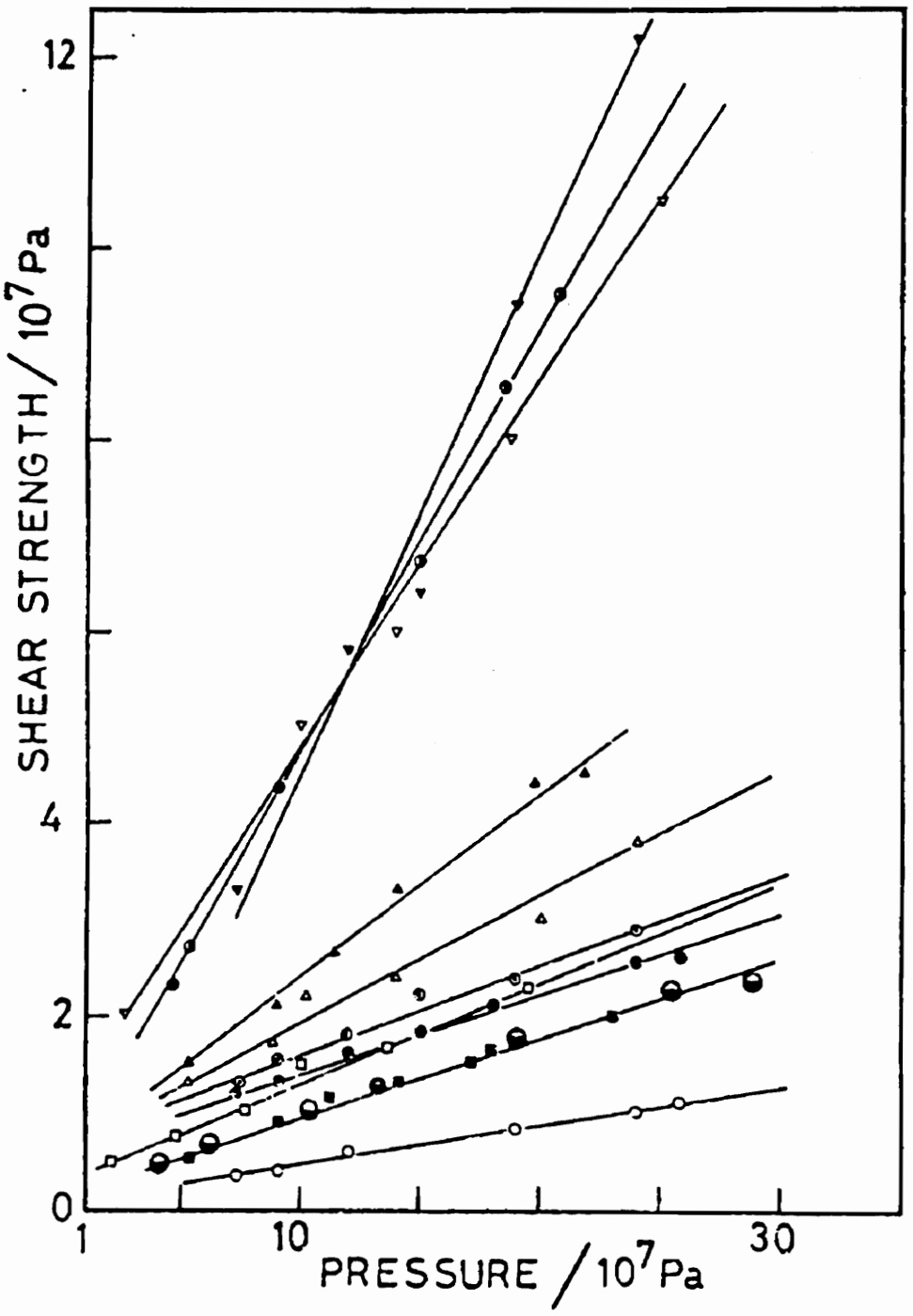

Figure 2.4 - Shear strength, τ, against mean calculated pressure P, at 20°C for ■,○, HDPE; □ PTFE; △ LDPE; ▲ Polypropylene; ▽ PMMA; ▼ PVC; ◑ Polystyrene; ⊙ oleamide; ● stearamide; ◒ CaSt. [16]

It is well known that the apparent strength of a polymer is determined by the deformation rate of the strength test. In the case of the shearing of surfaces in the interfacial zone the deformation rates are extremely high, up to six orders of magnitude higher than in the deformation zone [7, 10]. Therefore one must be careful when estimating the effective shear strength of a polymer interface.

Briscoe found experimentally that the velocity affects both τ and α. The following models were proposed for these parameters,

$$\tau = \tau''_o \ln(V/(h \cdot \phi)), \quad \alpha = \alpha_o \exp\{-V/(d \cdot \theta)\}$$

where V is the velocity, h is the polymer film thickness, d is the contact diameter, ϕ and θ are "characteristic" frequencies, and τ''_o is another intrinsic shear strength which is constant for a given polymer. Combining all of the above relationships results in the following equation.

$$\tau = \tau'''_o \ln(V/(h \cdot \phi))\exp\{-Q/RT\} + \alpha_o \exp\{-V/(d \cdot \theta)\}P$$

where τ'''_o is a combination of all the above intrinsic shear strengths and is a constant.

Area and Shear Strength

Ludema and Tabor [10] calculated a curve for friction vs. sliding speed taking into account the changes in shear strength and area with sliding speed. They used a hard slider on a rubber flat configuration. Figures 2.5a, 2.5b and 2.6 show how the shear strength, s, and area, A, were adjusted assuming that the shear rates involved in s (or τ) are about 10^5 times those involved in A. This illustrates how important area and shear strength are in determining the friction force and how they relate to each other.

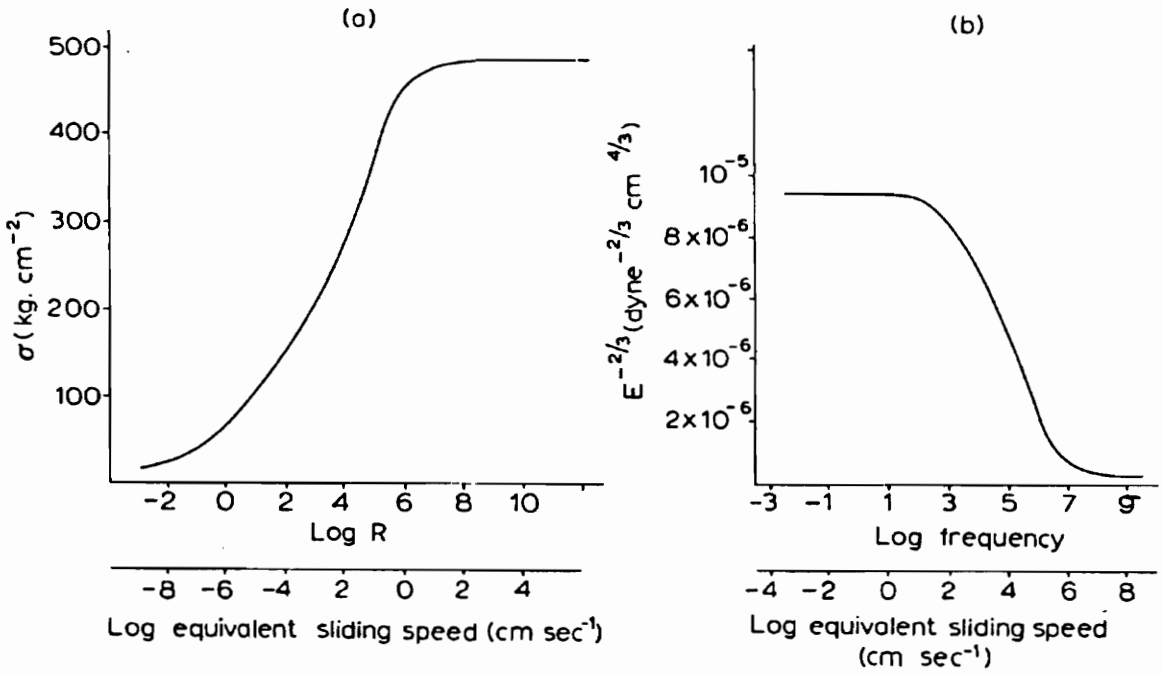

Figure 2.5 - (a) Tensile stress at failure of butadiene rubber as function of rate of strain. (b) Variation of $E^{-2/3}$ of butadiene rubber as a function of rate of deformation. [10]

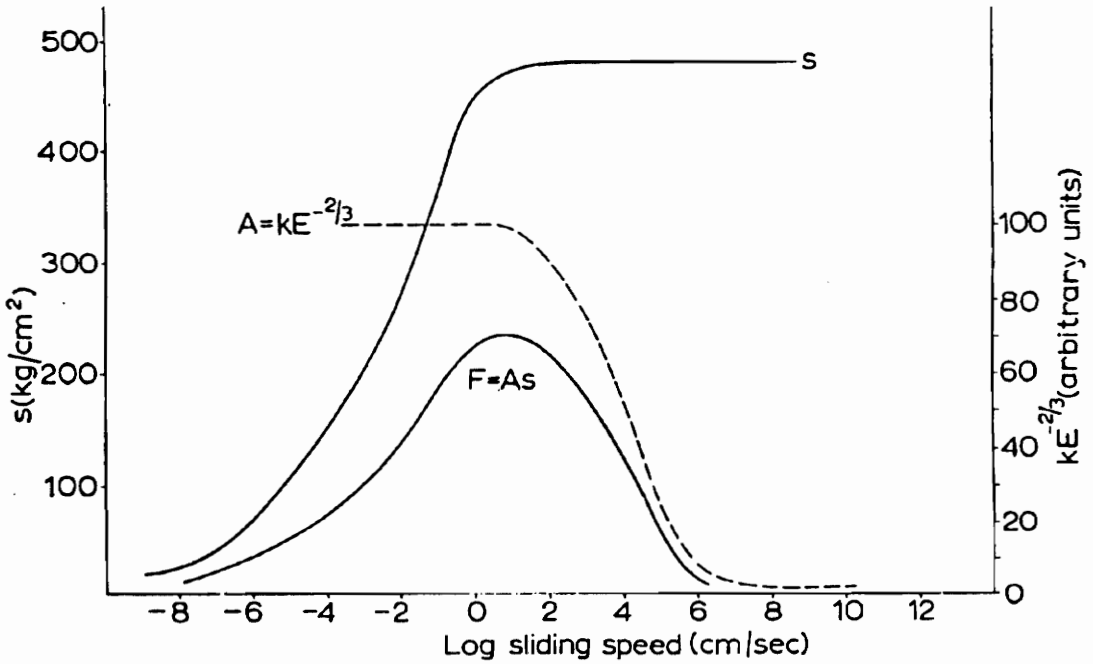

Figure 2.6 - Curves showing variation of s and A as functions of sliding speed assuming that the shear processes involved in s are about 10^5 times as rapid as those involved in A. [10]

2.3 Stick-Slip motion

Stick-slip motion is when two surfaces move in a recurring cycle of first sticking together then sliding for a short period of time followed by sticking together again. The process is often repeated over and over again as the surfaces are forced to move relative to one another.

Consider the general case of two sliding bodies, where one is driven at a steady uniform speed, v, and the other is supported by an elastic system so that its deflection is a measure of the frictional force between the surfaces, assuming that the mass is not accelerating (Figure 2.7). Also shown in Figure 2.7 is a stick-slip friction signal. There is a linear relationship between the friction force and the deflection of the mass, δ, and the constant of proportionality is equal to the stiffness of the spring, k. From point A to point B, the friction force between the two surfaces is increasing. At B, the force acting on the mass, $F_{applied}$, exceeds the interfacial force and the mass begins to move relative to the bottom surface. This force is called the static friction force. The interfacial force during sliding is called the kinetic friction force, F_k. If $F_k < F_{applied}$ then there is a force imbalance which accelerates the mass. Assume that F_k is constant during the entire slip process. Since there is no damping the mass will move in a sine wave motion. Because of the inertia the mass will pass the equilibrium position for F_k at point D and begin to slow down until its velocity is equal to v. Now, if there is enough friction force to allow the two surfaces to stick together again then the process is

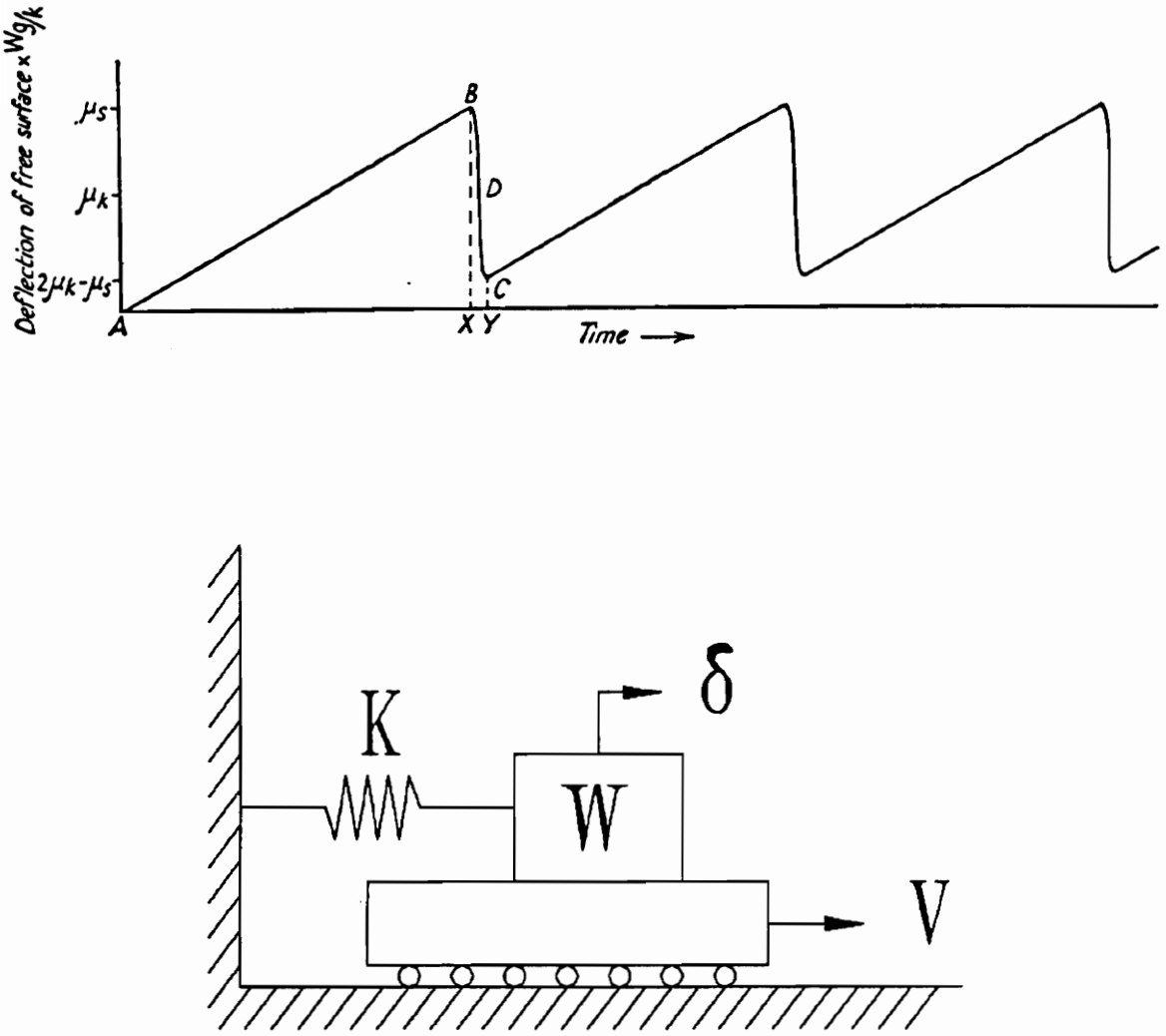

Figure 2.7 - Analysis of stick-slip or intermittent motion. Upper figure taken from [2]

repeated.

It has been accepted that at least two conditions of a system must be met before stick-slip motion will occur. 1) Potential energy must be stored somewhere in the system, and 2) the friction velocity curve must have a negative slope. Any friction apparatus which utilizes the deflection of a member to measure the friction force satisfies condition 1. Any pair of surfaces that exhibits a kinetic coefficient of friction less than the static coefficient of friction satisfies condition 2.

Research has shown that μ_k is not constant with velocity [1, 21, 22, 23]. Figure 2.8 shows typical friction-velocity curves which have the potential of stick-slip motion. Some researchers have found that stick-slip behavior will not occur for relative velocities above v_{min} and will occur for velocities where the slope of the friction-velocity curve is negative [1, 24]. At velocities above v_{min} or as a result of damping, the mass velocity does not have a chance to equal v and therefore the surface does not have a chance to stick again. If the mass does not stick again then the behavior is called single stick.

2.4 Surface Roughness

The effect of surface roughness on friction has been studied by many investigators. For metals, the friction force is thought to vary as in Figure 2.9 [25]. For smoother surfaces, the area of contact is greater and so the adhesion friction force is greater. For rougher surfaces, the slopes are steeper and so the deformation friction force is larger. In the middle, the friction force is relatively constant. Some say this

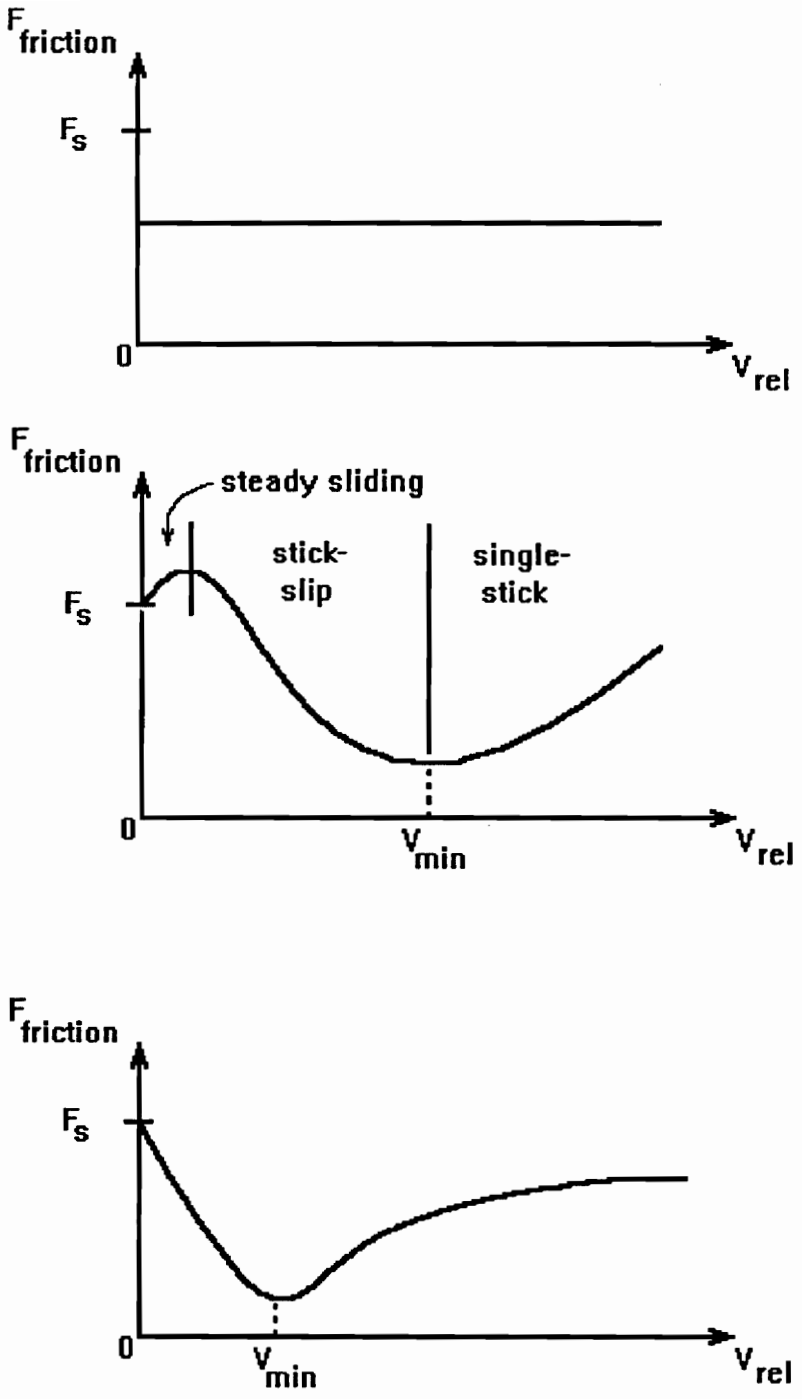

Figure 2.8 - Theoretical kinetic friction vs. velocity curves which have the potential for stick-slip behavior.

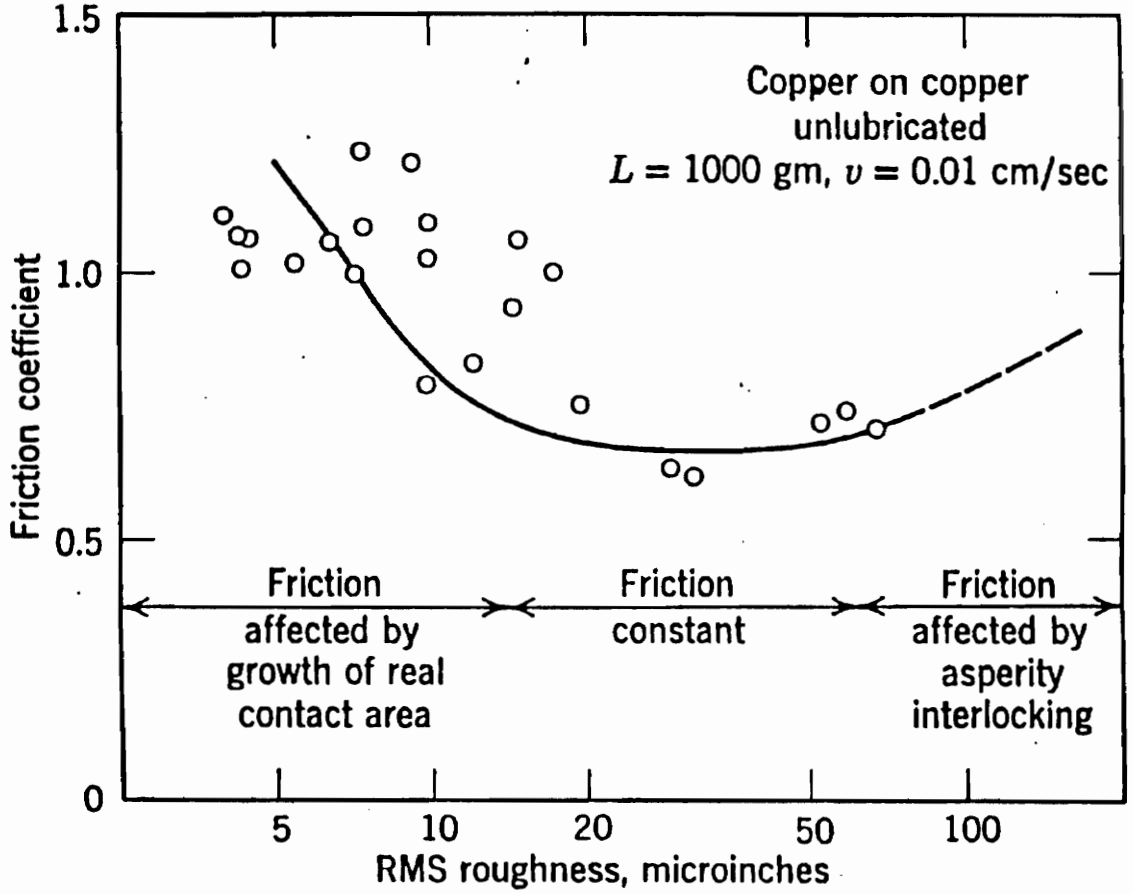

Figure 2.9 - Friction coefficient against RMS roughness for Copper on Copper. [25]

transition is the result of transition from elastic deformation in the smooth surfaces to plastic deformation in the rough surfaces [26].

B. McCann [1] investigated the relationship between frictional behavior and surface roughness for ABS plastics. He concluded that the rough surfaces (~ 0.82 R_a) exhibited steady sliding behavior ($\mu_s = \mu_k$) while the smooth surfaces (~ 0.042 R_a) exhibited single-stick or stick-slip behavior.

2.5 ABS Aging and Processing

How a polymer ages is very important in determining how a plastic will perform throughout its lifetime. It is important in the case of dashboard components where the plastic will be exposed to ultraviolet rays and a range of temperatures.

M. Wyzgoski [27] has studied extensively the effects of oven-aging on ABS. He found that oven aging affected some mechanical properties and these effects were dependent on whether the test specimens were injection or compression molded.

Figure 2.10 [27] shows the relative polybutadiene concentration vs. aging time for injection molded ABS. The three curves represent the three different crystals used in the FMIR (frustrated multiple internal reflection) attachment of an infrared spectrophotometer. Each crystal had a different penetration depth into the specimen (KRS-5,45:$d_p = 4.7\mu$, KRS-5,60:$d_p = 1.6\mu$, Ge-30:$d_p = 1.3\mu$). "This suggests that either the surface of an injection molded sample has a lower concentration of polybutadiene unsaturation or a depletion of rubber particles [27]." For the compression molded

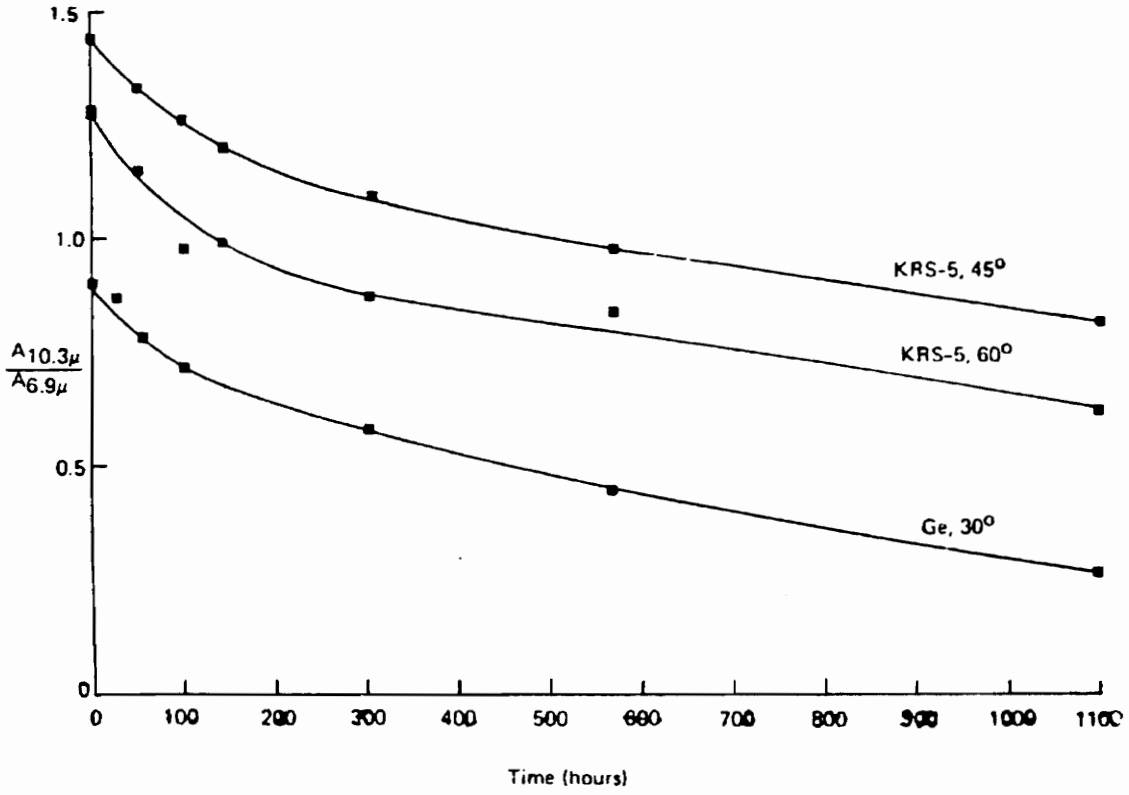

Figure 2.10 - Relative polybutadiene concentration (A10.3μ/A6.9μ) vs. aging time at 90°C for injection molded ABS. [27]

samples, the surface showed the same concentration of unsaturated polybutadiene regardless of the crystal used in the FMIR. Therefore, the surface of an injection molded sample is slightly different than the surface of a compression molded sample. The change in concentration vs. aging time for compression molded samples followed the same trend as the injection molded samples.

The oven aging did not affect the yield strength or modulus of ABS very much. However there was a change in the ultimate elongation. Figure 2.11 shows how the ultimate elongation changed and how the change is dependent on whether the sample is compression or injection molded.

Processing conditions such as temperature and pressure can affect the bulk properties of the polymer. Knowing the processing history of a polymer is important in determining the mechanical properties, especially when one is concerned with the properties of the polymer surface. Some researchers have found that the morphology of a plastic can vary across its thickness as a result of certain molding processes [16]. In the injection molding process, the polymer is subjected to much higher shear rates than in a compression molding process. This could affect the stress state of the material at the surface and hence the surface mechanical properties.

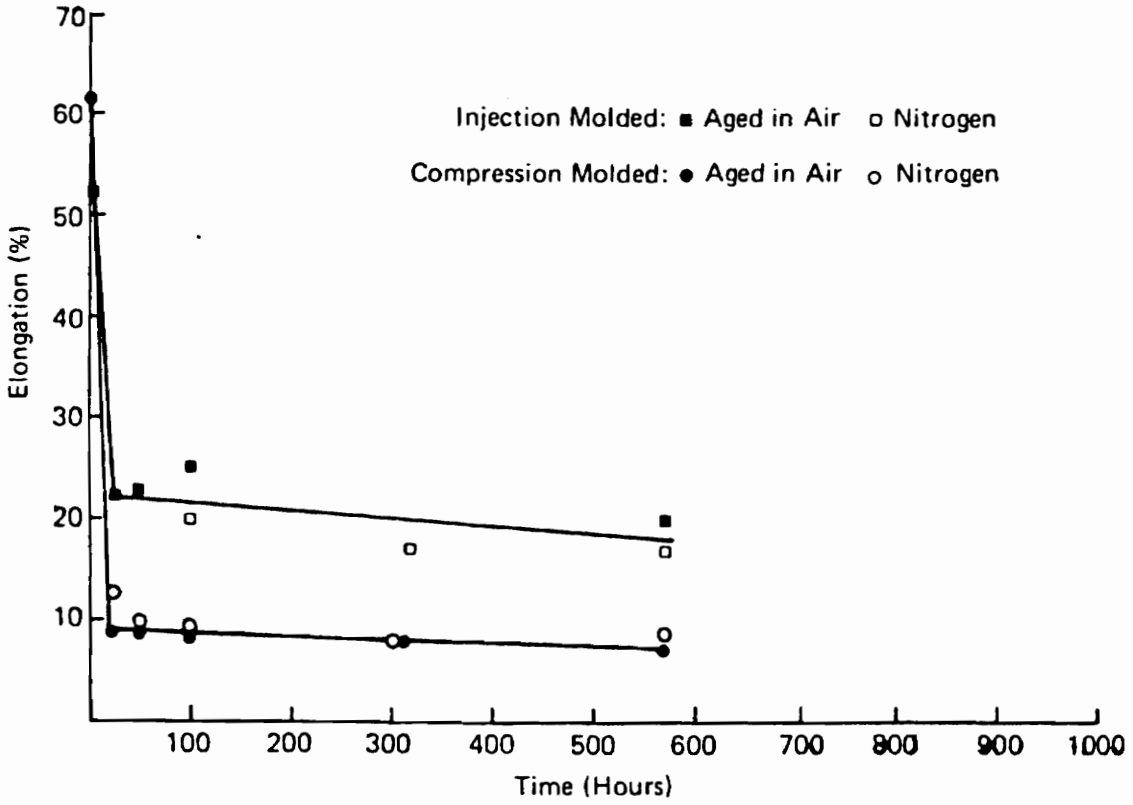

Figure 2.11 - Ultimate tensile elongation vs. aging time at 90°C for ABS. [27]

3.0 Experimental Apparatus and Procedures

This chapter details the test apparatus and procedures used in this study. First the pin-on-disk apparatus is described. Next, the modifications made to the test apparatus and the acquisition of data are explained. Section 3.3 reports the details of the materials used and the specifics of the handling of the polymer samples. A description of the testing conditions under which the experiments were performed are included in section 3.4. How the surface characteristics were obtained is described in section 3.5. The last section is a summary of the design of the new test apparatus.

3.1 Pin-on-disk Apparatus

The pin-on-disk machine shown in Figure 3.1 is used to measure the friction and wear of materials. The disk is attached to the platform which is forced to rotate at a constant rotational velocity by an electric motor. The velocity can be varied from 0.5 to 380 RPM (0.05 to 40 rad/sec) through a speed reducer and belt/pulley system. This results in a sliding velocity which can be varied from 0.0005 to 0.8 m/s. The pin is attached to a pneumatic cylinder which is used to apply the normal load (5 to 20 N

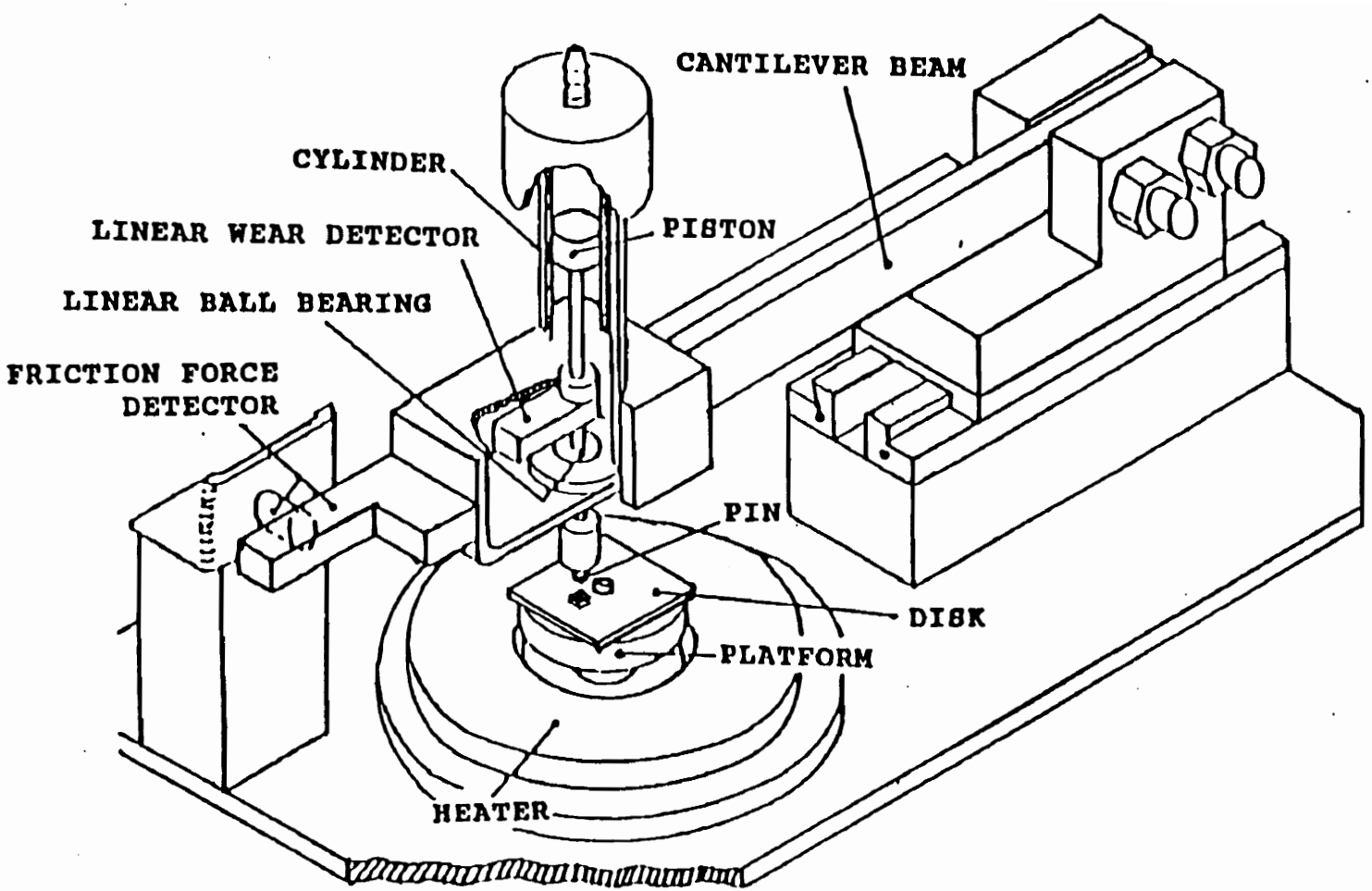

Figure 3.1 - Existing pin-on-disk friction measurement apparatus. [1]

range). The pneumatic cylinder is attached to the end of a cantilever beam. When the disk rotates the friction force pulls the cantilever beam away from the displacement sensor (Kaman KD-2400 Eddy current probe) causing the voltage output of the sensor to increase. It is important to emphasize that the sensor measures the displacement of the beam and not the actual friction force. This will be discussed further in section 5.1.2 and the next paragraph.

A typical stick-slip friction vs. time signal taken with this apparatus is shown in Figure 3.2. Notice the vibration at the beginning of each stick cycle. This vibration is the beam displacement not a variation in friction force. Figure 3.3 shows a detailed view of the sensor location. When the disk begins to move at a constant velocity, v, the two surfaces are stuck together, so the pin sample and the beam also move at constant velocity, v. When the static friction force is exceeded, the surfaces slip suddenly and stick again. The pin sample again moves at constant velocity, v, but the beam which has been given energy moves at velocity, v, plus a vibration component, $v_o \sin\omega_n t$, related to the natural frequency of the beam/piston rod system.

Another displacement sensor can be used to measure the normal displacement of the pin sample relative to the cantilever beam. This test apparatus is the same one used by B. McCann in previous research done for Ford Motor Company [1].

Following an evaluation of McCann's results, some changes were made to the test apparatus and data acquisition. These are discussed in the next section.

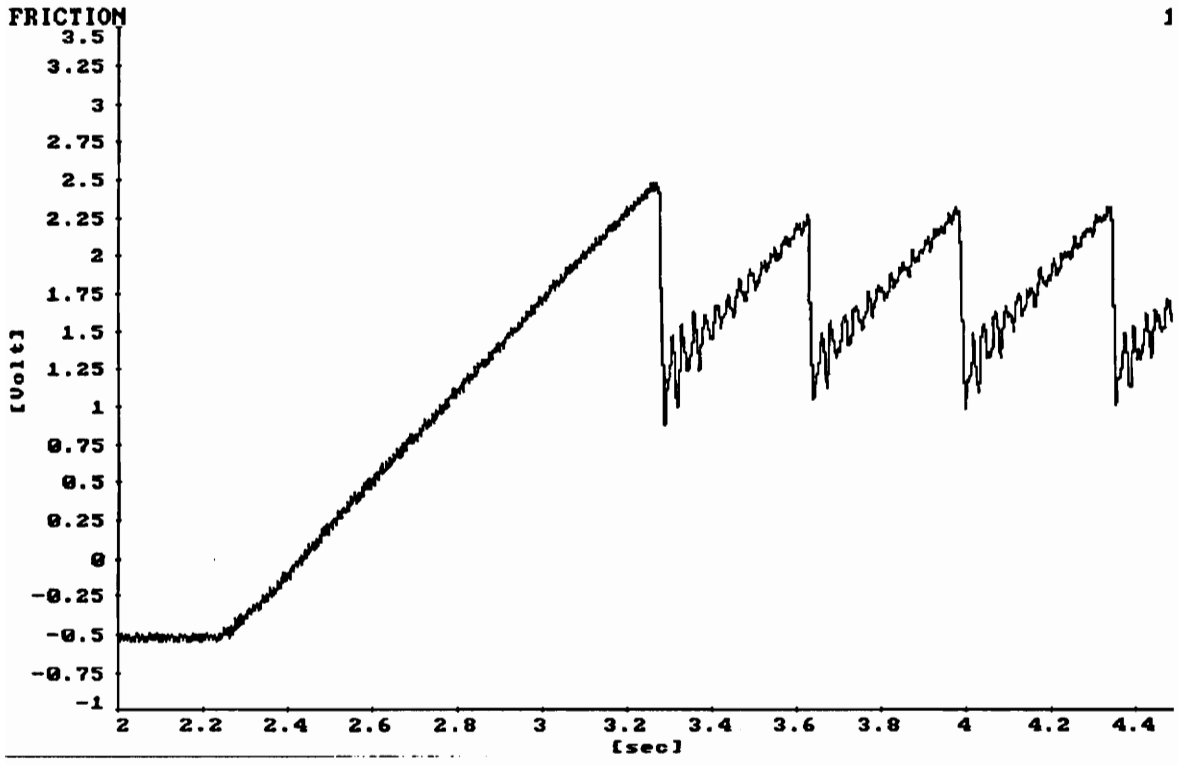

Figure 3.2 - Typical stick-slip friction signal showing beam vibration.

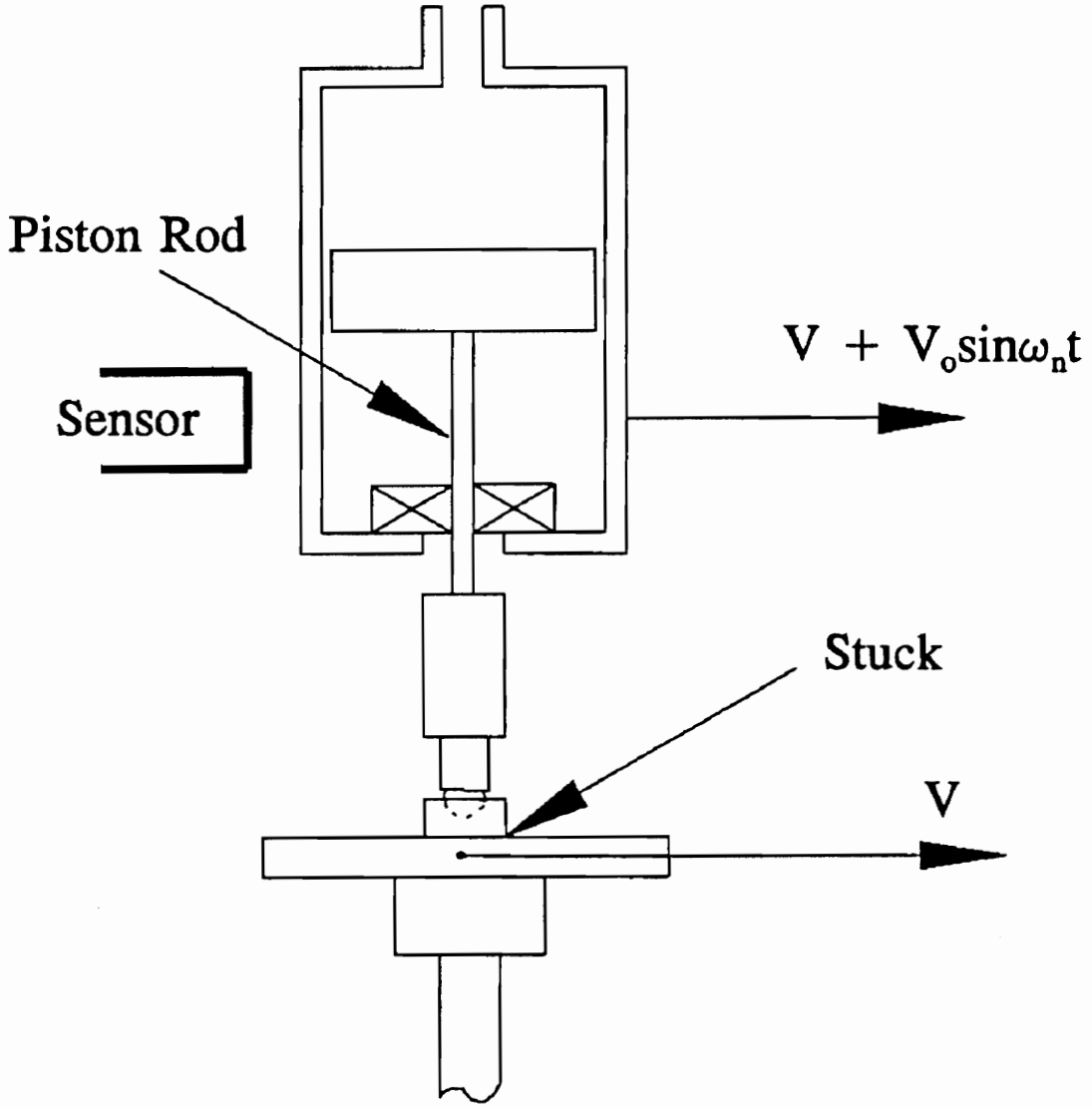

Figure 3.3 - End view of cantilever beam showing sensor location and beam vibration.

3.2 Vibration Problems

The electric motor and speed reducer were used to rotate the platform at constant velocity. Unfortunately, they were not completely isolated from the testing surface interface. So, the friction sensor picked up noise at the frequencies of the motor (1725 RPM or 29 Hz) and speed reducer (4 times 29 Hz or 115 Hz). The frequency of the noise did not change as the disk speed was changed. The noise had to be eliminated to achieve a signal which could be interpreted easily.

Mr. McCann used a low-pass filter while taking his friction data on a strip chart recorder. The filter successfully eliminated the noise in the friction signal. Figure 3.4a is a typical friction signal obtained by McCann, the static friction force was found from the strip chart by calculating the change in voltage between points A and B. Similarly, the kinetic friction force was found from points A and D, where D is the average of the signal beyond the first slip. The coefficients of friction were found by converting these voltage values to force values, using the calibration data for the sensor, and dividing by the normal load of the test.

The friction force in this study was sampled with a computer through a low pass anti-aliasing filter. Preliminary tests were run using a 150 Hz filter, and sampling at 1000 samples/sec. Figure 3.4b is a typical friction signal obtained in this way. To eliminate the noise, it was decided to continue to take the data through the 150 Hz filter but then filter the data again with a computer simulated 25 Hz low pass filter. Figure 3.4c is the filtered friction signal of 3.4b. Then the static and kinetic voltage values

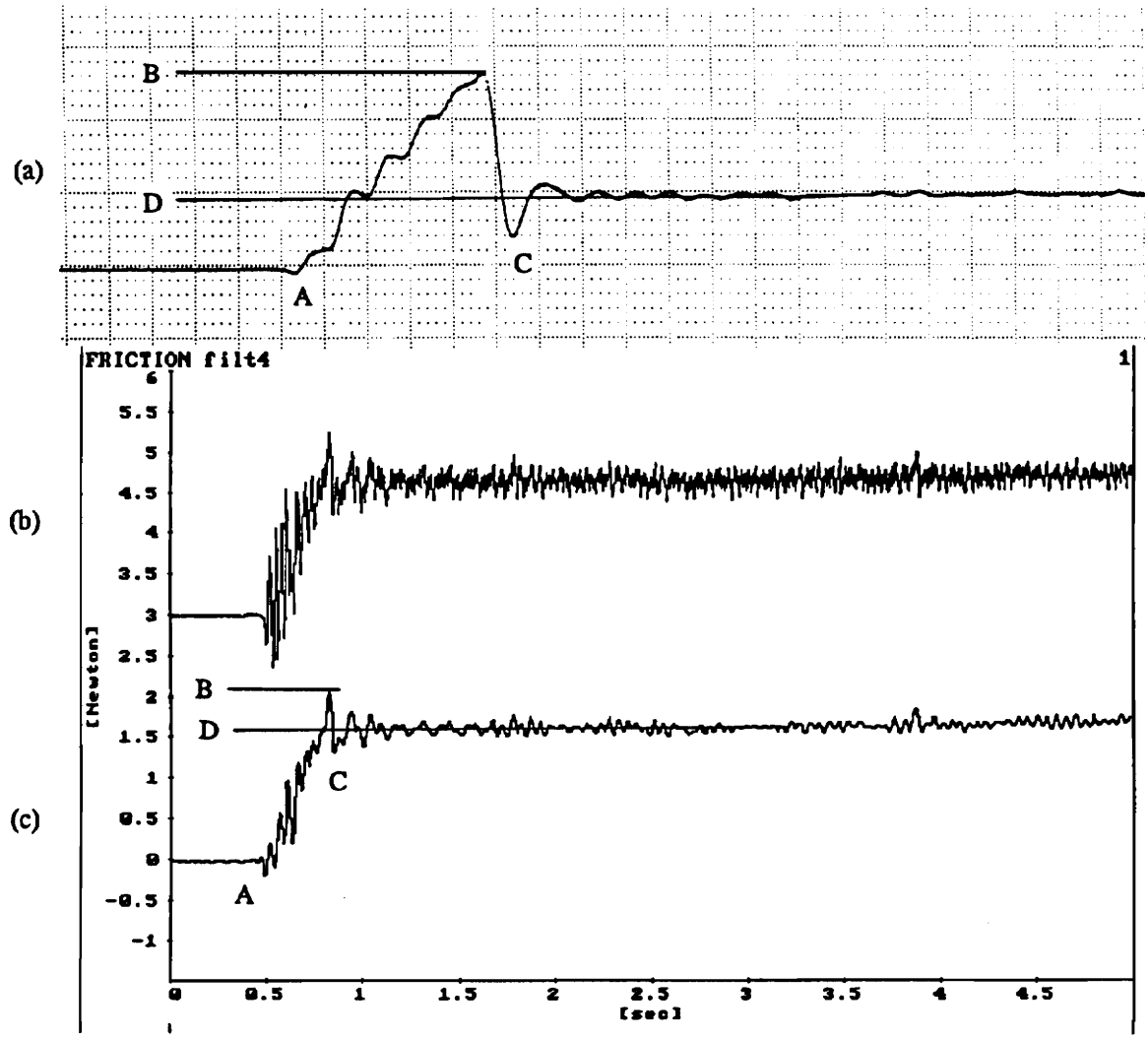

Figure 3.4 - (a) McCann's filtered friction signal. (b) Friction signal, 150 Hz filter. (c) Friction signal, 25 Hz filter.

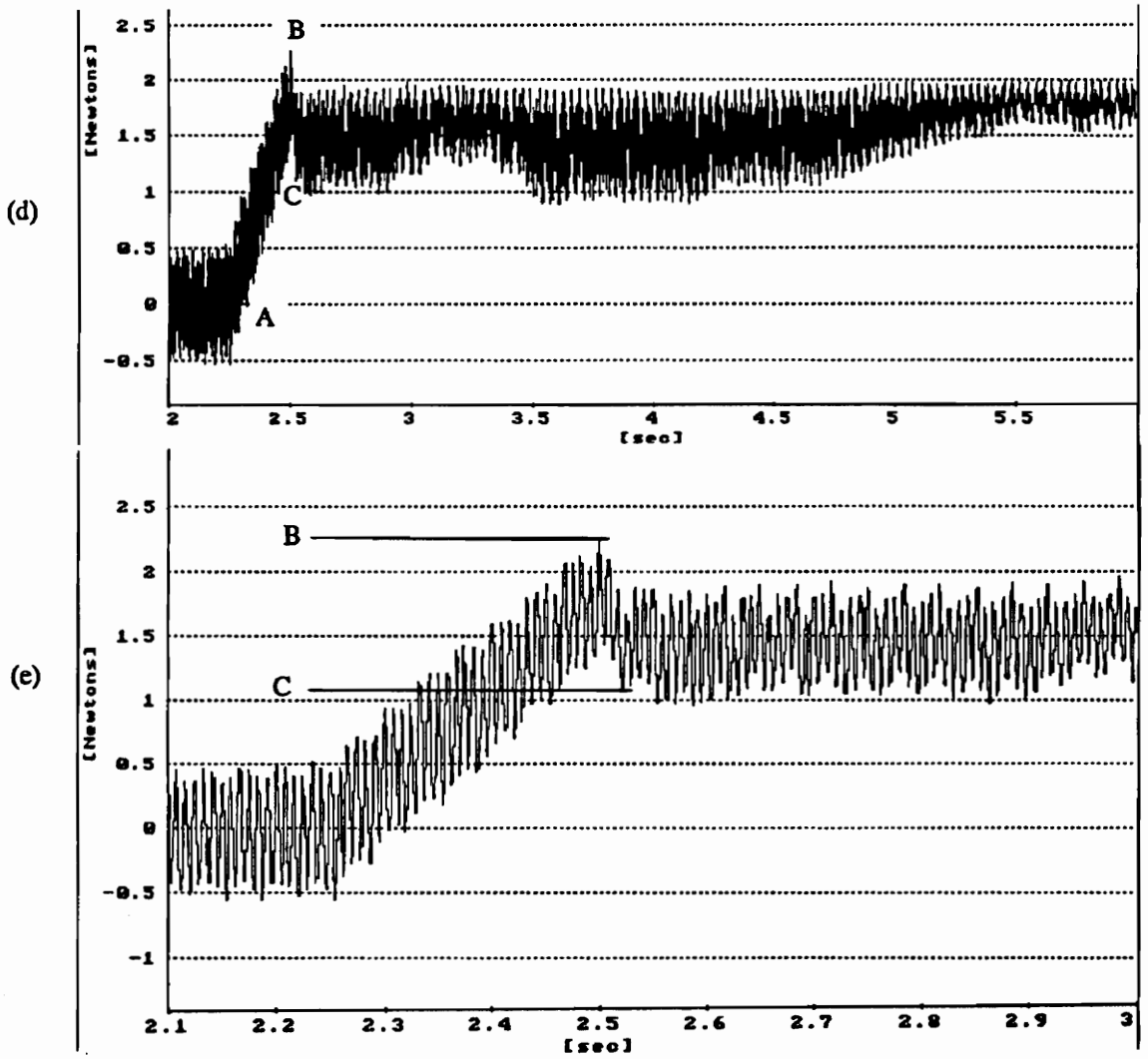

Figure 3.4 - (d) Friction signal showing variation in vibration amplitude. (e) Friction signal showing drop in friction force.

could be found in the same way as Mr. McCann.

Due to other experiments being run on the apparatus, the steel platform was replaced by a stainless-steel platform. This was done after the preliminary tests and before the actual tests. It was discovered about half way through the first set of actual tests that the vibration amplitude coming from the speed reducer was larger than before. Upon further investigation it was found that sometimes the amplitude of the noise varied during the friction test (Figure 3.4d). This variation might have been caused by the belt drive system. If the pulleys were slightly off-center, then the tension in the belts could have been changing. If the tension in the belts were changing then the dynamics (e.g. natural frequencies) of the whole system could have been changing which could affect the vibration amplitude transmitted to the disk.

If the noise was changing in amplitude but centered around the same voltage value, then the extra noise would not matter because the voltage signal is being filtered or averaged. But, as seen in Figure 3.4d, the noise is not centered around a single voltage value. The mean value of the noise is dependent upon the magnitude of the noise. The larger the noise amplitude the lower is the average voltage and hence, the lower is the measured value of kinetic friction force. This lower value of friction is misleading.

It is interesting that the peak of the vibration seems to be constant no matter what is the vibration amplitude. There may be some relationship between the peak of the vibration (which is essentially constant) and the kinetic friction force (which should be

constant).

A quick and inexpensive solution to the vibration problem was found. A clamp was used to secure the bottom plate of the test apparatus to the counter top. The clamp reduced the vibration amplitude significantly. After the clamp was added, the second half of the friction tests were run. After all the results were tabulated, statistical analysis was used to confirm the theory that the unclamped tests yielded friction coefficients which were lower than the clamped tests. So, a direct comparison could not be made between friction values obtained from the two different testing conditions. However, it was found statistically that the drop in friction force during slip (point B to point C in Figure 3.3d) was the same under the two different testing conditions. Therefore, the drop in friction force was used to evaluate surface roughness effects.

Actually, the drop in voltage from point B to C is not equal to the drop in friction force for the reason stated in Section 3.1. This drop in voltage is the beam response to a drop in friction force. The drop in friction force is directly related to the amount of potential energy converted to kinetic energy of beam vibration, and the kinetic energy of the beam controls the beam deflection. Therefore, we can say that the actual drop in friction force is proportional to the change in the beam deflection (drop in voltage), but the values obtained can be used for comparison purposes only.

Figure 3.4e is the exact same friction signal of 3.4d with an expanded x-axis. This illustrates how points B and C are defined. Both points are defined on the 150 Hz filtered signals. Point B is the maximum point just before slip and point C is the

minimum point just after slip.

The clamp was not the only change made to the test apparatus. The drive system of the test apparatus was modified before any of the actual tests were run. This was necessary because the start of the motor caused, a transient vibration which interfered with the friction signal. This vibration problem was corrected by modifying the belt/pulley system. A set of intermittent gears was added to the drive system which delayed the movement of the disk until after the motor transient had decayed. The design of the gear system is shown in Appendix A. As is seen in Figure 3.5, this made the friction signal much cleaner. This also affected the frictional behavior that is observed. The test run before the gears were added would be described as steady sliding while the test run after the gears would be described as single-stick. The motor transient could be responsible for a smooth transition from stick to slip. Without the extra vibration the potential energy is released into the beam more suddenly causing single stick behavior.

This test apparatus, with the clamp and the intermittent gears, is referred to as the "improved" test apparatus.

3.3 Test Samples

3.3.1 Materials

The work done over the past 18 months on this research project has been a continuation of the work done by Brian McCann. Some of the same materials were used

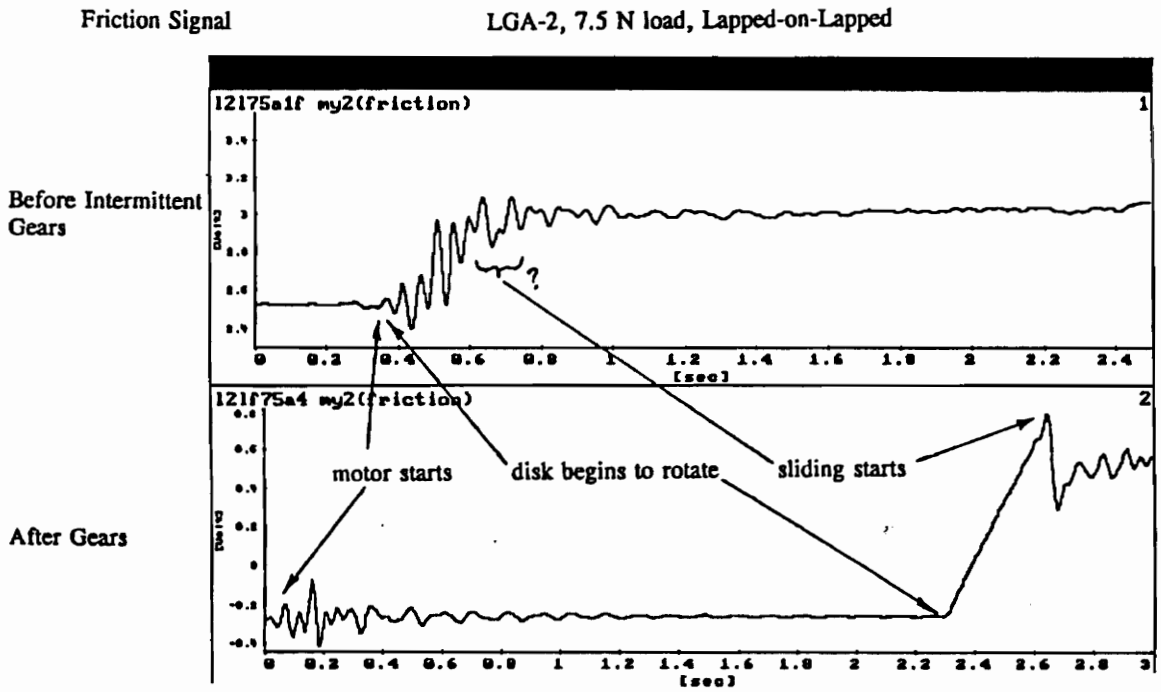

Figure 3.5 - Effect of intermittent gear system.

in both studies. Five different types of ABS, Poly(Acrylonitrile-Butadiene-Styrene), and one sample of Polypropylene were tested.

ABS is an amorphous polymer with a rubber component and a styrene component. "The rubber in a polybutadiene-in-water emulsion is swollen with a mixture of styrene and acrylonitrile monomers, which are then co-polymerized in situ under the influence of a water-soluble free radical initiator. The dried product is a blend of polybutadiene, styrene-acrylonitrile (usually called SAN) copolymer, and grafts of SAN on the rubber. The graft itself is a random copolymer. [28]"

Polypropylene is a semi-crystalline polymer. The five ABS materials used in this study are referred to by their trade names throughout this thesis; AL-4510, LGA-1, LGA-2, TG-38, and TG-72. Table 3.1 is a list of some of the properties of the materials. No other material characterization is available at this time.

3.3.2 Processing

In his Master's Thesis, Mr. McCann concluded that unstable frictional behavior decreases with increasing surface roughness. Tests run with a rough surface in contact with a rough surface exhibited stable frictional behavior. Tests run with a smooth surface in contact with a smooth surface exhibited some frictional instabilities. This roughness effect was observed for only the four materials which had different roughness values on the plaque surfaces. The other five samples had the same roughness on both surfaces of the plaque. It was decided to determine whether or not this roughness effect

Table 3.1 - Material Composition and Properties

		TG-38	TG-72	AL-4510	LGA 1	LGA 2	Poly-propylene
Silicone Oil (%)*		0	1	1	0	1	0
PTFE (%)* Poly(tetraflouro ethylene)		0	0	4	0	0	0
Impact Strength (kJ/m^2)		32.0†	32.0†	4.1†	16.2†	14.0†	21-53‡
Tensile Strength (MPa)		45.0†	45.0†	39.1†	38.7†	37.6†	30-40‡
R_a Roughness (μm) **							
Injection Molded	Smooth	0.041	0.05	0.10	0.18	0.12	0.2-0.3
	Rough	0.88	0.90				
Compression Molded	Lapped Smooth	0.12	0.12	0.12	0.13	0.13	0.12
	Ground Smooth	0.14	0.18	0.13	0.16	0.14	0.14
	Ground Rough	0.85	0.78	0.96	0.98	0.99	0.78

* Information obtained from the polymer manufacturers.
** Measured using the Talysurf 4.
† Information obtained from testing done by Ford Motor Company.
‡ Taken from [29].

would be observed for all the materials if they had the same range of roughnesses.

The least expensive way to obtain a range of surface characteristics was to reprocess some of the samples left over from McCann's work. All of McCann's samples were injection molded by the suppliers into square plaques. A compression molding machine was used to produce different surface roughnesses on the plaques.

The objective was to obtain three different roughnesses, one as smooth as McCann's smooth surface (0.04 μm R_a roughness), one as rough as McCann's rough surface (0.86 μm R_a roughness) and one in between the two. Steel plates for the compression molding machine were machined by grinding and lapping to the following R_a roughnesses; 0.09, 0.14, and 0.76 microns, while the lapped smooth (0.09 μm) and ground smooth (0.14 μm) surfaces had comparable R_a roughnesses, the surface textures produced by the finishing procedures were different. The impression of the steel plates on the plastic plaques resulted in slightly different surface roughnesses: lapped smooth= 0.12-0.13 μm R_a, ground smooth= 0.13-0.18 μm R_a, and ground rough= 0.78-0.99 μm R_a.

Before compression molding, the plastic plaque was placed between the two steel plates. The plaque and plates were placed between two hot plates each at 170°C. A thermocouple placed between the plaque and one of the plates was used to monitor the temperature of the plastic. When the temperature reached 160°C (well above the Tg for ABS and Polypropylene) the plaque and plates were placed between two cooling plates and pressed together with a hydraulic jack to 25,000 lb (about 1000 psi). The six

materials processed in this manner were Polypropylene and the five ABS compounds, TG-38, TG-72, LGA-1, LGA-2, and AL-4510.

The plaques were then cut into squares to be used on the pin-on-disk test apparatus. The disk sample was 2" square with a hole drilled in the middle so that it could be attached to the platform of the test apparatus. The pin sample was ¼" square with a spherical cavity drilled on one surface of the sample. The pin of the pin-on-disk apparatus fit into the spherical cavity allowing for the two samples to self-align (Figure 3.6). The edges of the samples were de-burred with a de-burring knife. All of this machining was done while being careful not to scratch the surfaces which would be in contact. The samples were then washed with a mild soap and allowed to air dry.

3.4 Test Conditions

3.4.1 Surface Roughness Tests

In the first series of tests, the test procedures and conditions for each of the six compression molded materials were the same as those used by McCann. The tests were run using normal loads of 5, 7.5, 10, 15, and 20 Newton. Three different surface roughness combinations were tested: Ground rough-on-Ground rough, Ground smooth-on-Ground smooth, and Lapped-on-Lapped. The velocity of the disk sample was 0.5 RPM which gave a surface velocity of 0.0005 m/sec. Four repeat tests were done for each set of conditions. Each test was six seconds in duration; therefore, only one disk sample was used for all twenty tests (5 loads x 4 repeats). To minimize the effect of

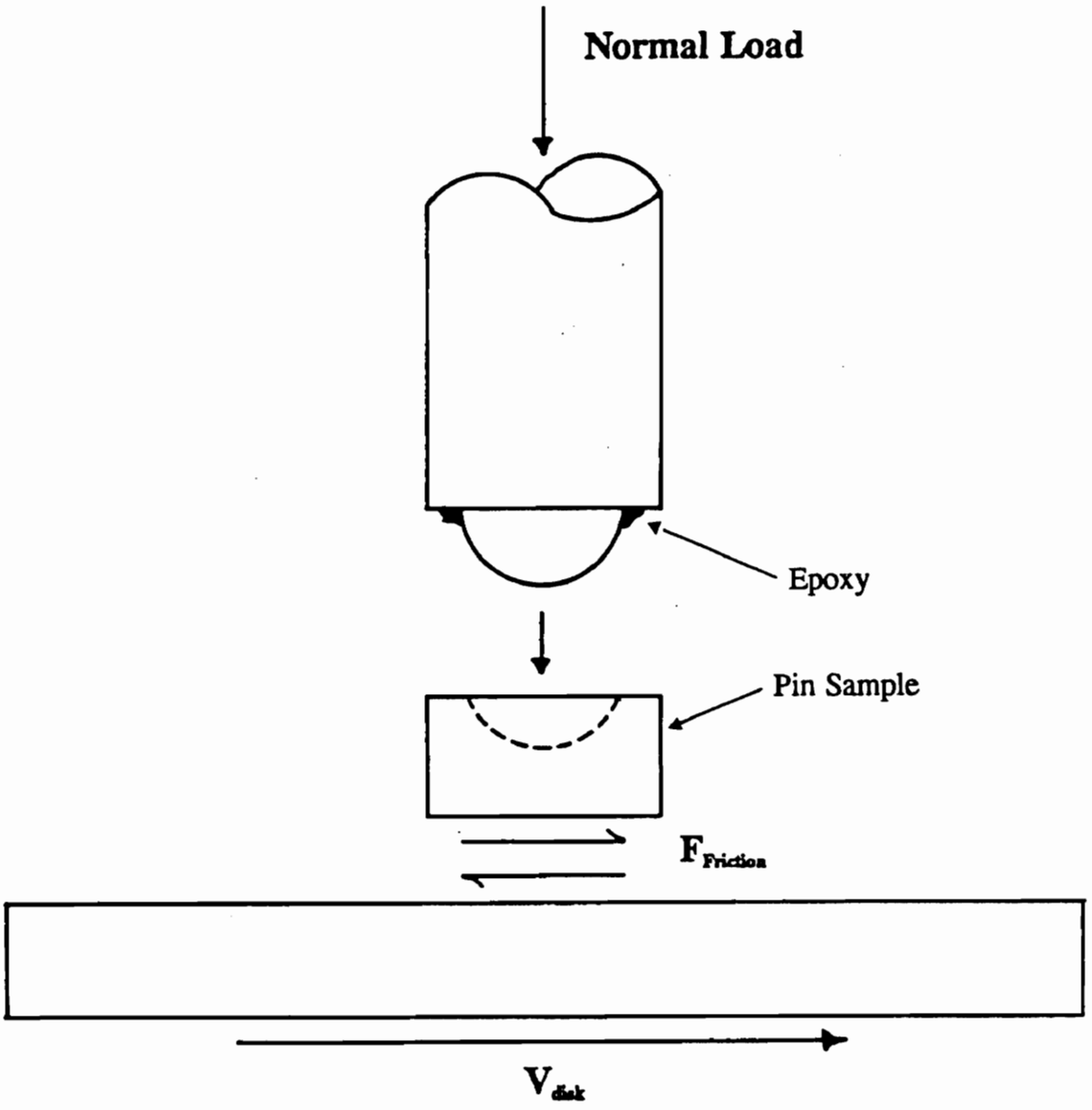

Figure 3.6 - Expanded view of loading system for polymer-on-polymer interaction [1].

wear, a new pin sample was used for each load when possible. For consistency, it was decided to keep the pin sample square with the direction of sliding (see section 5.4 and Figure 5.7). To minimize the effect of the normal load application time [1], the normal load was applied for three minutes before the start of every test. Half of the tests were run under the unclamped condition and half were run under the clamped condition, as discussed in section 3.2.

In the second series of tests, the materials used by Mr. McCann (injection molded samples) were tested on the "improved" test apparatus. Four different material/surface roughness interactions were re-tested: TG-72 Rough-on-Rough, TG-72 Smooth-on-Smooth, LGA-1 Smooth-on-Smooth and LGA-2 Smooth-on-Smooth. The same testing conditions as the first series were used: Normal load= 5, 7.5, 10, 15, 20 N; velocity= 0.0005 m/s; test duration= 6 seconds; and a three minute delay after applying the normal load, before starting rotation.

Table 3.2 illustrates how the results of all the friction tests will be referred to throughout this thesis. The results from tests run with the injection molded plaques on the old test apparatus will be referred to as McCann's results and can be found in their entirety in his thesis [1]. The results from tests run with the compression molded plaques on the "improved" test apparatus will be referred to as the A-series results. The results from tests run with the injection molded plaques on the "improved" test apparatus will be referred to as the B-series results.

Table 3.2 - Test Conditions

		Test Apparatus	
		"improved"	"old"
Sample Processing	Compression Molded	A-Series	
	Injection Molded	B-Series	McCann's

3.4.2 Friction-Velocity Tests

A few tests were run to find the relationship between friction force and velocity. Injection molded samples of TG-72 Smooth-on-Smooth and LGA-1 were tested under a 15 N normal load. Tests were run at mean surface velocities of 0.0005, 0.001, 0.0027, 0.0079, and 0.03 m/sec. Mr. McCann had done similar tests but because the motor transient obscured the static-kinetic transition he only recorded the kinetic coefficient of friction at each velocity. The new gear system on the improved apparatus made it possible to record both the static and kinetic coefficient of friction at each velocity.

3.5 Surface Roughness

A Talysurf 4 surface profile meter was used to find surface characteristics of the materials tested. A computer was used to digitally sample the output of the Talysurf 4. A computer program was modified to read these data files and calculate the surface characteristics of the materials (the program is listed in Appendix B).

The surface roughness parameters used to characterize the surfaces included the

profile height R_a, RMS, skewness, and kurtosis; along with the RMS values of slope and curvature. Formulas for these parameters can be found in Appendix C.

3.6 New Test Apparatus

McCann's research on Ford materials used an existing pin-on-disk apparatus, which was designed for wear tests, to measure friction. This system measured the friction force by measuring the deflection of the beam. While this system could measure steady state friction, the deflection of the beam during transient conditions such as stick-slip was caused by the sum of the friction force and the inertial forces of the moving beam. To accurately measure the friction force during transients, the measuring system must be very stiff so that the inertial forces are small compared to the friction forces.

Since relative velocity is known to affect the magnitude of friction, both must be known accurately if friction-velocity relationships are to be determined. On the old apparatus, the beam motion during transients caused fluctuations in relative velocity which could not be measured accurately. A new test apparatus was designed and built to correct these deficiencies.

Figure 3.7 is a drawing of the new test apparatus. The following is a summary of how the apparatus was designed.

The most accurate measurement of relative velocity would be to attach each end of a velocity transducer to each sliding member. However, to change specimens would require disconnecting and reconnecting the transducer as well as complicating the

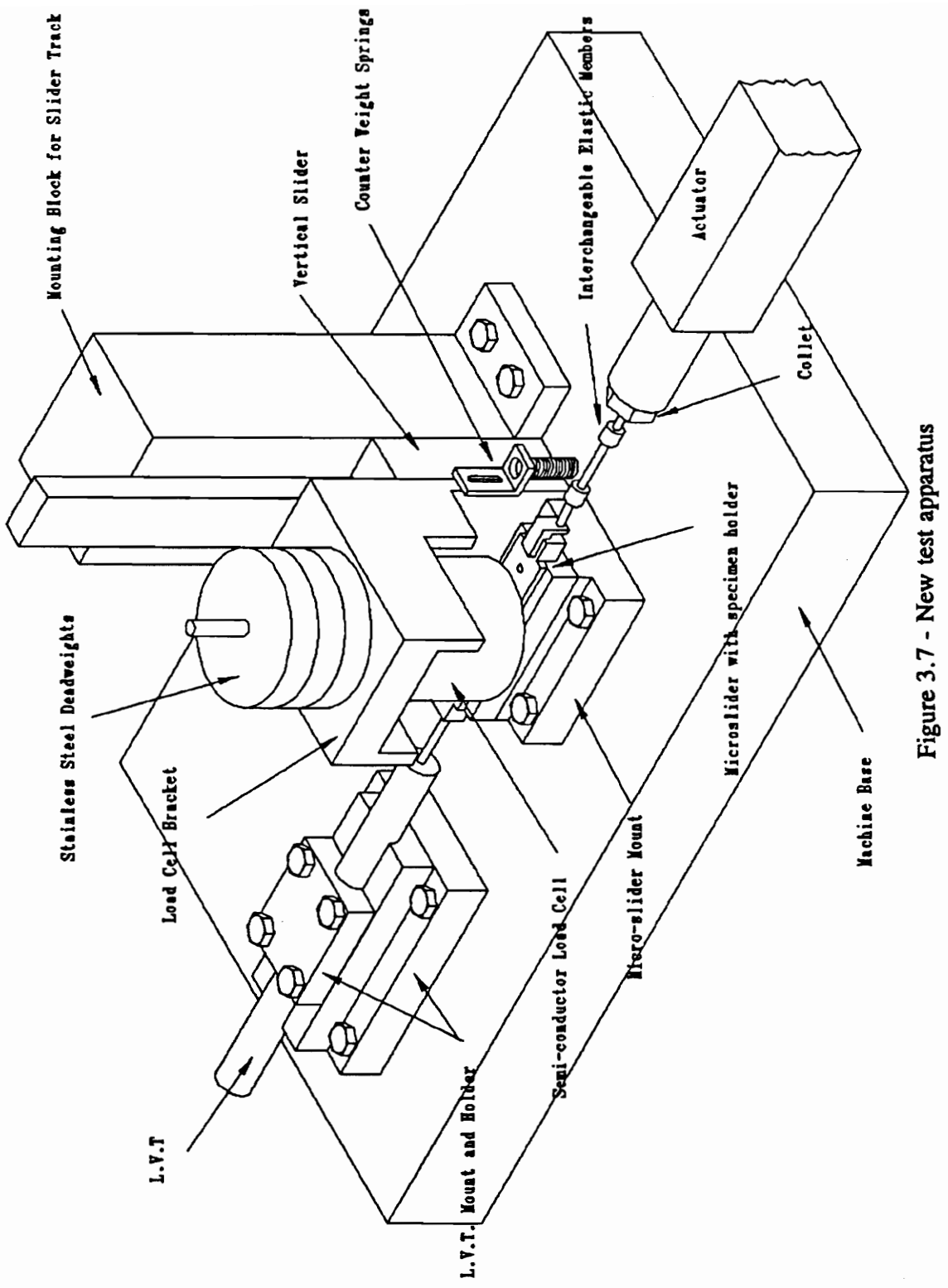

Figure 3.7 - New test apparatus

transducer mounting. Therefore it was decided to keep one surface stationary and measure the absolute velocity of the other. The normal and friction forces must be measured through the stationary sample, as attaching the force transducer to the moving sample would lessen the accuracy of its measurements due to the inertia of the internal components of the force transducer.

Since the apparatus may eventually be used in an industrial laboratory, a simple, safe, and portable method of normal load application was desired. Dead weights best meet these criteria. Since dead weights are to be used to apply the normal load, a frame is necessary to maintain stability and alignment of the sample contact. Because the sample attached to the force transducer must be held stationary when subjected to changing friction forces, the portion of the frame which supports the force transducer must be significantly stiffer than the force transducer. The stiffness requirements are based on the velocity resolution desired. As the stiffness of the stationary sample mounting is increased, the maximum velocity possible by the stationary sample during a specified step change in force is decreased. And it is required that the maximum velocity of the stationary sample be small so that the absolute velocity of the moving sample (which is measured) is close to the actual relative velocity (v_{moving}-$v_{stationary}$). The samples will need to be changed between tests, so the frame must be separable at the sample contact point.

To provide the stiffness which is necessary in the direction of the sample velocity, and to allow for separation at the sample contact point, a linear bearing system is used.

When material samples need to be changed, the carriage can be raised approximately eight inches above the contact position. The pre-loaded roller bearings prevent the vertical slider carriage from rattling, and provide the necessary rigidity. A bracket is used to connect the force transducer to the slider carriage and to hold the weights. The bracket design is optimized for stiffness and weight. A lightweight bracket is necessary so that tests could be run at low loads (5 N). The total weight of the slider carriage, bracket and force transducer is about 15 N; therefore a counterweight system using compression springs was designed to offset the extra 10 N.

To measure the friction force and normal load, a biaxial force transducer is used. The simultaneous measurement of friction and normal forces permits the calculation of instantaneous values of coefficient of friction. The force transducer was chosen taking into account cost and stiffness. The force transducer which uses semi-conductor strain gages can measure normal forces from 0 to 20 N and friction forces from 0 to 10 N.

A linear actuator driven by a stepper motor is used to drive the forced sample. The actuator is designed to move at constant velocity despite varying forces at the end of the actuator which is very important since the friction force changes. The actuator is capable of speeds from 0.000237 to 23.7 inches/second; however, at the lower speeds the stepping action of the motor causes a variation in the actual velocity. The actuator can accelerate to 5.9 in./sec in about 50 milliseconds.

The driver is isolated from the velocity and force transducers by rubber pads placed underneath the two bases. This eliminates most of the noise caused by the motor

vibration.

The forced sample is mounted on a sliding table which is guided by linear motion bearings. An interchangeable elastic member is installed between the driver and the table to control the characteristics of the stick-slip oscillations. Thus, the elasticity of the traveling table is completely independent of the elasticity of the friction force transducer. Hence, the characteristics of the stick-slip and other instabilities can be altered easily. A Linear Velocity Transducer (L.V.T.) is used to measure the velocity of the table and hence the relative velocity of the samples. The L.V.T. is accurate to ± 1 percent and has a 2 inch stroke.

4.0 Results

4.1 Surface Roughness Effects

Figures 4.1-4.6 show the drop in friction force during slip at each load for the six materials and three surface combinations tested (A-series), including the 90% confidence intervals. There appears to be no consistent evidence of surface roughness effects on the drop in friction force.

Since this result was different from McCann's conclusion about roughness, the A-series results were compared directly to McCann's results for materials which had comparable R_a roughnesses in each study. These included TG-72 Ground rough-on-Ground rough (GR), LGA-1 and LGA-2 Ground smooth-on-Ground smooth (GS), and AL-4510 Ground smooth-on-Ground smooth and Lapped-on-Lapped (L). Figures 4.7, 4.8, and 4.9 show the coefficients of friction for these materials for 5, 10, and 20 N normal loads and the comparison between the A-series results and McCann's results. The conditions marked N/A mean that these results were run before the excessive noise problem was corrected.

As seen in Figure 4.9, for smooth surfaces at 20 N normal load, both the A-series results and McCann's results show a drop in the friction force after relative motion

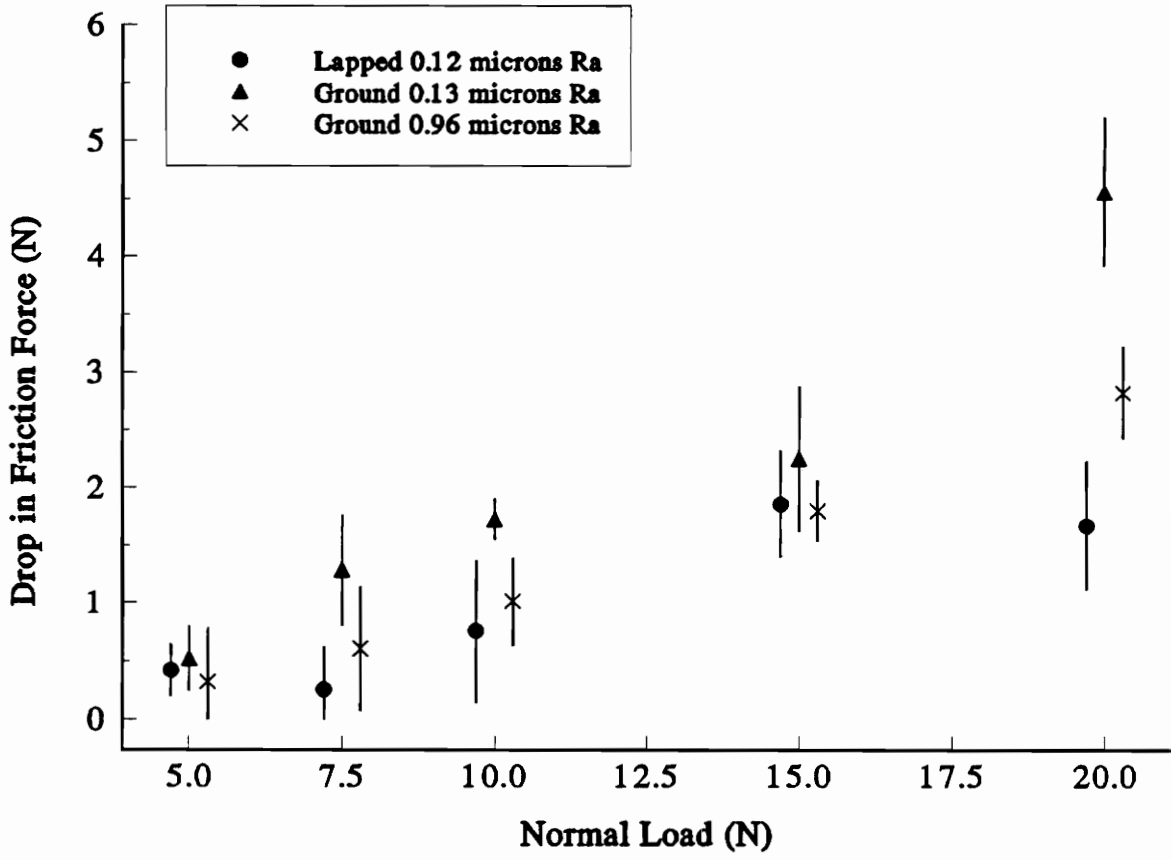

Figure 4.1 - Drop in friction force during slip for AL-4510, different surfaces, A-series, with 90% confidence intervals.

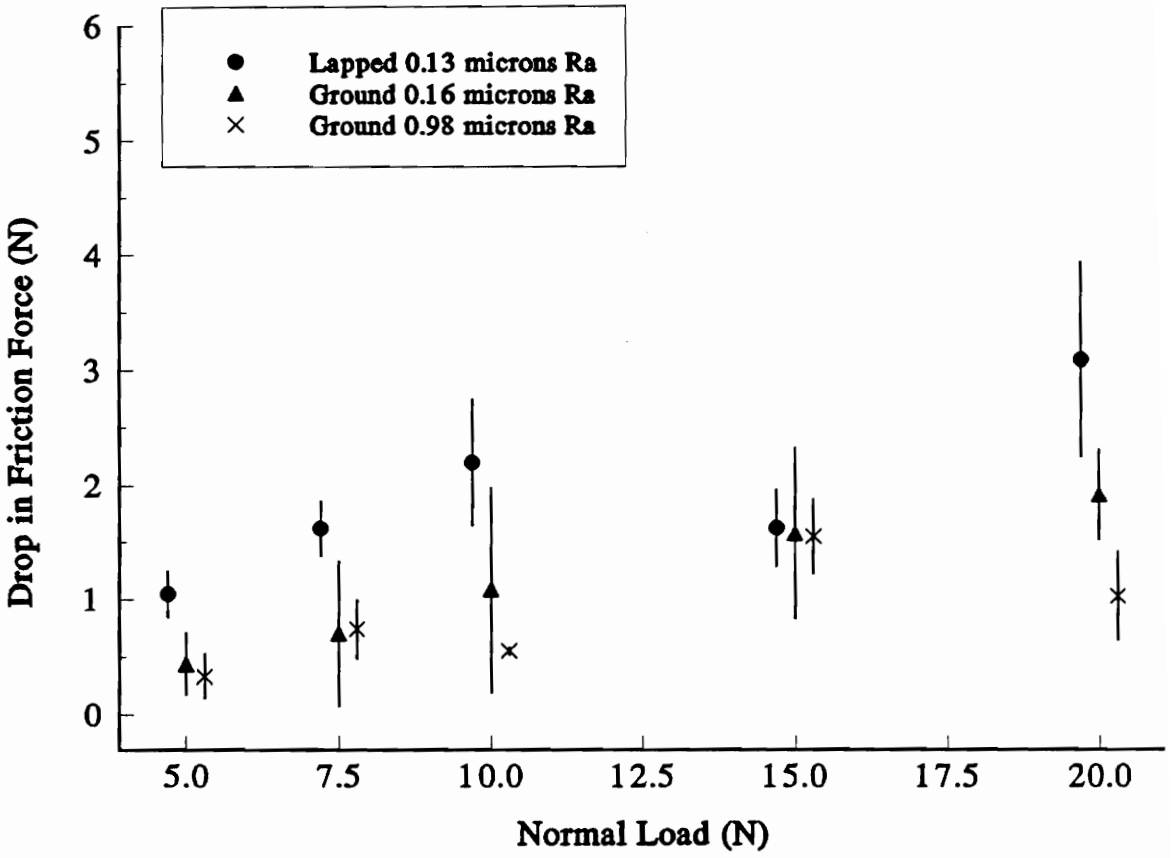

Figure 4.2 - Drop in friction force during slip for LGA-1, different surfaces, A-series, with 90% confidence intervals.

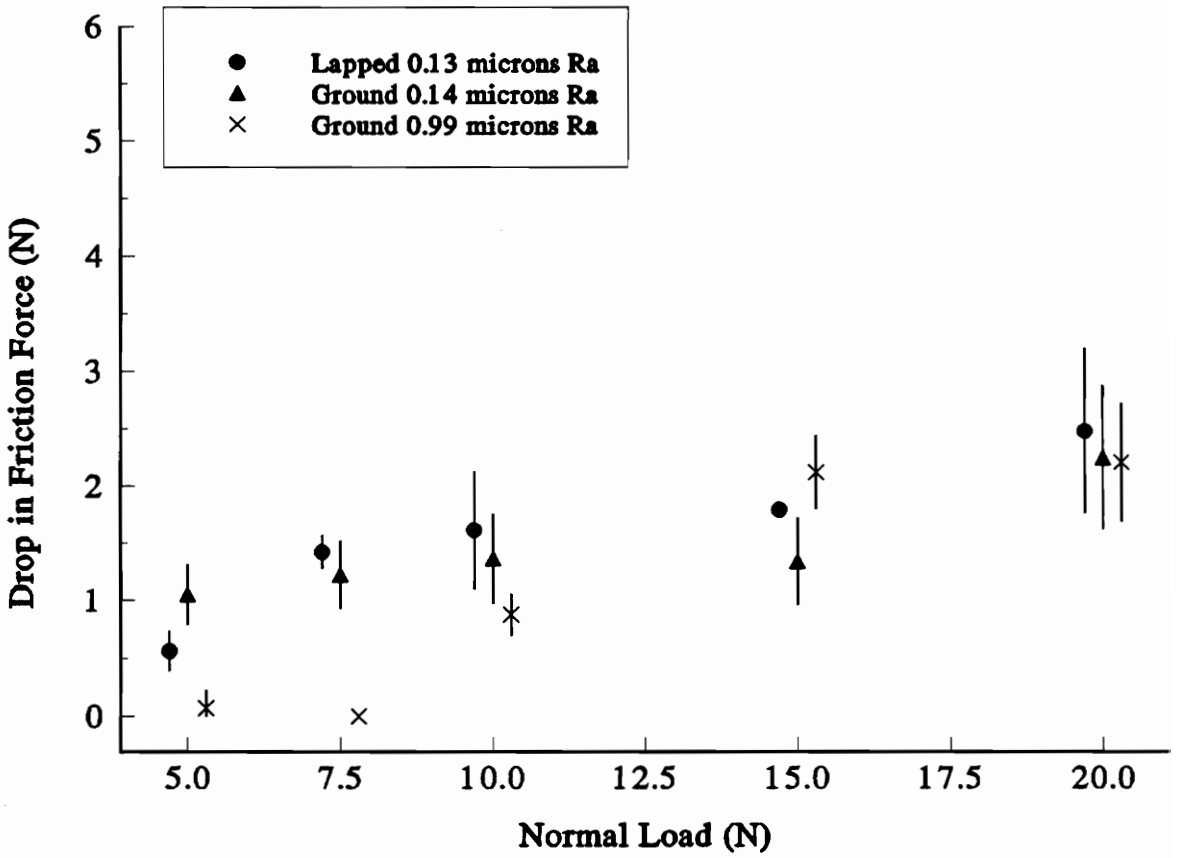

Figure 4.3 - Drop in friction force during slip for LGA-2, different surfaces, A-series, with 90% confidence intervals.

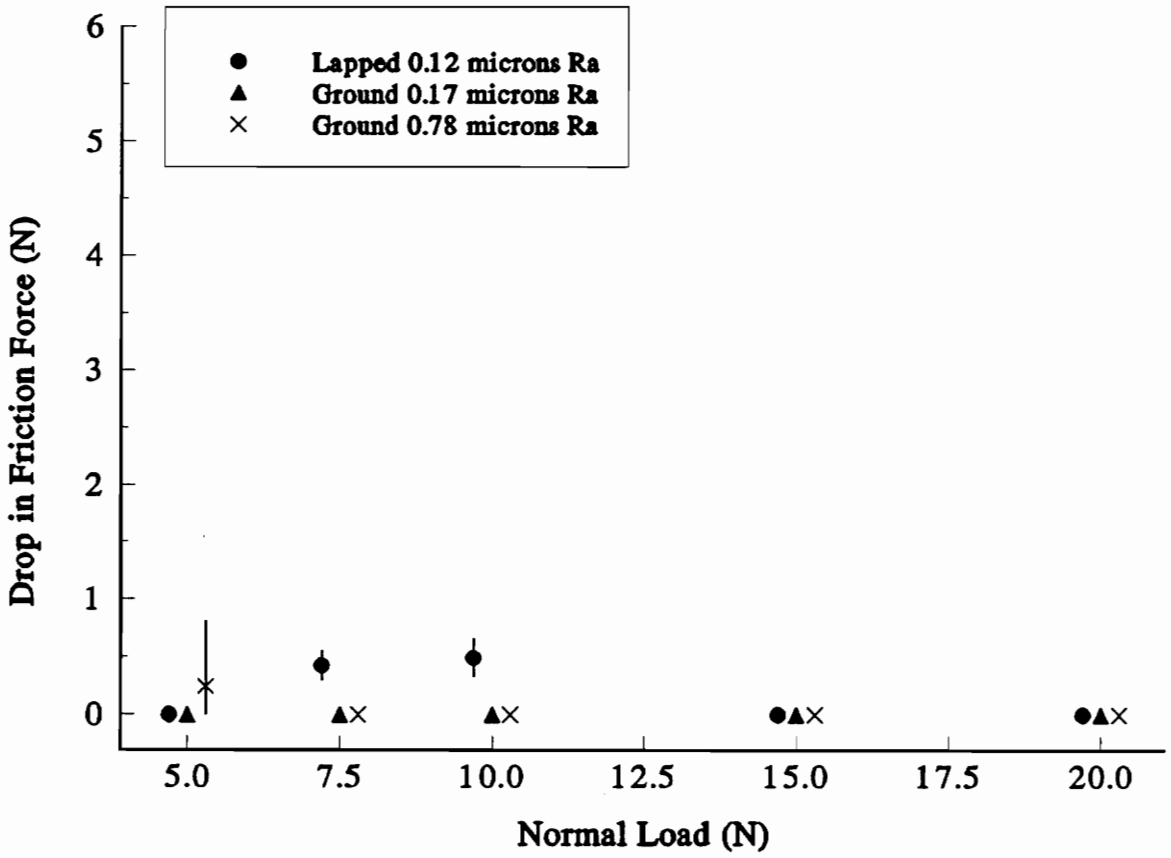

Figure 4.4 - Drop in friction force during slip for Polypropylene, different surfaces, A-series, with 90% confidence intervals.

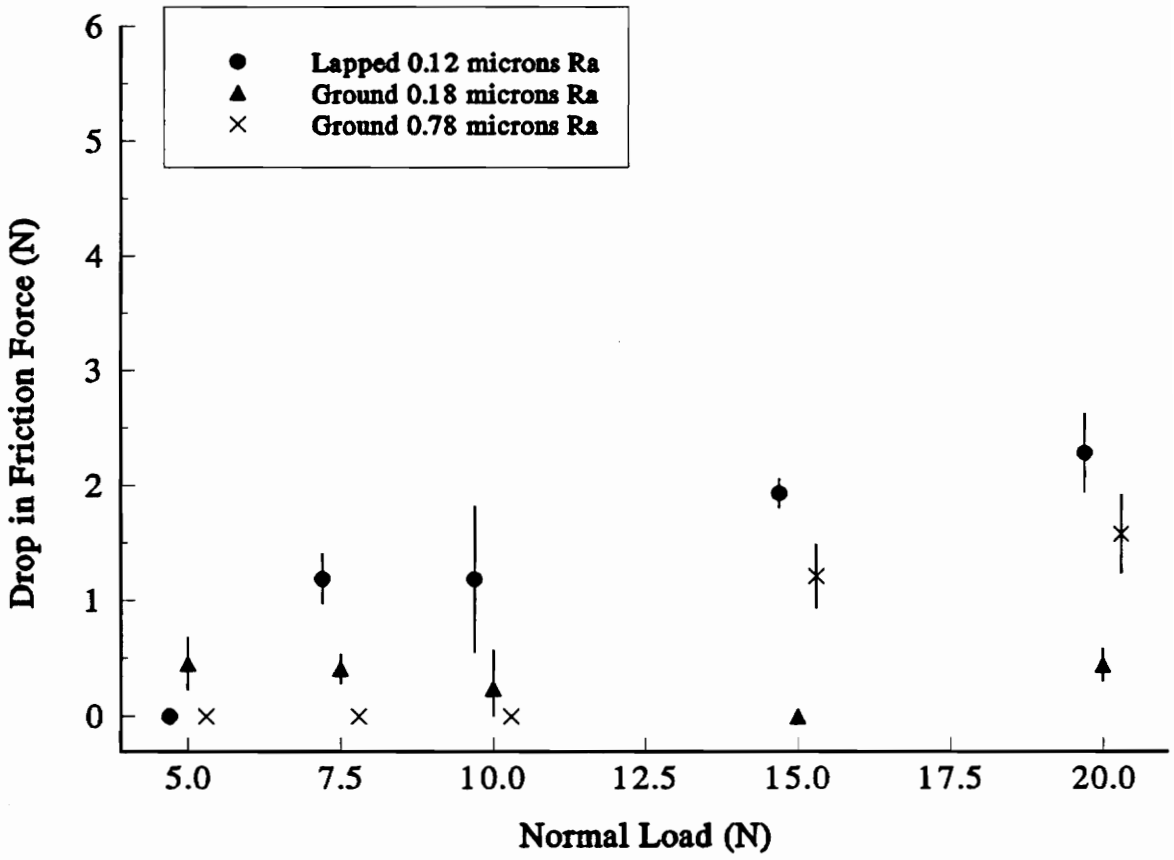

Figure 4.5 - Drop in friction force during slip for TG-38, different surfaces, A-series, with 90% confidence intervals.

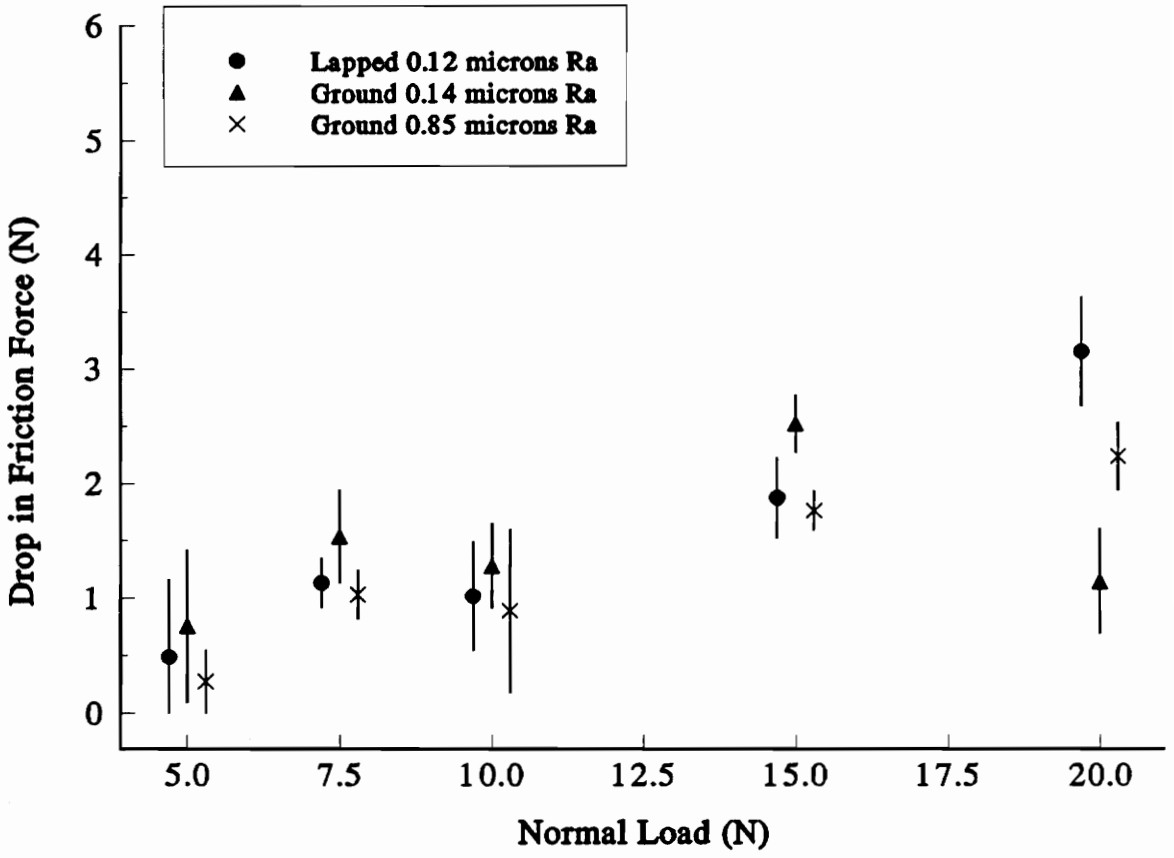

Figure 4.6 - Drop in friction force during slip for TG-72, different surfaces, A-series, with 90% confidence intervals.

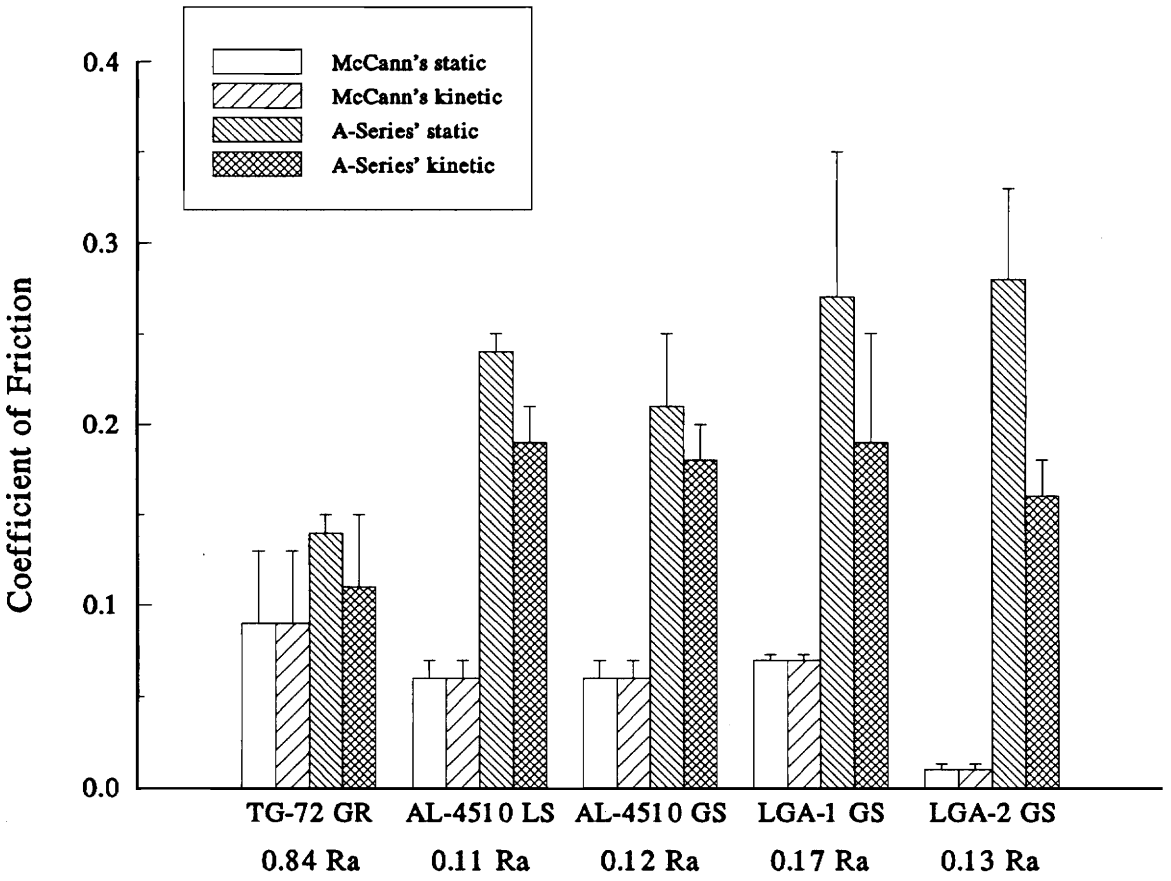

Figure 4.7 - Comparison of A-series results with McCann's results, 5 N load.

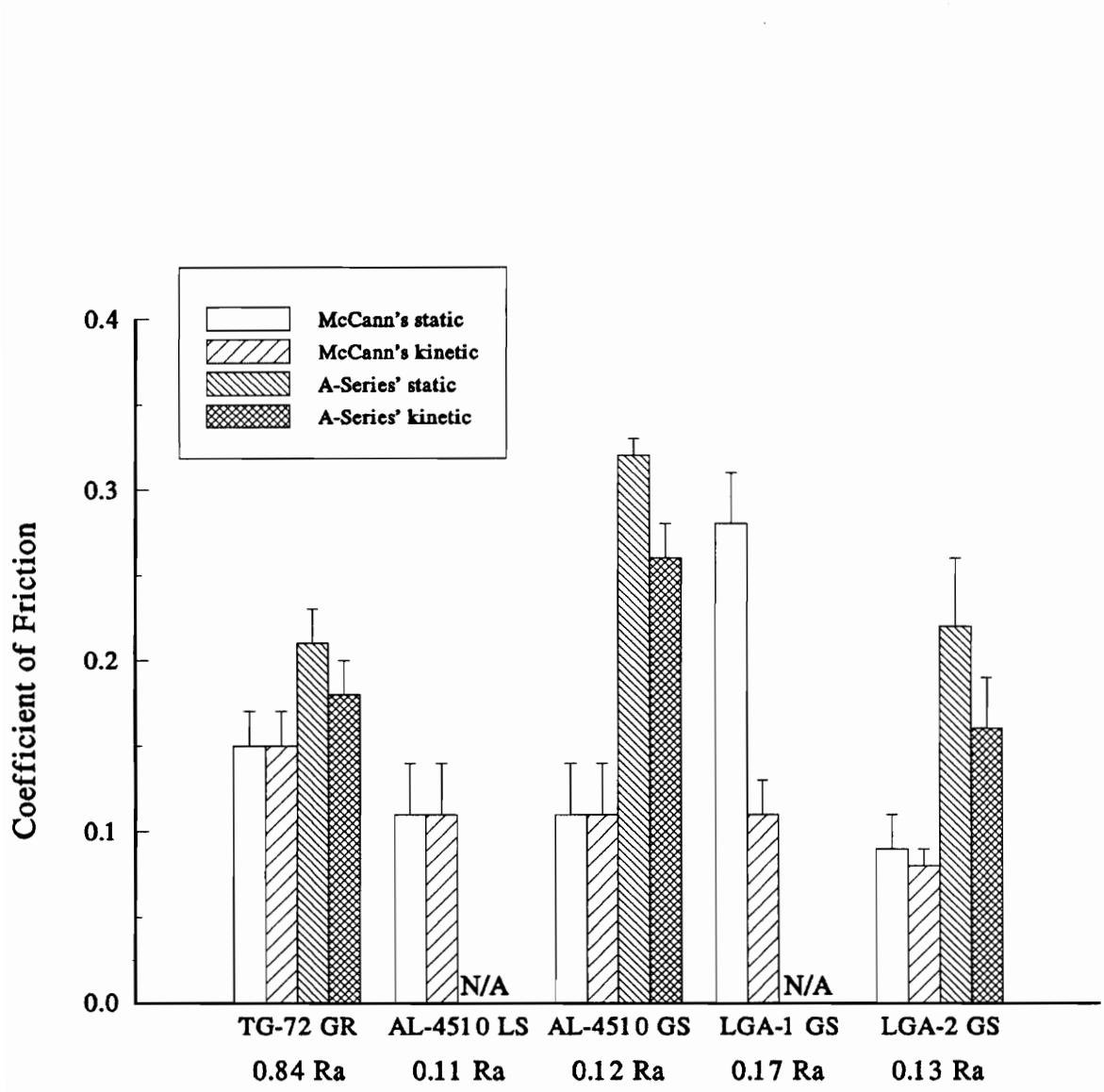

Figure 4.8 - Comparison of A-series results with McCann's results, 10 N load.

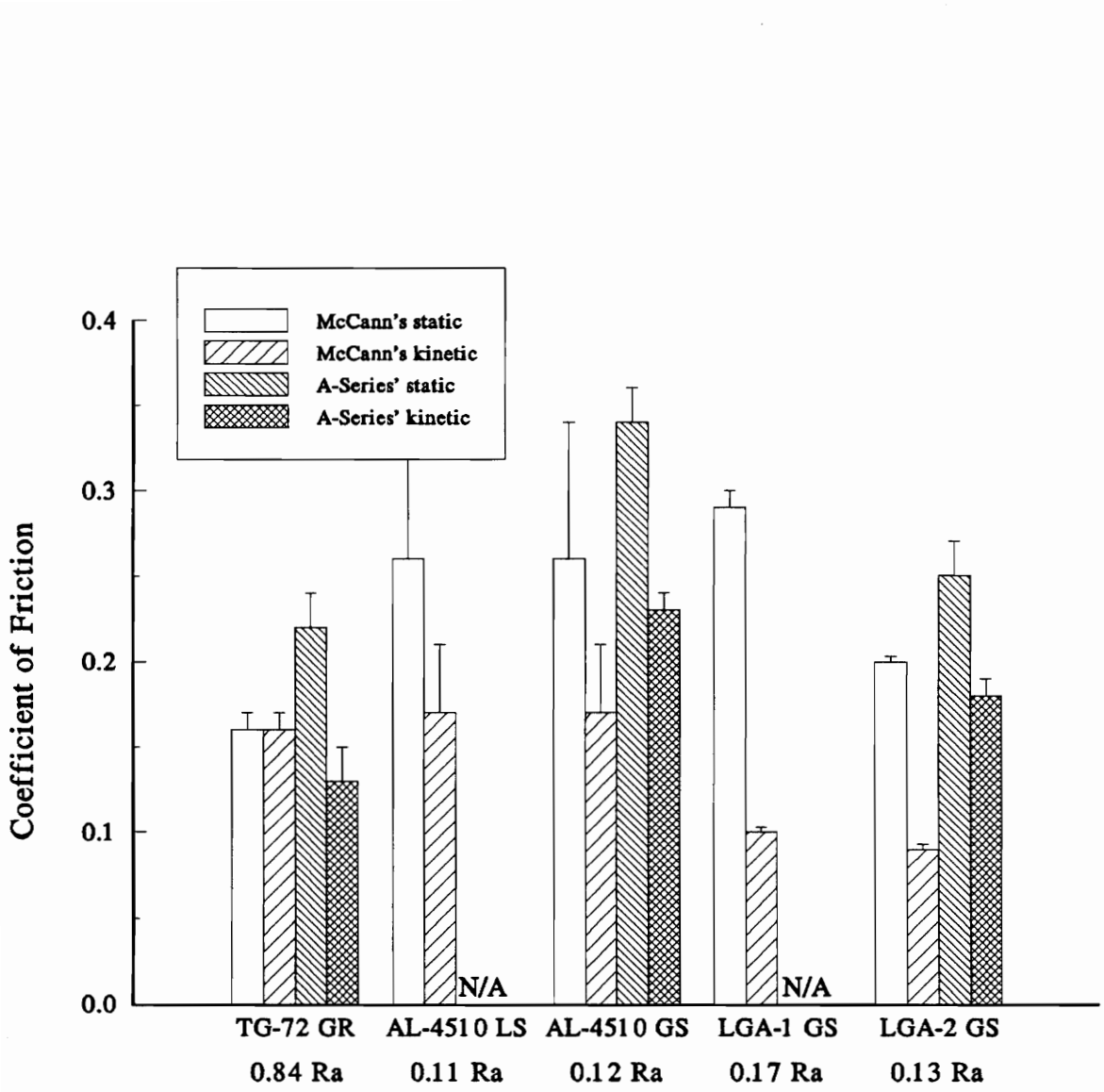

Figure 4.9 - Comparison of A-series results with McCann's results, 20 N load.

starts. In Figure 4.7 and 4.8, the A-series results show that a drop in friction force occurs for all materials tested, while McCann's results show no difference in the static and kinetic friction force (except LGA-1 10 N). Also, for rough surfaces at all loads, McCann's results show no difference in the static and kinetic friction force and concluded that rough surfaces should not produce a noise problem. The rough surfaces for the A-series tests, at all loads, exhibit a difference in the static and kinetic friction force.

There is one very important similarity between McCann's data and the A-series data. The Polypropylene samples yield little or no difference in the static and kinetic friction force at all loads and surface combinations (see Figure 4.4 and 4.10 [1]).

To investigate the differences between McCann's results and the A-series results, the injection molded samples were tested on the "improved" test apparatus (B-series).

The B-series results match the A-series results much more closely than McCann's results at 5, 7.5, and 10 N loads (See Figure 4.11-4.13). For 15 and 20 N loads the B-series' kinetic coefficients of friction match the A-series' μ_k much more closely than McCann's μ_k (Figure 4.14 and 4.15). But, for 15 and 20 N loads no conclusions can be made about the static coefficients of friction as to which set of results match the B-series results more closely. This will be discussed further in section 5.2.

4.2 Rise in Friction Force

It was also found in the B-series results that sometimes the friction force increased gradually after the first slip; in some cases μ_k was greater than or equal to μ_s (Figure

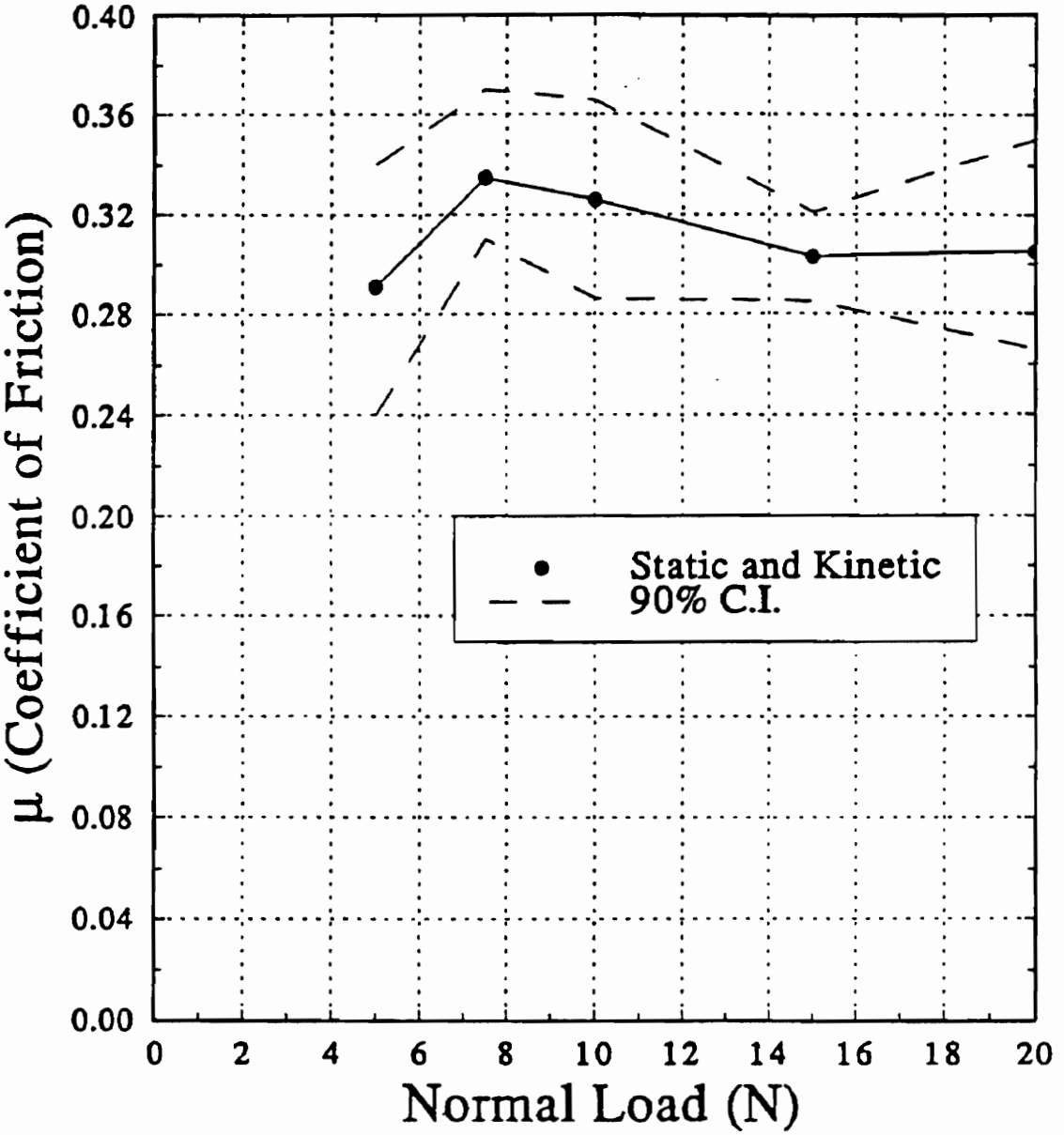

Figure 4.10 - Coefficient of friction vs. normal load for Polypropylene, with 90% confidence intervals. [1]

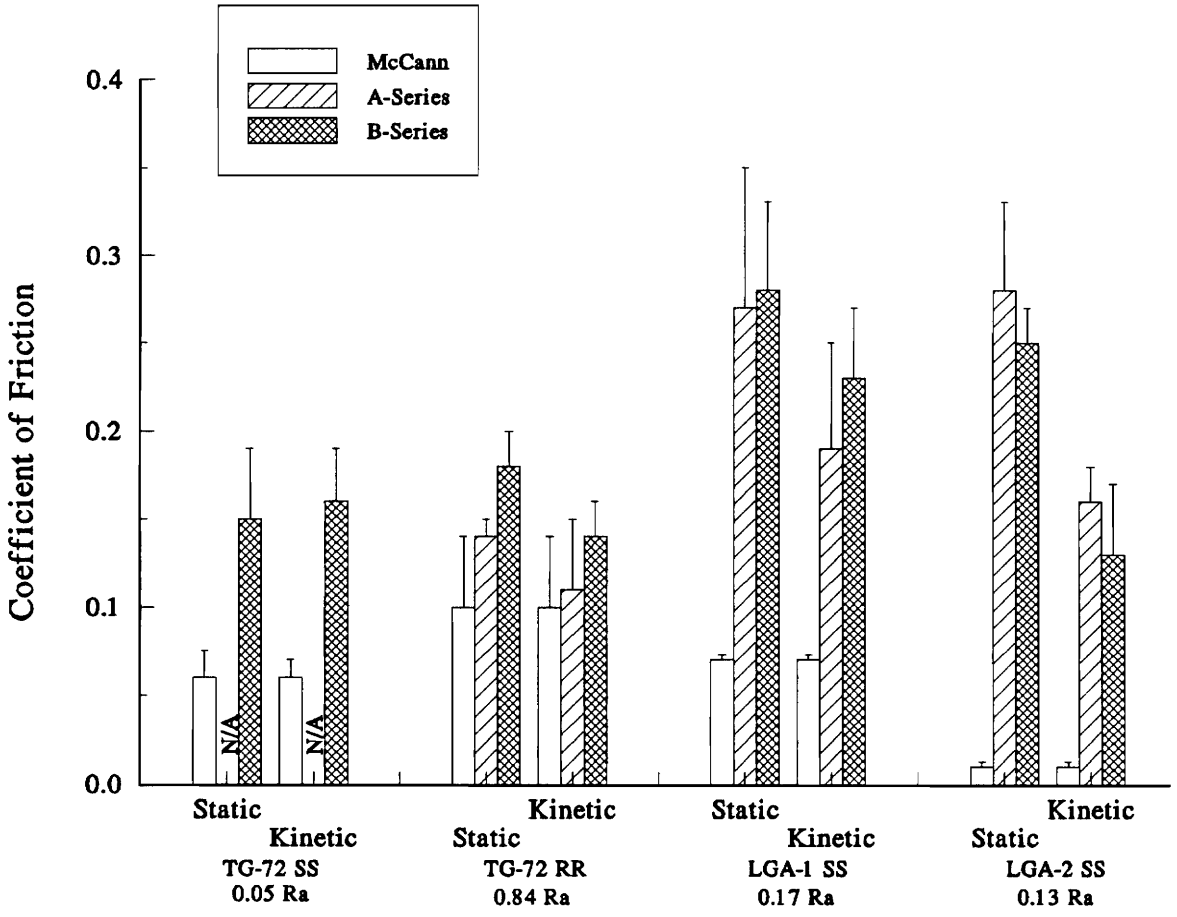

Figure 4.11 - Comparison of A-series, B-series, and McCann's results, 5 N load, with error bars.

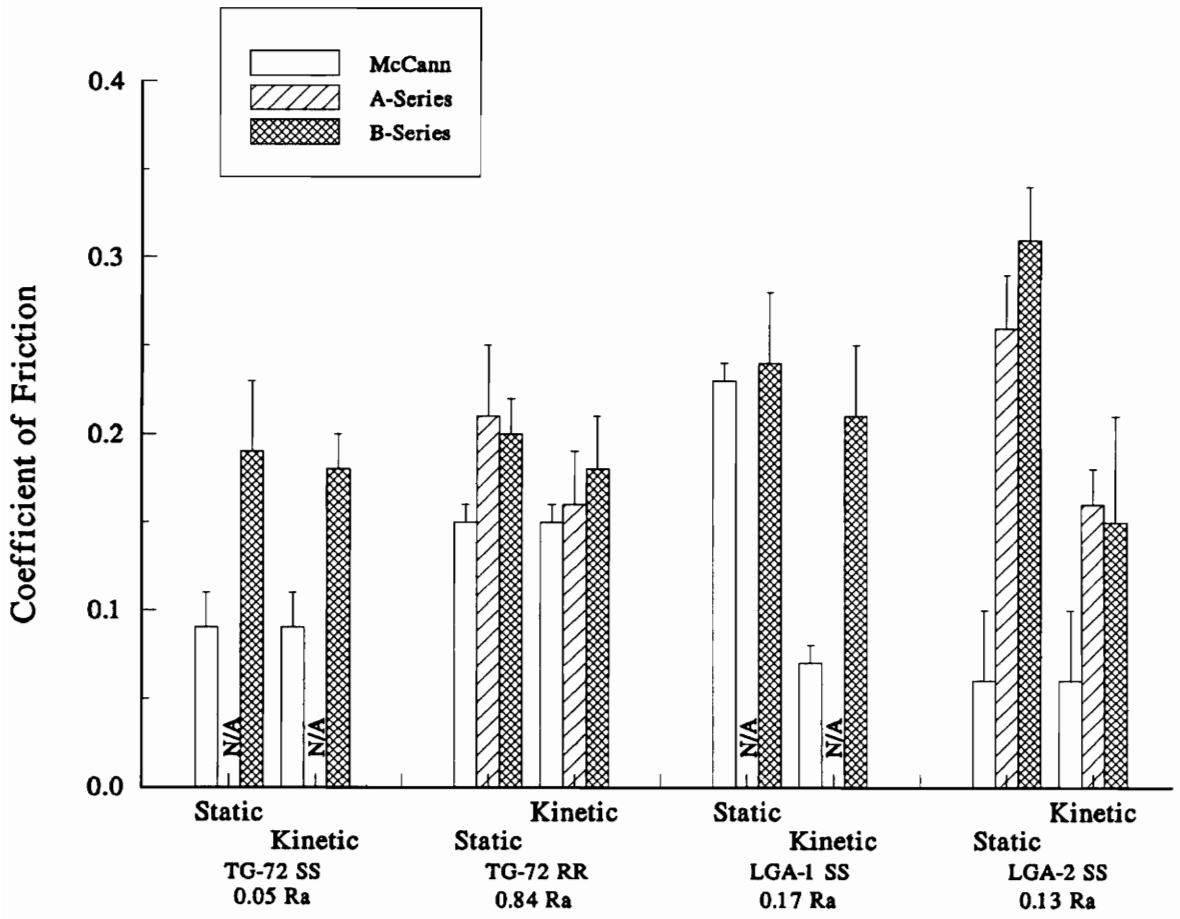

Figure 4.12 - Comparison of A-series, B-series, and McCann's results, 7.5 N load, with error bars.

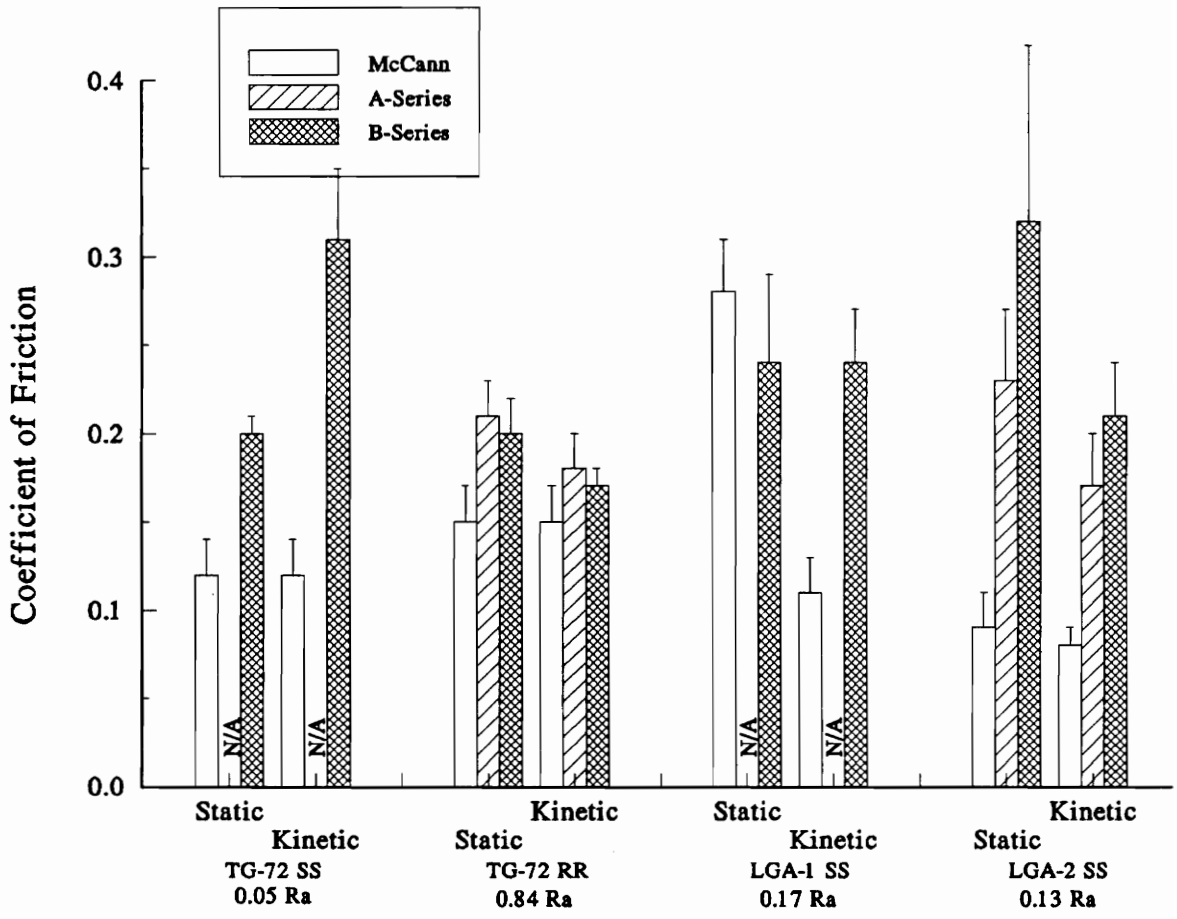

Figure 4.13 - Comparison of A-series, B-series, and McCann's results, 10 N load, with error bars.

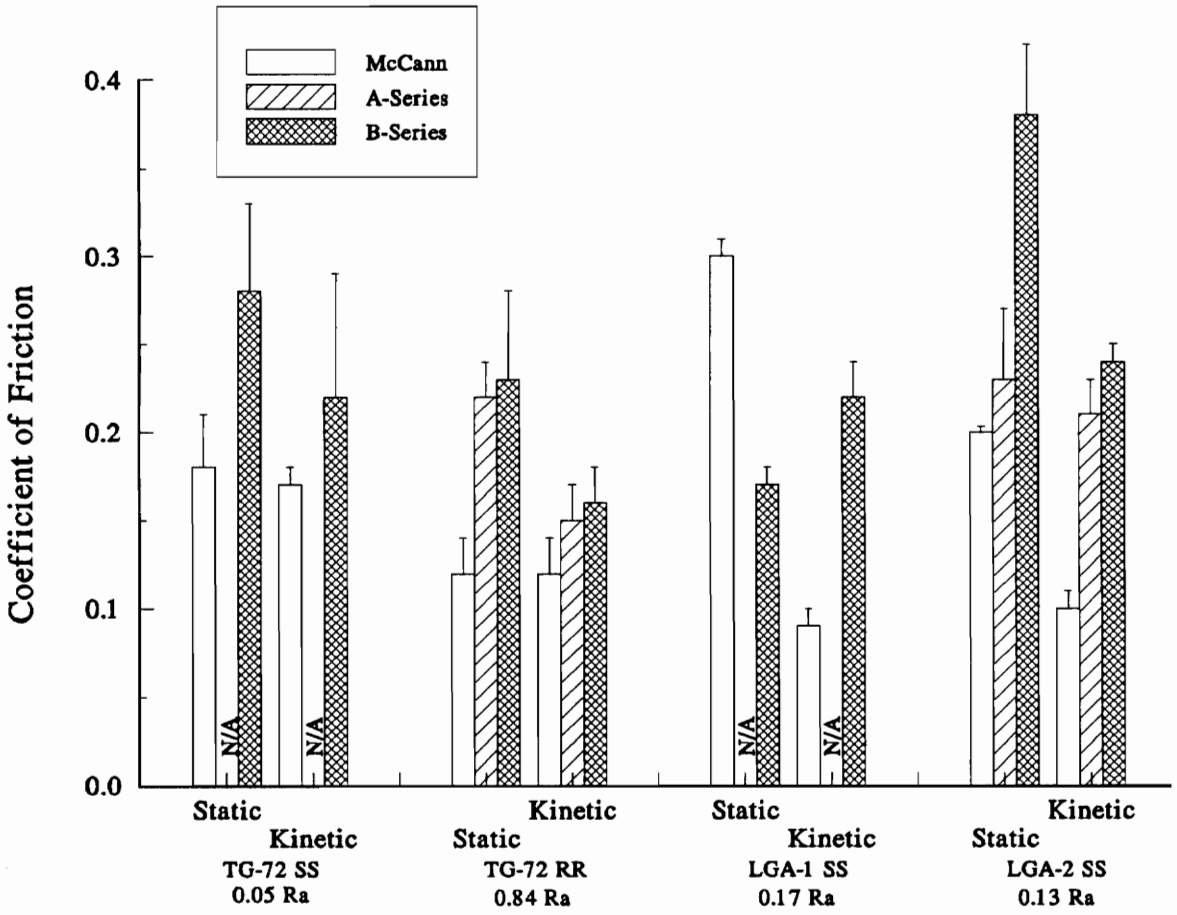

Figure 4.14 - Comparison of A-series, B-series, and McCann's results, 15 N load, with error bars.

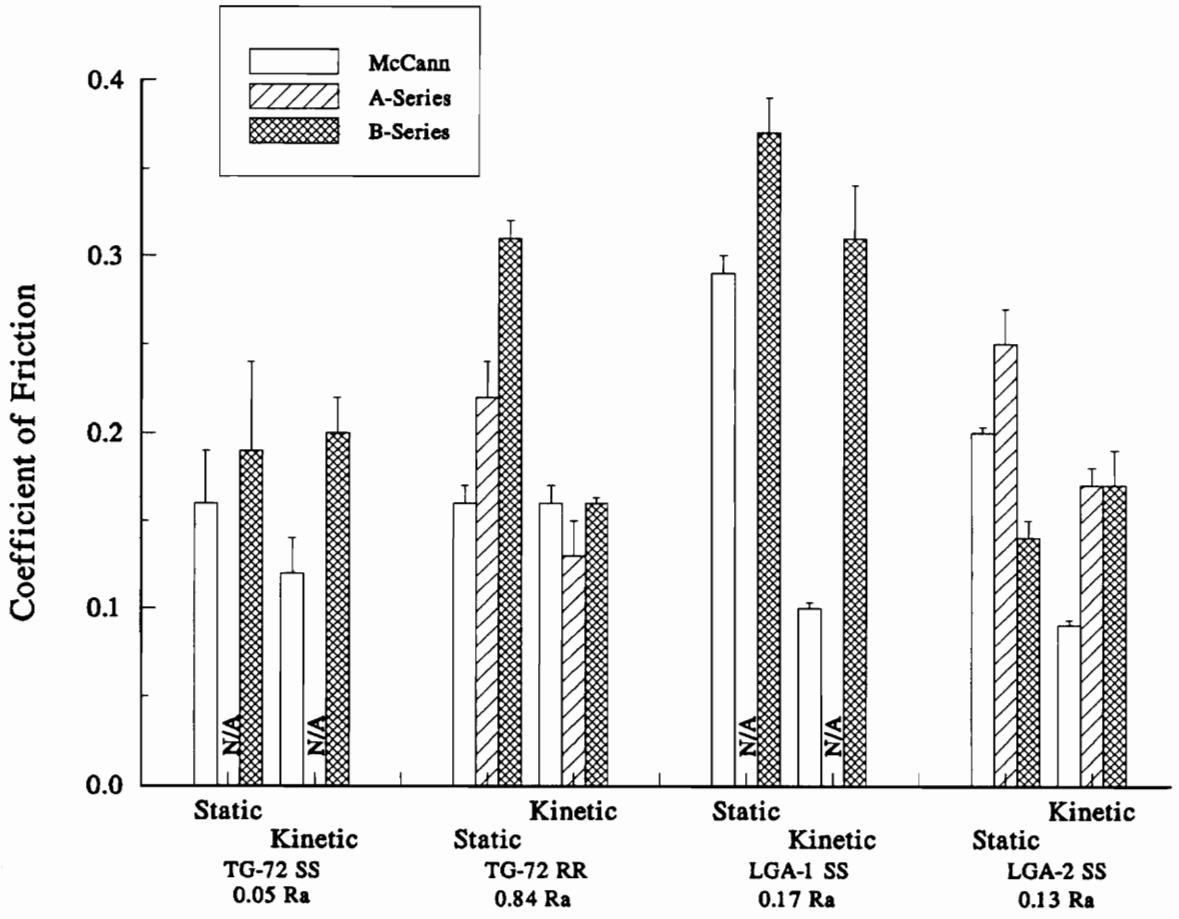

Figure 4.15 - Comparison of A-series, B-series, and McCann's results, 20 N load, with error bars.

4.16). A catalog of friction-time data was assembled relating frictional behavior to materials and roughnesses (Table 4.1). No definitive conclusions could be made. The only consistent behaviors observed were that LGA-1 and LGA-2 had repeated stick-slip, while TG-72 had mostly single stick. And that smooth surfaces exhibited stick-slip more often than the rough surfaces. A relationship could not be found between surface conditions (materials, roughnesses, and loads) and the behavior of μ_k being greater than μ_s.

4.3 Testing For Plastic Deformation

It is thought that if the plastic deformation of a surface interface is small compared to the elastic deformation, then the adhesion component of friction dominates the friction forces. The importance of plastic vs. elastic deformation of the samples prompted an investigation of the normal deflection under load. The deflection was measured using the pin-on-disk apparatus and the normal displacement sensor. Figure 4.17 illustrates how the plastic vs. elastic deflection was estimated. Since the sensor measures the relative displacement between the pin sample and the cantilever beam, the deflection of the beam had to be subtracted out. The deflection of the beam was found by loading the steel ball on the end of the pin against the steel platform. The deflection of the steel ball is nearly 100% elastic and can be calculated using Hertzian contact equations and turned out to be very small. The beam deflection (δ_{beam}) was equal to the total deflection measured by the sensor minus the calculated deflection of the steel ball.

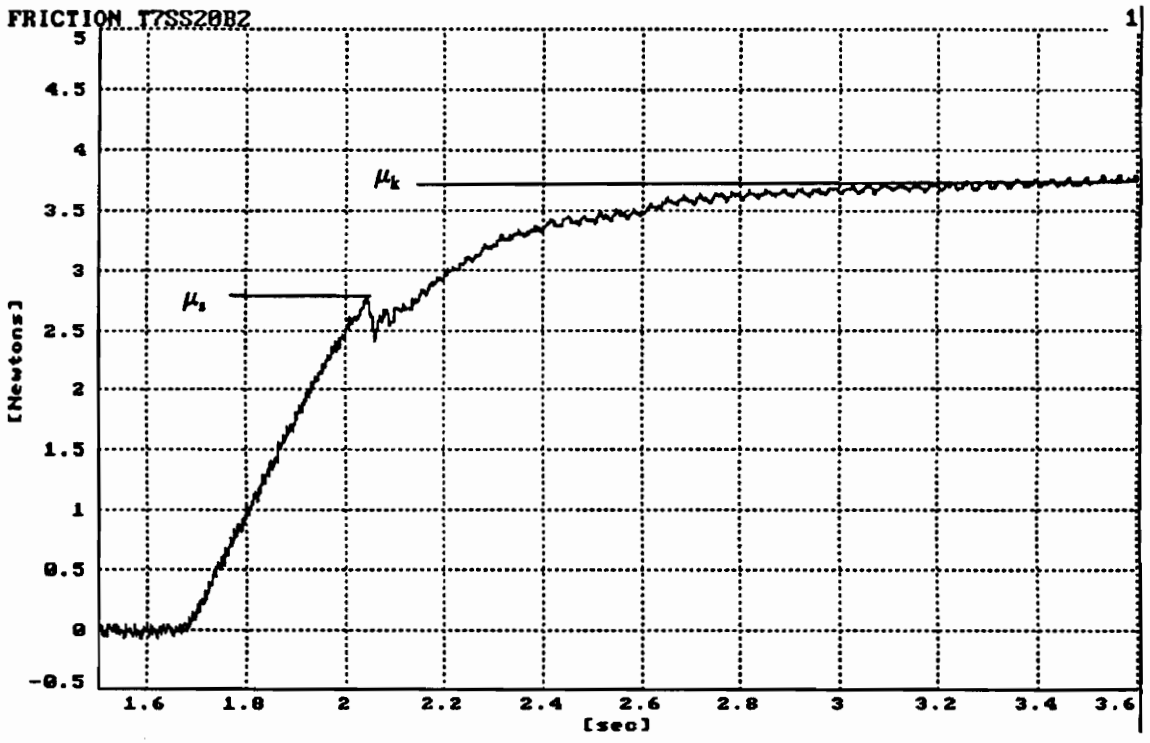

Figure 4.16 - Example of a friction signal showing $\mu_k > \mu_s$.

Table 4.1 - A catalog of frictional behaviors, A-Series (Clamped), B-Series

		Single-Stick		Stick-Slip		Steady Sliding	
μ_k increases	$\mu_k < \mu_s$	L1SS05B L2LL10A L2GG05A L2SS05B PPGG75A 10A T3GG75A	T7RR05A 75A 10A 15A T7GG75A 10A 20A	A4GG10A L1LL05A 75A 10A 15A 20A L1SS75B 10B 20B	L2LL75A 10A 15A 20A L2GG05A 75A 10A 15A 20A T7RR05A T7SS15B		
	$\mu_k = \mu_s$	T3GG75A 20A T7RR05B 75B 10B	T7SS05B 75B	A4GG05A L1SS75B 10B L2GG15A L2LL15A			
	$\mu_k > \mu_s$	T3GG15A 20A T7GG20A T7RR75B 10B	T7SS05B 10B 20B	L2LL20A L2SS20B L1SS10B 15B T7SS10B			
μ_k constant		L1LL05A L2GG05A L2LL05A L2SS05B PPGG05A PPLL75A 10A T3GG05A 75A 10A 20A	T7GG05A 10A 15A T7RR05A 15A 20A T7RR05B 75B 10B 15B 20B T7SS75B 15B	A4GG05A 75A 10A 15A 20A L1LL05A 75A 20A L1SS20B	L2LL75A 10A L2GG75A 15A 20A L2SS75B 10B 15B T3GG05A T7SS20B	PPLL05A 75A 10A 15A 20A PPGG05A 75A 10A 15A 20A	T3GG10A 15A T7RR10A T7RR10B T7GG05A T7SS05B 20B
μ_k decreases						PPLL05A 15A 20A PPGG05A 75A 10A 15A T3GG15A	

Test I.D. Code-- Materials-- A4 : AL-4510, L1 : LGA-1, L2 : LGA-2, PP : Polypropylene, T3 : TG-38, T7 : TG-72
Surface-- LL : Lapped, GG : Ground Smooth, RR : Ground Rough, SS : Smooth
Load-- 05 : 5 N, 75 : 7.5 N, 10 : 10 N, 15 : 15 N, 20 : 20 N

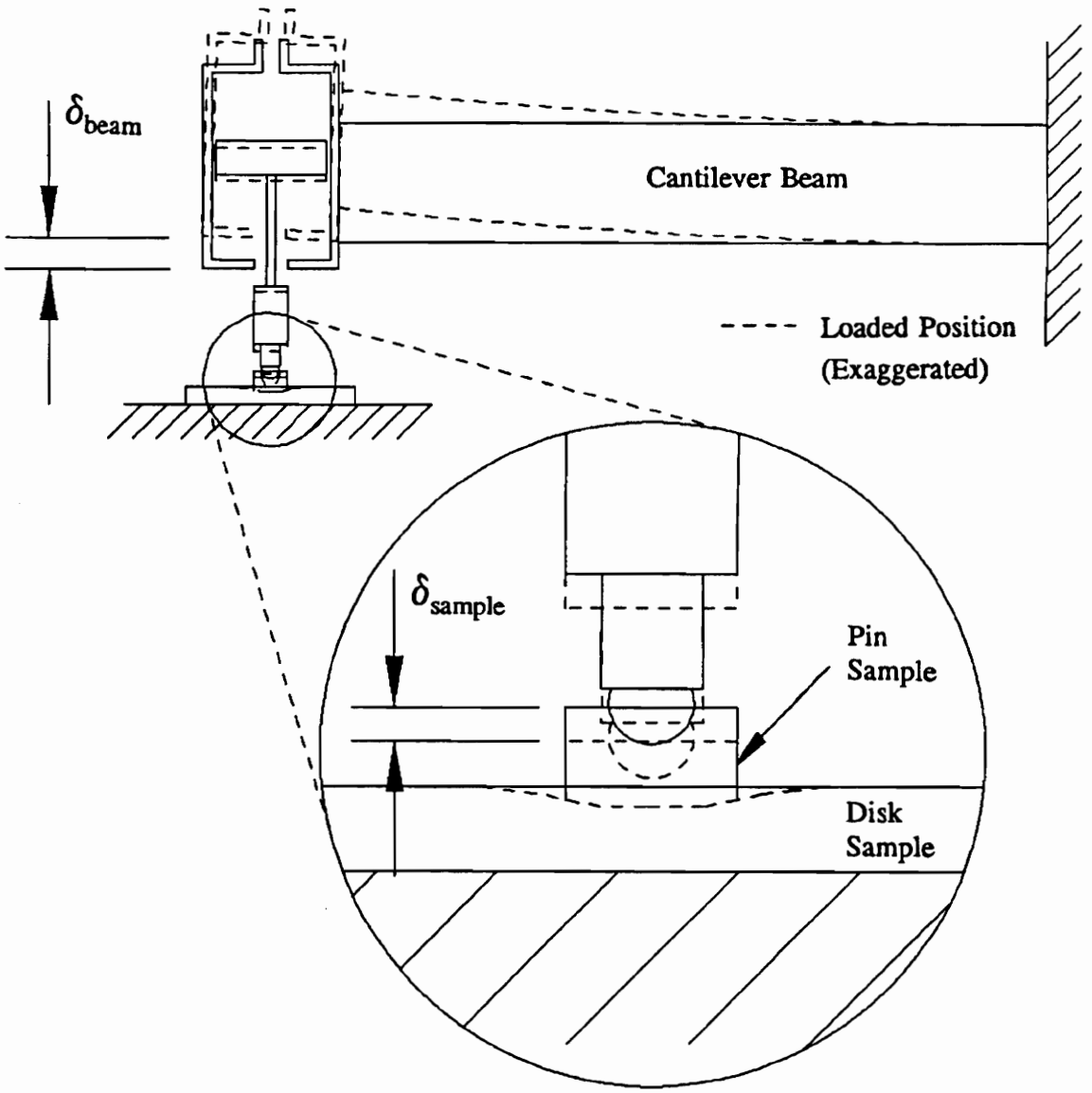

Figure 4.17 - Detailed view of the apparatus used to find the extent of plastic deformation of the samples.

The beam deflection was about 80 μm under a 20 N load and about 35 μm under a 10 N load.

The injection molded samples of TG-72 were used to estimate the extent of plastic deformation in the ABS samples. Two surface interactions were measured: Rough-on-Rough and Smooth-on-Smooth. First, the samples were put on the apparatus and a zero deflection reading was taken from the wear sensor. Then a normal load was applied to the samples through the pneumatic cylinder. Another reading was taken from the sensor and subtracted from the zero deflection reading. This was equal to the total deflection (δ_{total}). The deflection of the samples was equal to the total deflection minus the beam deflection: $\delta_{sample} = \delta_{total} - \delta_{beam}$. Next, the samples were unloaded and another reading was taken from the sensor and subtracted from the zero deflection reading. This was equal to the deflection which was not recovered by the sample and therefore was defined as the plastic deformation ($\delta_{plastic}$). The elastic deformation is equal to the sample deformation minus the plastic deformation: $\delta_{elastic} = \delta_{sample} - \delta_{plastic}$. Then as a check, the samples were loaded again without moving the samples at all. This time the plastic deformation should have been zero and the elastic deformation should have been the same. As shown in Table 4.2, this was nearly the case. The extent of plastic deformation was found in terms of a percentage using the following equation:

$$\% \text{ plastic deformation} = (\delta_{plastic}/\delta_{sample}) \times 100$$

For rough surfaces, the deflection is about 31% plastic under a 20 N load and 22% plastic under a 10 N load. For smooth surfaces, the deflection is about 26% plastic

for a 20 N load. This means that most of the deflection is elastic; therefore, friction components which result from plastic deformation will be overshadowed by the other friction components. Hence, the viscoelastic deformation below the surface along with the adhesive component of friction will dominate the friction forces. Further discussion can be found in the next chapter.

Table 4.2 - Extent of plastic deformation

			Deflection (μm)			
Surface	Load (N)	Application	δ_{sample}	$\delta_{plastic}$	$\delta_{elastic}$	% Plastic Deformation
Rough	20	First	61	19	42	31
Rough	20	Second	43	3	40	
Rough	10	First	27	6	21	22
Rough	10	Second	20	-1	21	
Smooth	20	First	62	16	46	26
Smooth	20	Second	47	2	45	

The Talysurf 4 was used to "look" at the surface profile before and after the tests. The plastic deformation of asperities was barely detectable.

4.4 Friction-Velocity Tests

Some friction-velocity tests were run with the injection molded samples on the

improved test apparatus. The materials (TG-72 Rough-on-Rough and LGA-1) were tested under a 15 N load at forced velocities of 0.0005, 0.001, 0.0027, 0.0079, and 0.03 m/s. Both the static and kinetic friction force were recorded. As shown in Figure 4.18 and 4.19, both the static and kinetic friction force seem to have the same relationship with velocity. The shapes of the curves are similar to those obtained by McCann, specifically the sharp drop in friction force near zero velocity followed by a rise in friction force with increasing velocity.

4.5 New Test Apparatus

Figure 4.20 shows the friction and velocity signals vs. time for a preliminary friction test taken with the new test apparatus. Test conditions were: load = 13 N, steel-on-ABS plastic, velocity = 0.0025 m/sec. Notice the friction force during the first slip is relatively constant from point C to D. Also notice the rise in friction force after the first slip from point E to F.

As is seen by the stick phase (from A to B) of the friction force signal, it appears that the friction force is not rising at a constant slope. This could be caused by the actuator not moving at a constant velocity. One might be tempted to look at the stick phase of the velocity signal and conclude that the velocity is constant, but this is the velocity of the sample not the velocity of the actuator. Subsequent to this test the actuator was hooked up directly to the L.V.T. and it was determined that the end of the actuator was not moving at a constant velocity. When the stepper motor was chosen for

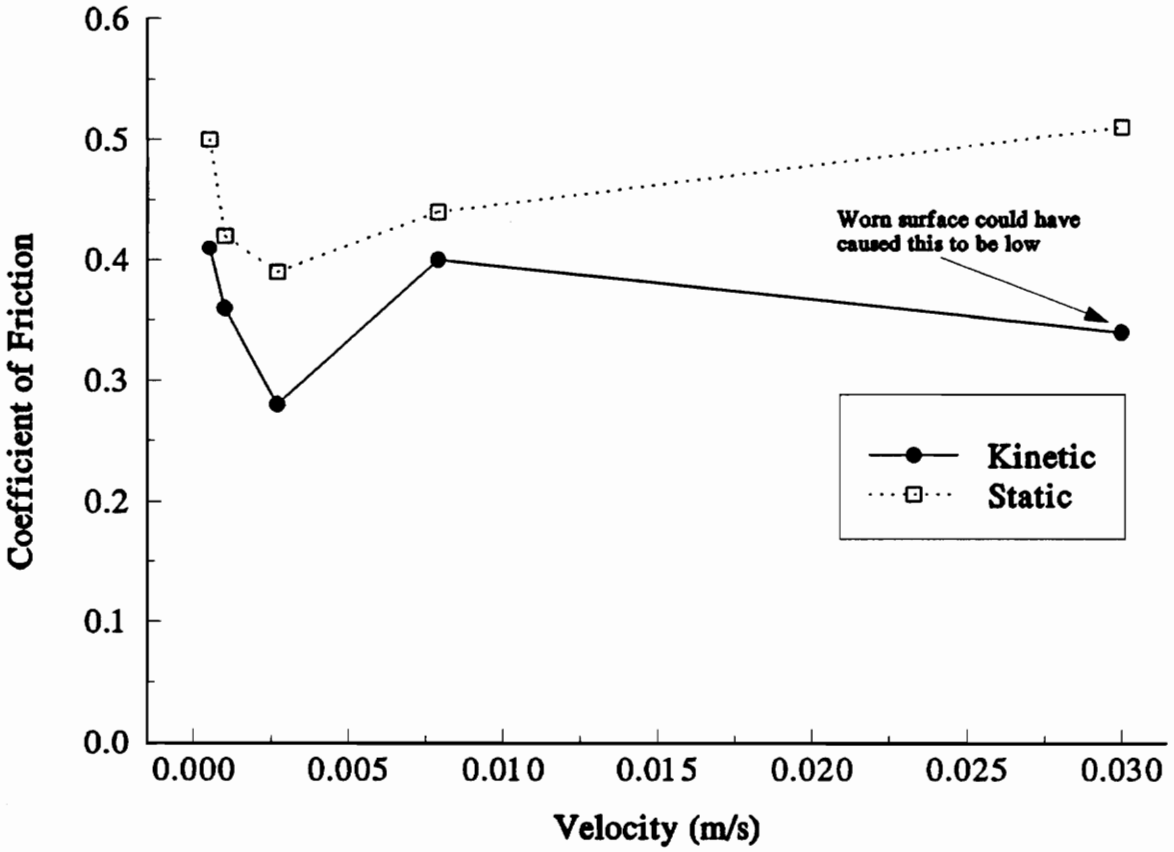

Figure 4.18 - Friction vs. velocity for TG-72, 15 N load, Smooth (0.05 μm R_a), B-series.

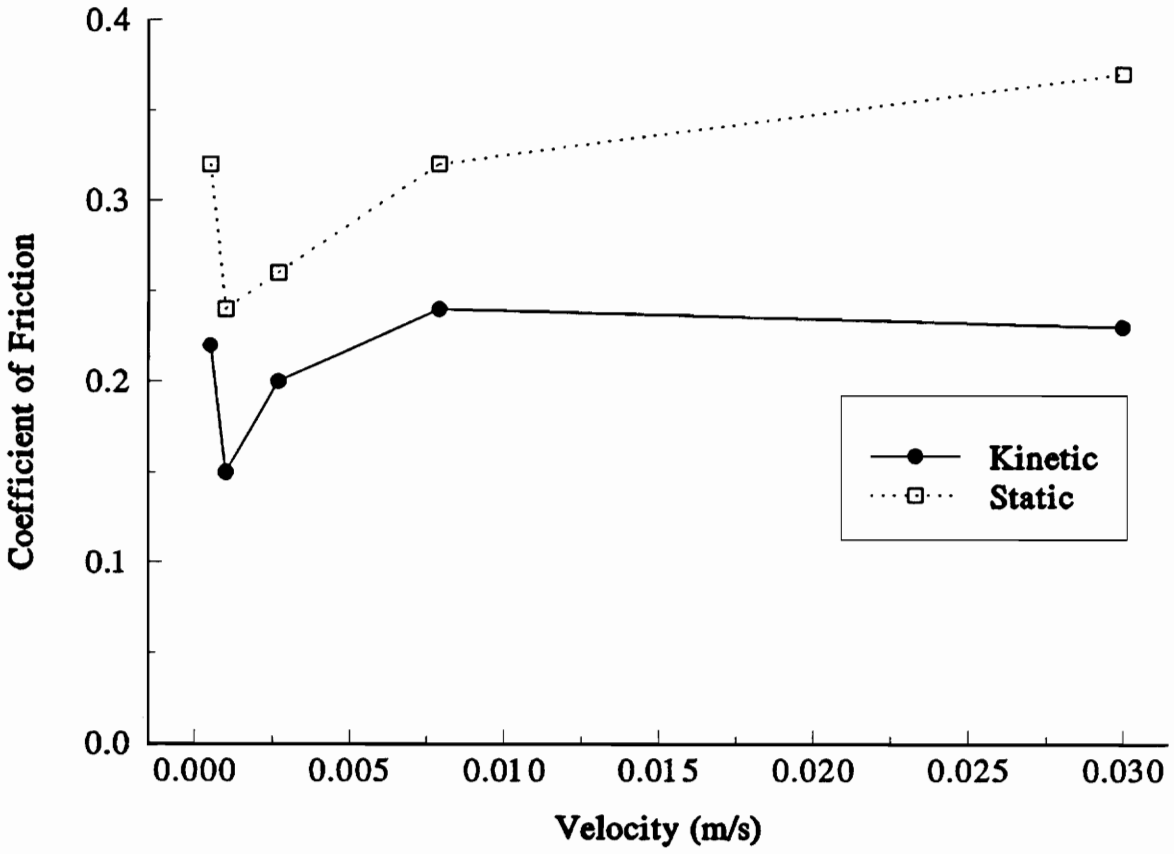

Figure 4.19 - Friction vs. velocity for LGA-1, 15 N load, Smooth (0.18 μm R_a), B-series.

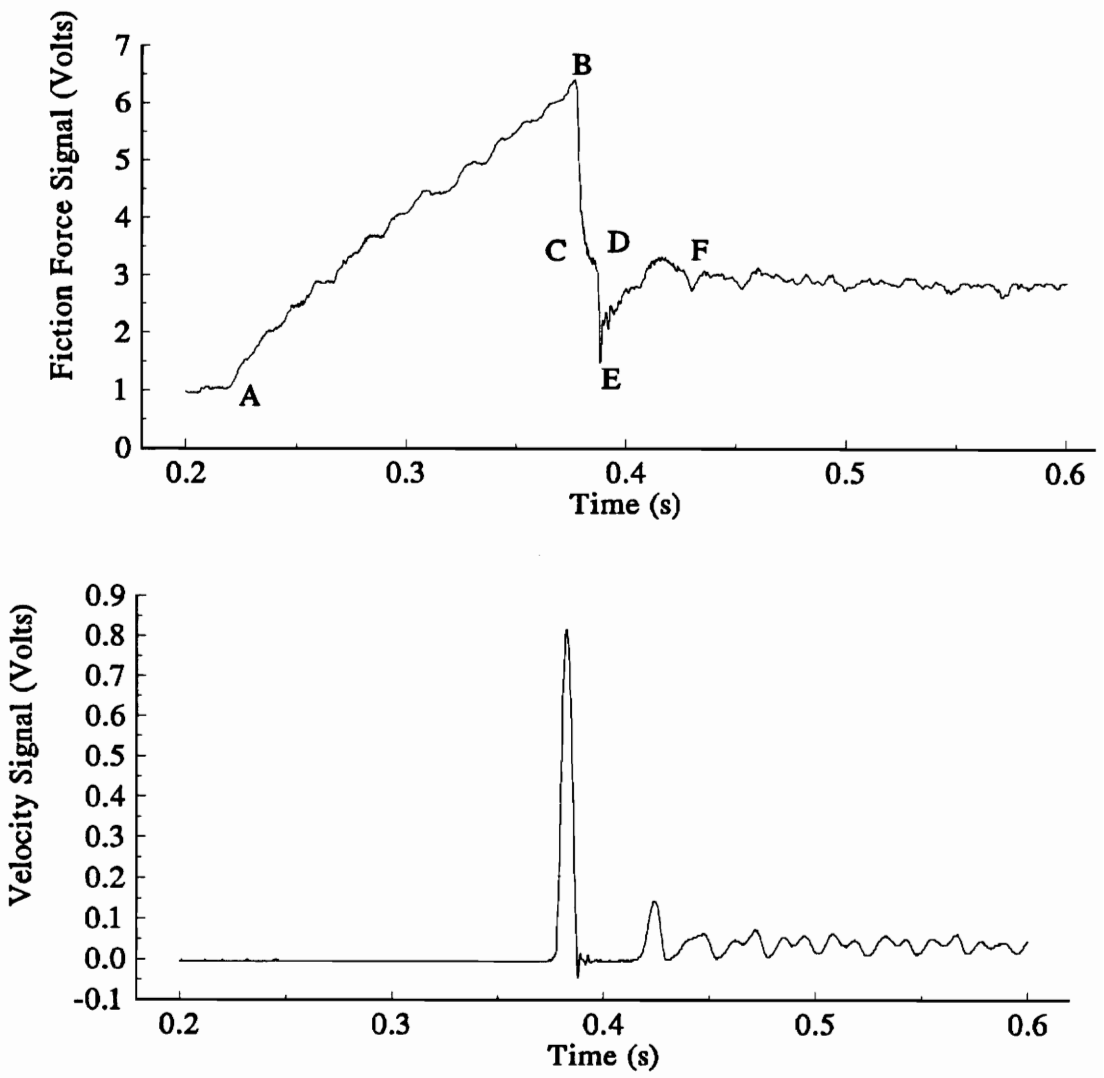

Figure 4.20 - Friction and relative velocity vs. time signals obtained with new test apparatus, 13 N load, steel-on-ABS plastic, V_{forced} = 0.0025 m/s.

this application, it was thought that the actuator would move at constant velocity despite the stepping action of the motor. It was anticipated that the mass of the actuator cylinder would act as a mechanical filter and eliminate the high frequency variation due to the stepping (427 steps/second at 0.0025 m/sec). But this was not the case.

5.0 Discussion

In this chapter, the results are discussed while trying to gain a better understanding of what is actually happening with the friction force and friction mechanisms during the transition from static to kinetic conditions. First, a computer model is used to aid in the understanding of this transition. Specifically the model is used to investigate how the friction-velocity curve affects frictional behavior. The analytical results and the experimental results are used to formulate theories about the friction mechanisms. Next, the experimental results are discussed with respect to the unexplained variation in values of friction force and frictional behavior. The friction-velocity tests are discussed in section 5.3. Section 5.4 addresses some of the concerns associated with the testing position of the pin and disk samples. Section 5.5 discusses another peculiarity associated with the old test apparatus.

5.1 Computer Modeling

Raouf A. Ibrahim [22, 23] presents some very complex analytical models for the frictional behavior of sliding surfaces. In particular, he is concerned with friction

induced vibration and stick-slip behavior. The models cover multi-degree of freedom systems with damping, non-linearites, and chaos terms. Application of these models to the test apparati used in this study is beyond the scope of this thesis; however, a very simple analytical model was developed to gain a better understanding of what is happening during the transition from static to kinetic conditions.

5.1.1 The Models

A computer model was developed to simulate the friction characteristics of the polymer system. The Personal Simulation Language (PSL) software was used to model a one degree-of-freedom dynamic system. Both the old test apparatus and the new test apparatus could be modeled in this way. Figure 5.1 shows the two systems and the equations of motion. For the old test apparatus, it is assumed that the disk and the drive system are rigid and that V_{disk} is constant. For the new test apparatus, it is assumed that the force transducer is rigid and that $\dot{z}$ is constant. The block diagrams for the software input can be found in Appendix D. The variables of the systems are: the mass of the moving sample, the stiffness of the elastic member used to store energy, the input velocity, the static friction force, and the kinetic friction force as a function of relative velocity. The models use a fixed time step Runga-Kutta numerical solution.

For each time step the models pick a value of friction force based on the relative velocity. If the relative velocity is zero, the friction force equals the force in the spring or the static friction force, whichever is less. It is necessary to define a range of

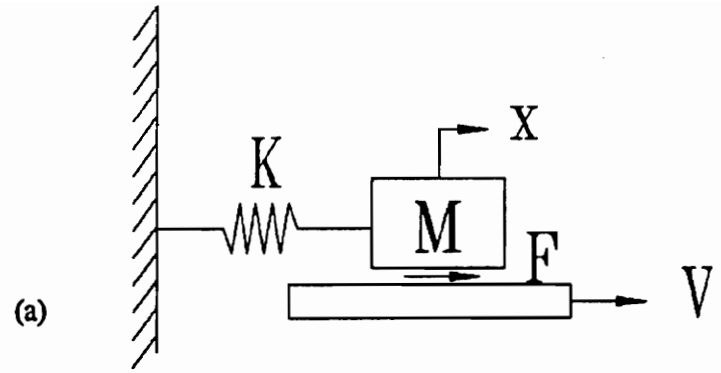

$$\ddot{x} = \frac{1}{M}(F - Kx)$$

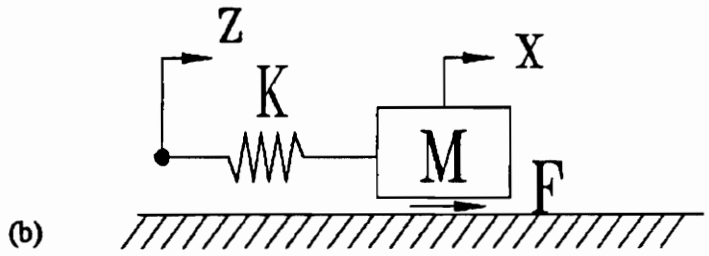

$$\ddot{x} = \frac{1}{M}(Kz - Kx + F)$$

Figure 5.1 - (a) Old test apparatus, single degree of freedom model and equation of motion (b) New test apparatus, single degree of freedom model and equation of motion.

velocities over which the velocity is considered to be zero (e.g. -1e-6 to 1e-6 m/s). If the relative velocity is not in this range then the friction force equals the kinetic friction force. The models pick the kinetic friction force value from the friction-velocity curve which is defined by the user. The range of relative velocities over which the kinetic friction force can be defined is unlimited; however, the value of friction force can only be defined at eleven discrete points (V_1,V_2, V_3, ...V_{11}) evenly distributed over the range in the function generator in PSL. The model will interpolate between points but if the velocity is above V_{11} then the friction force at V_{11} is used. If the velocity is below V_1 and above the velocity at which the static friction force takes effect then the friction force at V_1 is used.

5.1.2 Results

A variety of frictional behaviors resulted for a given set of system parameters simply by changing the shape of the kinetic friction force vs. velocity curve. These behaviors included stick-slip motion, steady sliding motion, and the gradual rise in friction force after the first slip.

The following graphs are examples of the output of the old test apparatus computer model with the following parameters: mass= 0.5 kg, k= 14000 N/m, F_{static}= 4.5 N, zero velocity= $1x10^{-6}$ m/s, v_{forced}= $0.5x10^{-3}$ m/s, and $F_{kinetic}$ at V_{forced}= 2.7 N. These parameters were chosen to simulate an actual test run with the improved apparatus (TG-72, Ground Rough-on-Ground Rough, 20 N). The range of velocities over which

the kinetic friction force is defined was chosen such that the forced velocity ($0.5x10^{-3}$ m/s) was in the center of the velocity range ($0.1x10^{-5}$ to $0.1x10^{-2}$ m/s). The shape of this kinetic friction vs. relative velocity curve was defined such that the output of the displacement of the mass, X, matched the actual test. Figure 5.2a shows the actual friction test output. It is assumed that the fluctuations after the slip are due to the beam vibration and not the actual friction fluctuations (as in Figure 3.2). Figure 5.2b shows the output of the simulation including the friction force, which is what we tried to measure, and the displacement of the mass, which is what we actually measured. The computer model reveals the limitations of the improved apparatus. The improved apparatus can only record the displacement of the mass, X. With the new test apparatus it will be possible to obtain the friction force directly.

Next, the shape of the kinetic friction vs. relative velocity curve was changed slightly to see what effect it had on the output variables of the system during a friction test. The value of the kinetic friction at the forced velocity was set at 2.7 N for all simulations. The output parameters included the friction force at the interface, and the displacement, and velocity of the mass in Figure 5.1a. Figures 5.3a, 5.4a, and 5.5a are the input (kinetic friction vs. relative velocity curves) for the different simulations.

Figure 5.3a-d shows the effect of changing the smoothness of the friction-velocity curve. The fluctuations in the output parameters during sliding is sometimes called quasi-harmonic frictional behavior.

Figure 5.4a-d shows the effect of changing the kinetic friction force at higher

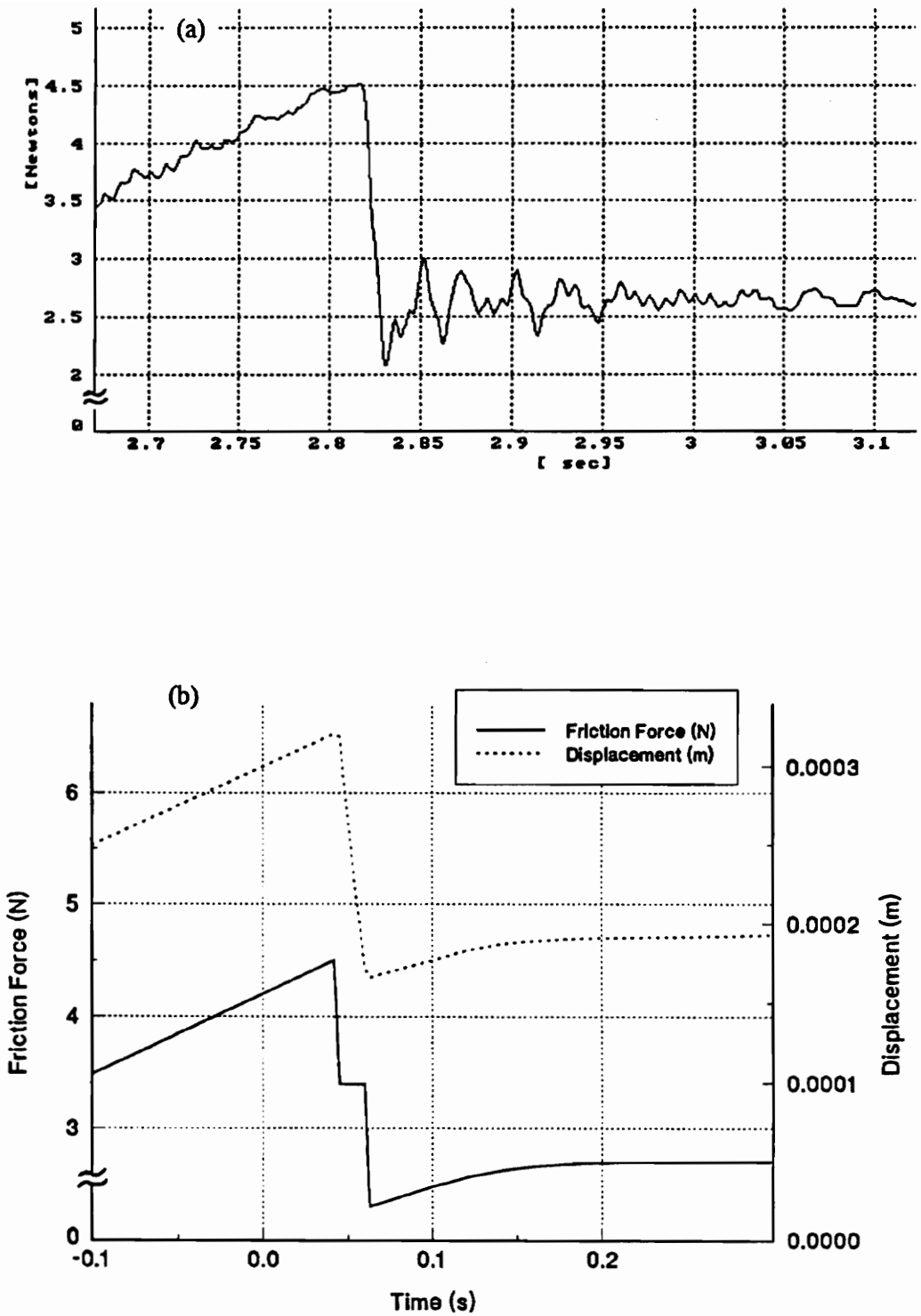

Figure 5.2 - (a) Actual friction test, TG-72, Ground Rough-on-Ground Rough, 20 N (b) PSL simulation.

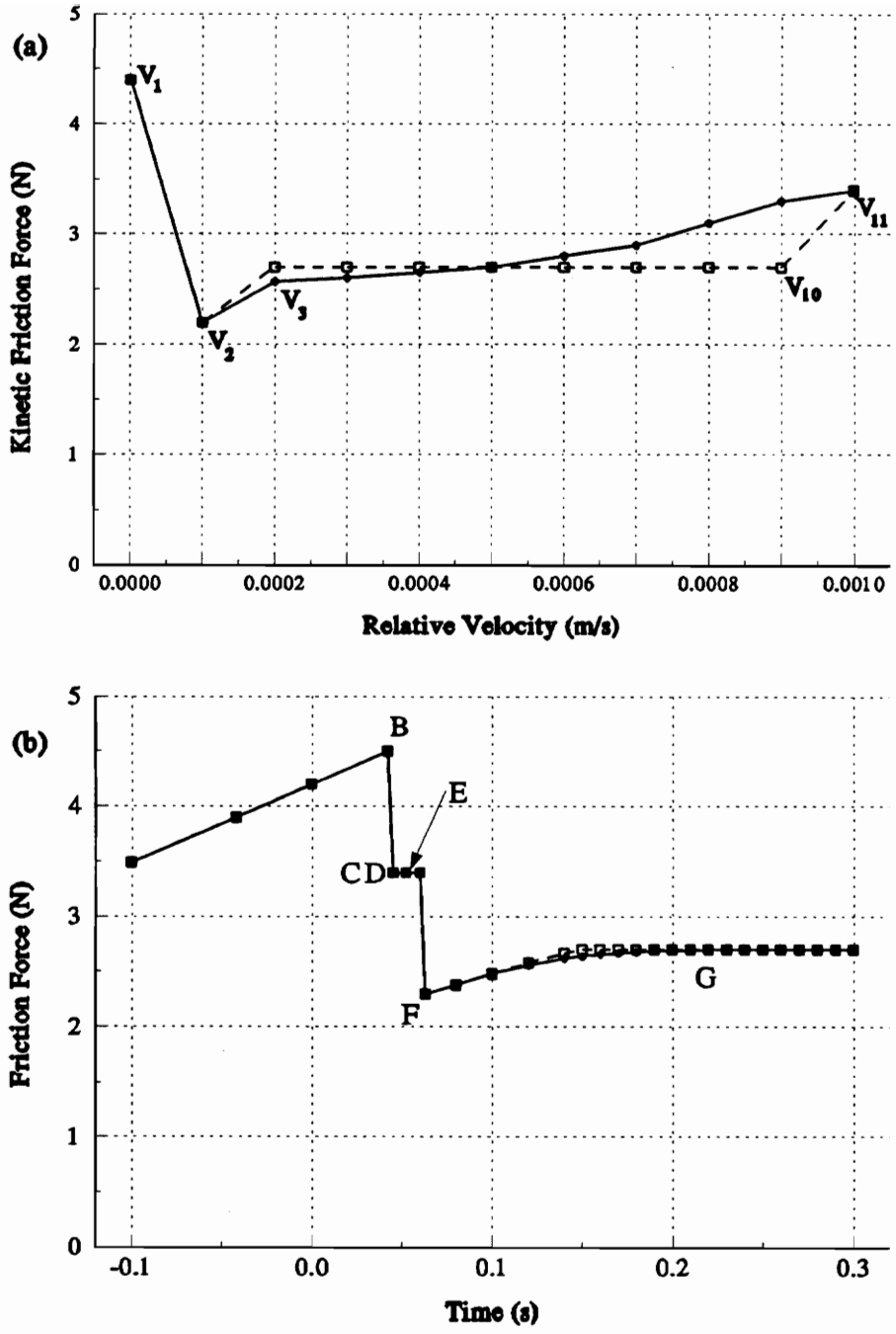

Figure 5.3 - PSL simulation, (a) kinetic friction vs. relative velocity, (b) friction force vs. time, effect of shape of F_k vs. V_{rel} curve.

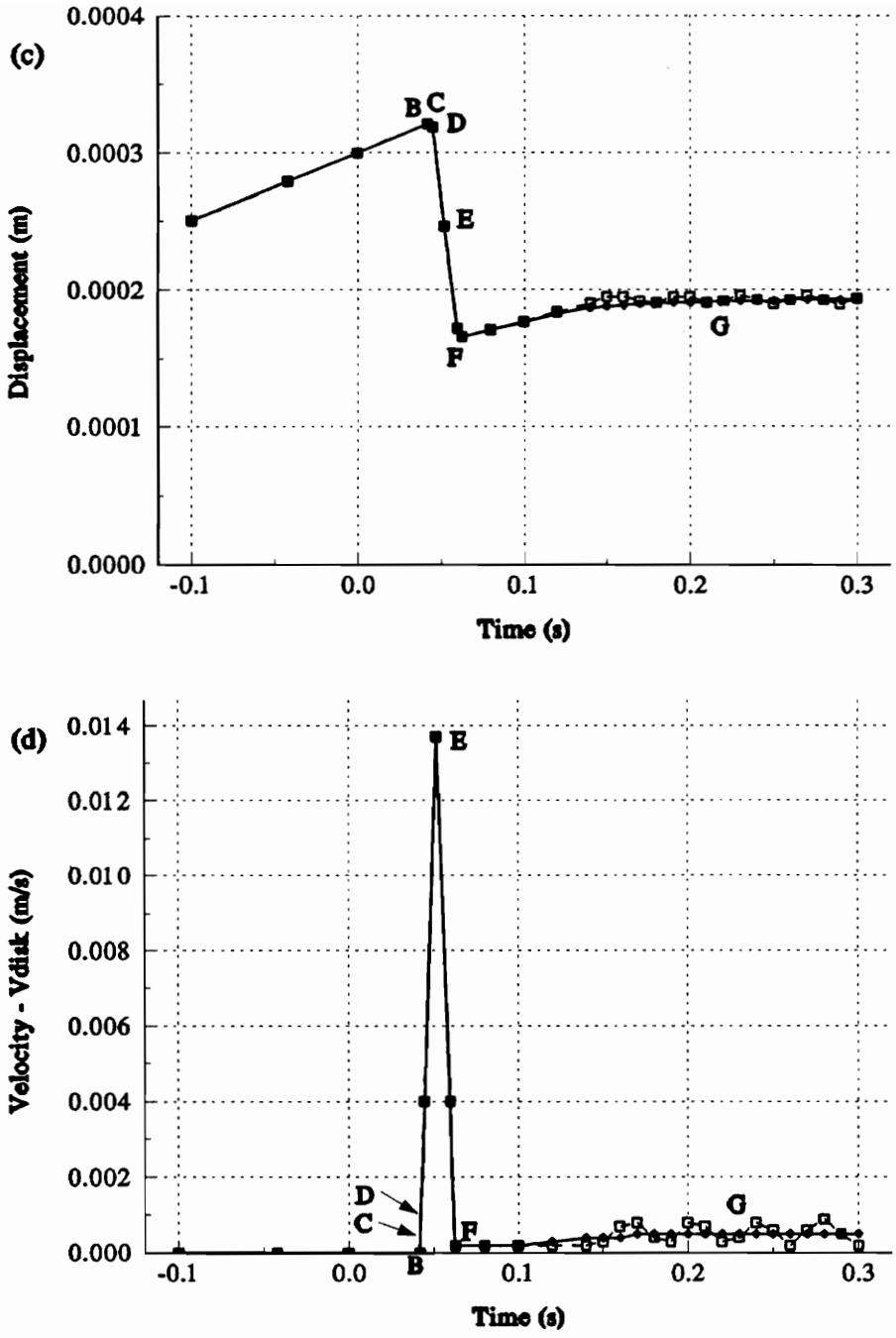

Figure 5.3 - PSL simulation, (c) displacement vs. time, (d) relative velocity vs. time, effect of shape of F_k vs. V_{rel} curve.

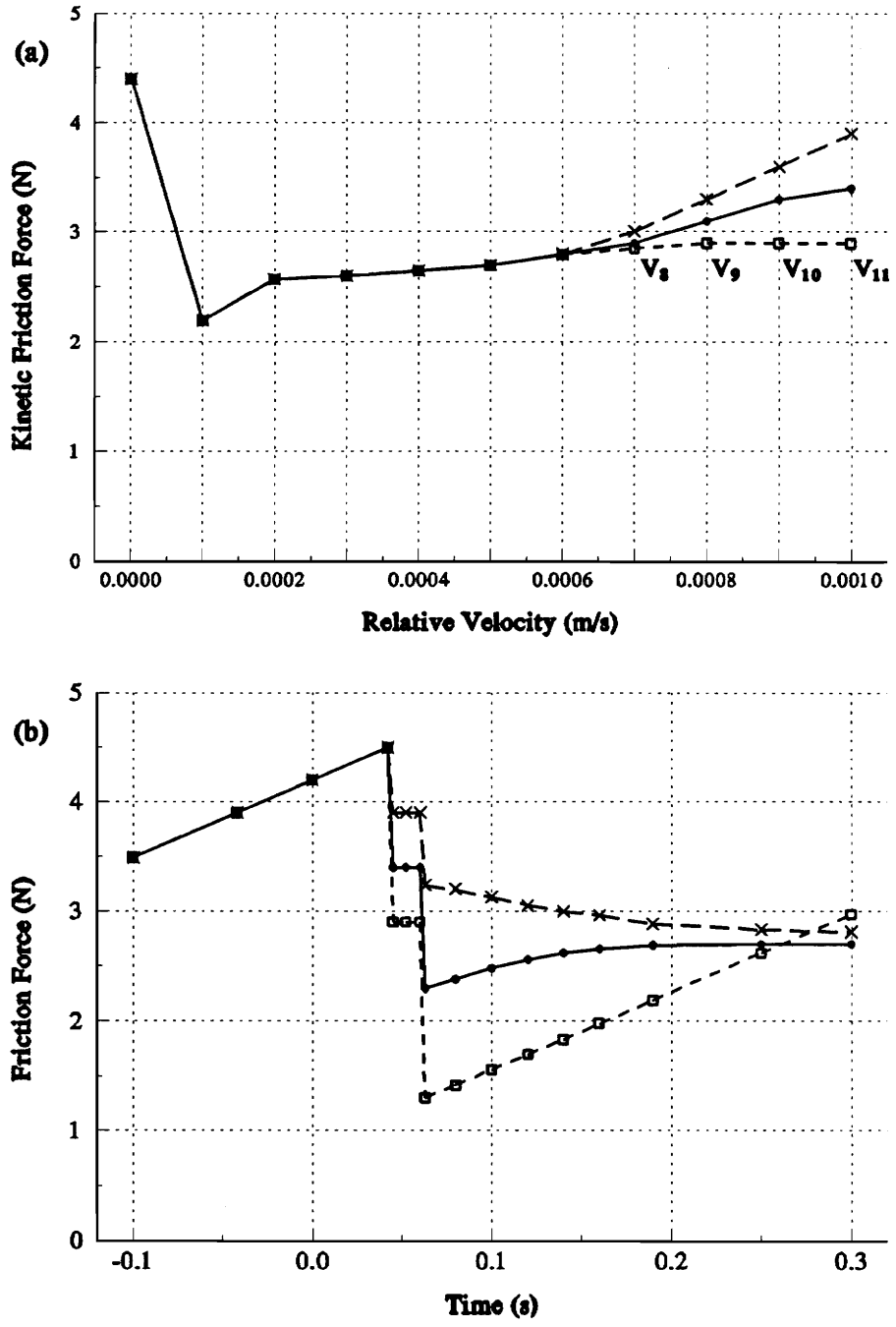

Figure 5.4 - PSL simulation, (a) kinetic friction vs. relative velocity, (b) friction force vs. time, effect of F_k at higher velocities.

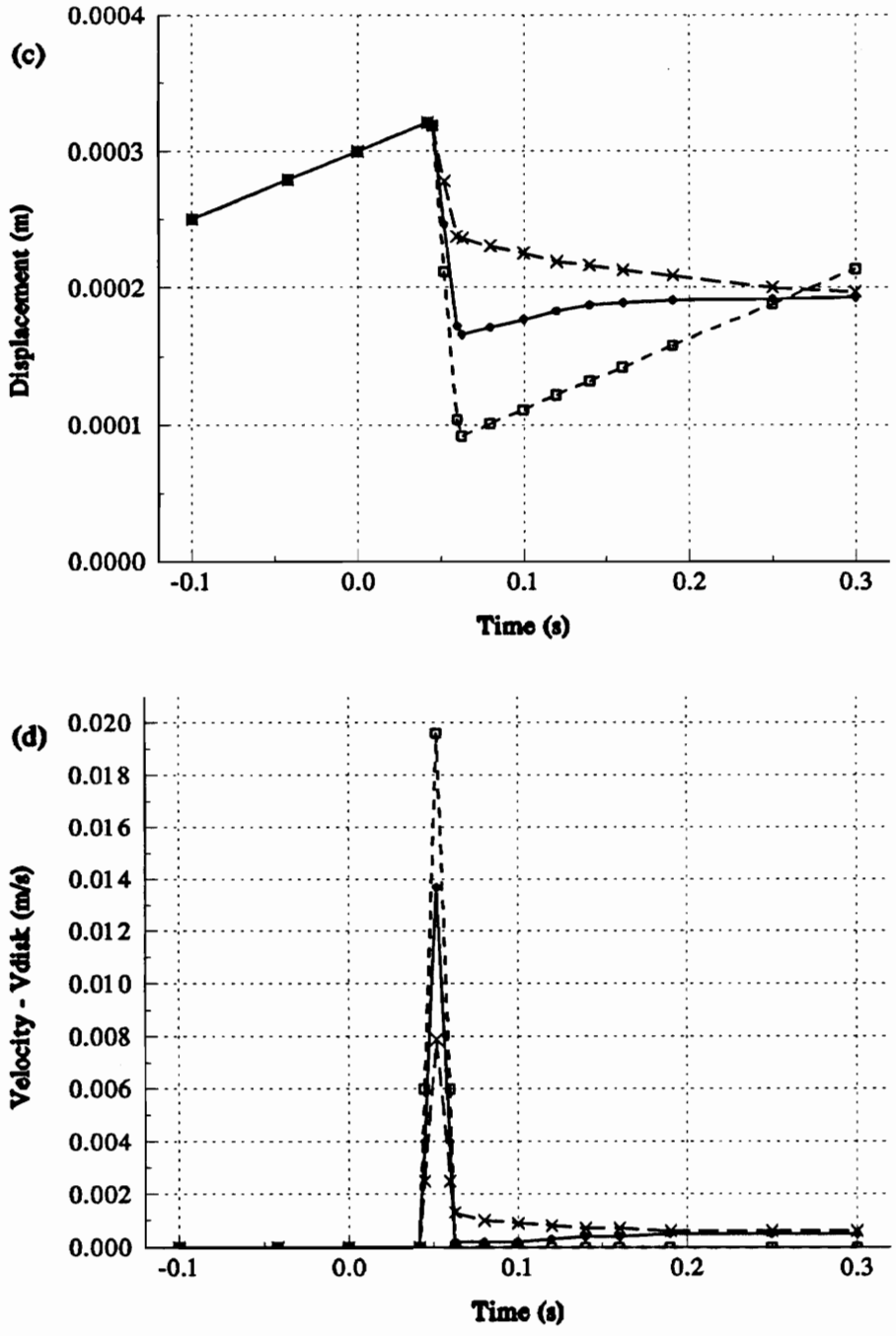

Figure 5.4 - PSL simulation, (c) displacement vs. time, (d) relative velocity vs. time, effect of F_k at higher relative velocities.

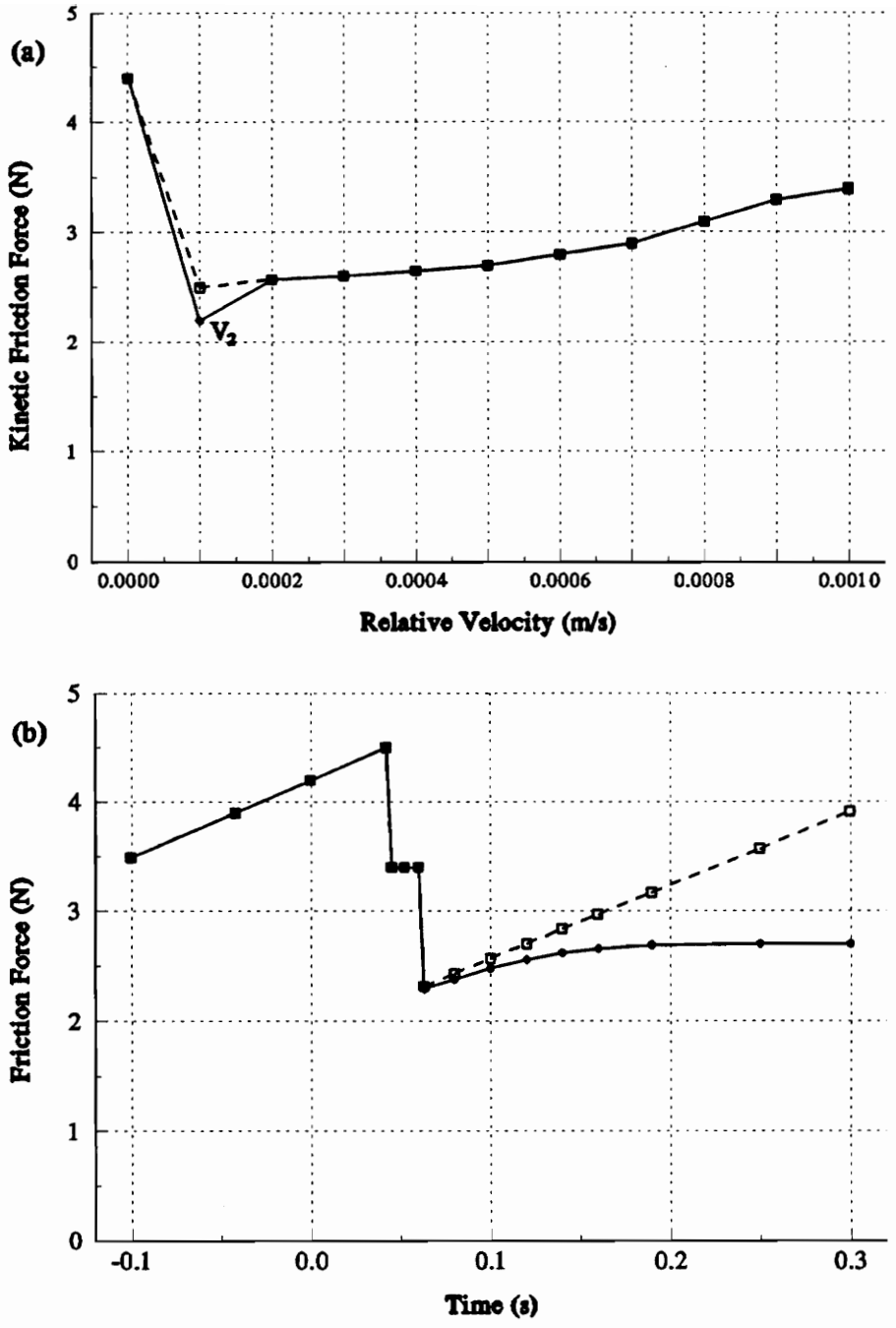

Figure 5.5 - PSL simulation, (a) kinetic friction vs. relative velocity, (b) friction force vs. time, effect of F_k at V_{min}.

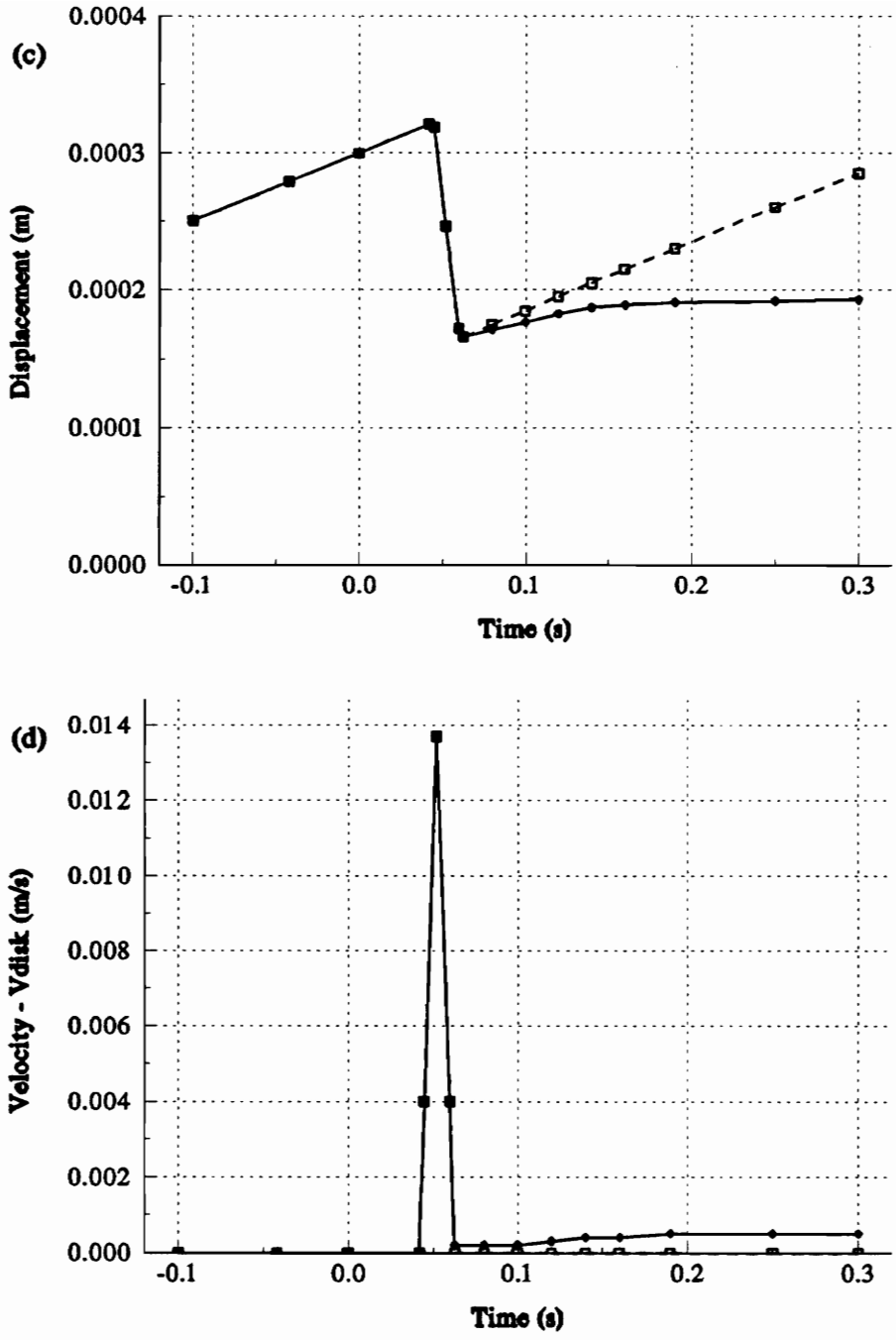

Figure 5.5 - PSL simulation, (c) displacement vs. time, (d) relative velocity vs. time, effect of F_k at V_{min}.

velocities (V_8, V_9, V_{10}, and V_{11}). The friction force during slip controls how far the mass overshoots its equilibrium position.

Figure 5.5a-d shows the effect of changing the kinetic friction force at V_2 ($0.1x10^{-3}$ m/s). This is the point defined as v_{min} by other investigators [1, 24]. Since the forced velocity is above v_{min} then both simulations should yield single-stick behavior. But, when the kinetic friction force at V_2 was raised from 2.2 N to 2.5 N, stick-slip motion resulted. Other investigators have consistently found that if the forced velocity is greater than v_{min} that stick-slip behavior will not occur.

Obviously, the friction force vs. relative velocity curve is very important in determining the frictional behavior of a system. Often the slightest change in the curve could change the behavior significantly. This may explain the range of behaviors observed experimentally when it seemed all the test conditions were exactly the same, such as shown in Table 4.1.

5.1.3 Rise in Friction Force

The model indicates that the rise in friction force after the first slip is due to the shape of the friction velocity curve. Referring to Figure 5.3a-d, when the mass begins to slide (pt.B), the velocity increases and the friction force varies as defined by the friction-velocity curve. Since the mass has momentum, it passes through the point where the relative velocity = v_{forced} (pt. C). Since the graph resolution is not nearly as small as the time step ($0.2x10^{-4}$) the drop and then rise in friction force (from pt. B to D) as

the mass increases in velocity is not seen in these graphs but has been seen for other input parameters (Figure 5.6). During the slip the velocity quickly reaches and exceeds V_{11} (pt.D), so the friction force is constant and equals the friction force value defined at V_{11}. When the mass begins to slow down (pt. E) the friction force again varies with velocity and again this happens very quickly. The relative velocity settles at a value below v_{forced} and above the zero velocity criteria (pt. F). The friction force then rises slowly as the relative velocity approaches equilibrium at v_{forced} (pt. G). The location of point F on the friction-velocity curve is dependent on all the input parameters.

The model does not predict a rise in friction force under stick-slip conditions. More than a few experimental tests showed a rise in friction force under stick-slip conditions (Table 4.1, tests labeled stick-slip, μ_k increases). An explanation for this behavior must be related to how the static friction force changes during a friction test. If it was simply the variations of the surface then the changes would be random; however, there may be a gradual change in the surface which may cause this rise, possibly sample machining directionality (see Section 5.4).

The local heating at the surface was investigated as a possible explanation, but the frictional heat generation was estimated and found to be very small due to the low mean sliding velocity. Besides, if the ΔT caused the rise in friction, why didn't it cause a rise in friction for all the tests, unless all the tests do not have the same ΔT.

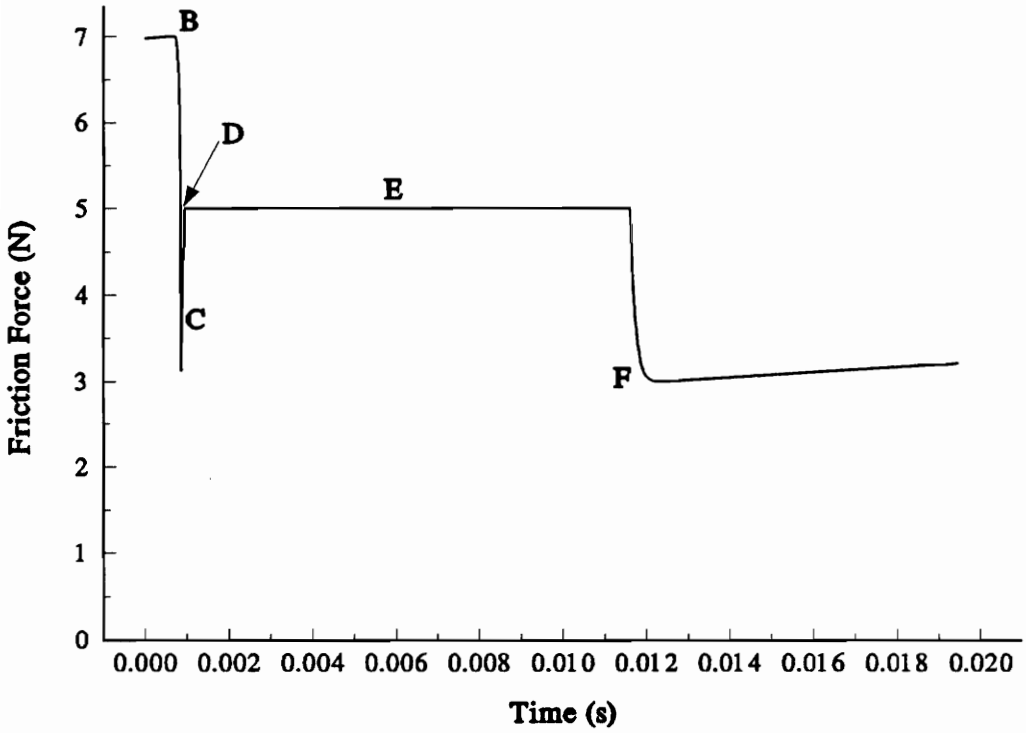

Figure 5.6 - PSL simulation, a detailed plot of friction force vs. time showing the rapid fall and rise of friction force at the very beginning of relative motion.

5.1.4 Drop in Friction Force

As seen in Figure 5.4c, the displacement of the mass during slip decreases as the friction force at the higher velocities (V_8, V_9, V_{10}, and V_{11}) is increased. For the tests run on the improved apparatus the drop in friction force is defined essentially by the displacement of the mass during slip. The A-series results indicate that the drop in friction force is not dependent on surface roughness; therefore, the actual friction force at high velocities is not dependent on surface roughness. Since the extent of plastic deformation is relatively small then it can be assumed that the friction force is dominated by the adhesion component of friction and/or the deformation losses below the surface.

Another conclusion can be made if we assume that the adhesion component of friction, F_{adh}, is a function of surface roughness. Referring to equation (3), section 2.1, F_{adh} is dependent on the real area of contact. Since the real area of contact is thought to increase with a decrease in surface roughness, the above assumption could be true. This could possibly be tested experimentally by running lubricated tests (section 2.2.2).

Case A:

If it is assumed that the adhesion component is a function of surface roughness,

and it is known that the kinetic friction force at the higher velocities is not a function of surface roughness,

then the deformation losses below the surface must be controlling the friction force at the higher velocities.

So, if it is desired to reduce the sudden drop in friction force (the sudden

displacement of the mass), increase the kinetic coefficient of friction at the higher velocities by increasing the loss tangent of the material.

The other possibility is if the adhesion component of friction is controlling the friction force at the higher velocities.

Case B:

If it is assumed that the kinetic friction forces due to deformation losses are small compared to the adhesion forces,

and it is known that the kinetic friction force at the higher velocities is not a function of roughness,

then the adhesion component of friction is not a function of surface roughness.

5.2 Frictional Behavior

The results shown in Figures 4.11-4.15 are a direct comparison between McCann's tests, the A-series tests, and the B-series tests. These results support the theory that the discrepancy between McCann's results and the A-series results was due to the improvements made to the test apparatus. It appears that the motor start-up transient interfered with McCann's friction measurements at lower normal loads. The motor start-up transient interferes more at the lower loads because sliding begins at the lower friction forces before the transient has decayed.

While this explains the difference in the static coefficients of friction, the kinetic coefficients should be the same. For TG-72 Rough-on-Rough this is precisely the case.

At all loads there is no significant difference between McCann's μ_k, A-series' μ_k, and B-series' μ_k. However, for almost all the smooth surfaces, the A and B-series tests show a higher kinetic coefficient of friction than McCann. This could be due to the filtering done by McCann.

Since TG-72 was the only sample that showed no difference in the μ_k's and it is the only rough-on-rough sample tested, then perhaps roughness has an influence on the differences between the A-series and McCann's results. Another explanation for the differences between the A-series and McCann's results is the material processing. The reprocessing of the materials may have changed the surfaces in more ways than one. Perhaps the morphology of the plastic changed. The reprocessing might have increased the rubber content at the surface [27] or changed the mechanical properties of the surface in some way [16]. But even if this were true it would only explain the differences between the compression molding (A-series) results and McCann's results; not the differences between the B-series and McCann's results.

McCann's samples were stored at room temperature for months before any testing was done. So the extended storage time for the B-series tests has been discounted as a possible explanation of the differences between McCann's results and the B-series results.

Through extensive testing on the old test apparatus it has been found that there is a high degree of randomness associated with the polymer-on-polymer system which can initiate different kinds of frictional behavior. The randomness may be due to surface roughness variations; non-linear relations between friction, velocity, contact area, and

surface roughness; drive system non-linearities; and humidity [22, 23]. The PSL models show that small changes in the friction force vs. relative velocity curve can result in different frictional behaviors. Therefore, if the factors mentioned above cause small changes in the friction-velocity curve then different frictional behaviors may result.

There is some consistency in the results (Table 4.1). For example TG-72 tended to exhibit single stick motion while LGA-1 tended to exhibit stick-slip motion. For LGA-1, the rough surfaces tended to exhibit single stick behavior while the smooth surfaces exhibited stick-slip behavior. It is obvious that the frictional behavior is dependent on surface roughness and material properties.

Also, for both sets of results the Polypropylene samples obviously exhibit a more desirable frictional behavior. This could be due to the significant difference between ABS plastic and Polypropylene. Polypropylene is semi-crystalline whereas ABS is amorphous. Polypropylene has a percent elongation between 200 and 700 percent whereas ABS is between 5 and 60 percent. However, no connection between these mechanical properties and frictional instabilities has been made at this time.

5.3 Friction-Velocity Tests

5.3.1 Experimental

As shown in Figure 4.18 and 4.19, both the static and kinetic friction force seem to have the same relationship with velocity. This means that the velocity affects both the static and kinetic friction mechanisms in the same way. This is essentially the same

conclusion made by Simkins [30]. He was one of the first to talk about the mutuality of static and kinetic friction. He states that the static friction coefficient is merely a local maximum of the friction force. This is easiest to describe using the asperity deformation model of friction. When two rough surfaces are put into contact and loaded tangentially, the asperities interlock with each other and prevent motion. As the tangential load increases the weakest asperities break and the surfaces move microscopically until stronger asperities come into contact with each other. This is called microslip and cannot be measured by most friction testers. This microslipping continues to occur until the strongest asperities are broken. The tangential load at this point is called the static friction force and gross sliding begins. The average tangential load during subsequent sliding is called the kinetic friction force and is equal to the average tangential load required to break the asperities, which is less than the static friction force.

This theory can be extended to other friction mechanisms and it can be said that the static friction force is merely a local maximum and the kinetic friction force is the average friction force. For example, just as the asperity strength controls the microslips in the asperity deformation model, the shear strength of the interface may control the microslips in the adhesion model of friction. The friction mechanisms are the same in both static and kinetic friction and therefore should follow the same trends with velocity.

In another vein, one possible factor contributing to the B-series tests which exhibited a $\mu_k > \mu_s$ is that the local maximum friction force is less than the average friction force.

Another observation during the friction-velocity tests that is worth mentioning is that TG-72 at a forced velocity of 0.001 m/s exhibited single-stick motion despite the fact that 0.001 m/s is below v_{min} (Section 2.3). This does not agree with other investigators [1, 24] and with additional evidence may disprove the theory that stick-slip motion will result for tests run at velocities on the negative slope of the friction-velocity curve. There is no explanation for this behavior at this time.

5.3.2 Constructing the Friction-Velocity Curve

There is some question about the validity of the method used in constructing the friction-velocity curve [24]. The curve is constructed by running independent friction tests at various velocities and plotting the kinetic friction force vs. forced velocity. The problem lies in the definition of the kinetic friction force. Usually it is defined as the average friction force after the first slip occurs. For steady-sliding or stick-slip behavior, this definition is valid. But for stick-slip behavior the average friction force is equal to the average friction force during slip (higher velocities). This may or may not be equivalent to the actual kinetic friction force for the velocity being tested. The new test apparatus will be able to measure relative velocity and friction force simultaneously. So, it will be possible to plot the friction force vs. relative velocity curve during a single slip.

5.3.3 Friction Mechanisms

Again further conclusions can be made if the conditions in section 5.1.4 are

assumed to be true.

Case 1:

If 1) The friction mechanisms are the same for static and kinetic friction forces. (Section 5.3.1)

and 2) The kinetic friction force at higher velocities is controlled by the deformation losses below the surface. (Section 5.1.4, Case A)

then the static friction force at the higher velocities is controlled by the deformation losses below the surface.

Case 2:

If 1) The friction mechanisms are the same for static and kinetic friction forces. (Section 5.3.1)

and 2) The kinetic friction force at higher velocities is controlled by the adhesion forces, $F_{adh}=A\tau$. (Section 5.1.4, Case B)

and 3) The static real area of contact is a constant with respect to sliding velocity

then the changes in the static friction force with respect to velocity are due to changes in the shear strength of the interface with strain rate.

and the changes in the kinetic friction force with respect to velocity are due to changes in the shear strength with strain rate.

5.4 Surface Orientation

Plastic plaques were compression molded using steel plates which had been

machined. For the ground surfaces, the directionality of the machining was reproduced on the plastic surfaces. Some of the injection molded samples also had surfaces which exhibited the machining direction. In the A and B-series tests, the machining direction of the pin sample was recorded. Since the pin sample was kept square with the direction of sliding, the pin machining direction was either parallel or perpendicular to the sliding direction (Figure 5.7); although the pin did rotate slightly on occasion. It was also decided to keep the orientation of the pin machining direction >45 degrees relative to the orientation of the disk machining direction.

Tests were done to investigate the dependence of the friction values on the orientation of the pin with respect to sliding. It was found that there was no difference between sliding parallel and sliding perpendicular to the pin machined direction at the 90% significance level.

For the new test apparatus the pin machined direction with respect to the disk machined direction will be constant throughout the sliding.

Another variable which may be affecting the friction data is the depth of the spherical cavity on top of the pin sample. Referring to Figure 3.6, if the cavity is too deep the epoxy may push on one side of the sample so that the load is not evenly distributed over the surface of the pin and self-alignment is not realized. The possibility that this was happening was not discovered until most of the tests had been completed. Even so, it is difficult to tell if the epoxy is touching the pin sample during a test or not. The new test apparatus was designed so that this would not be a problem. A larger

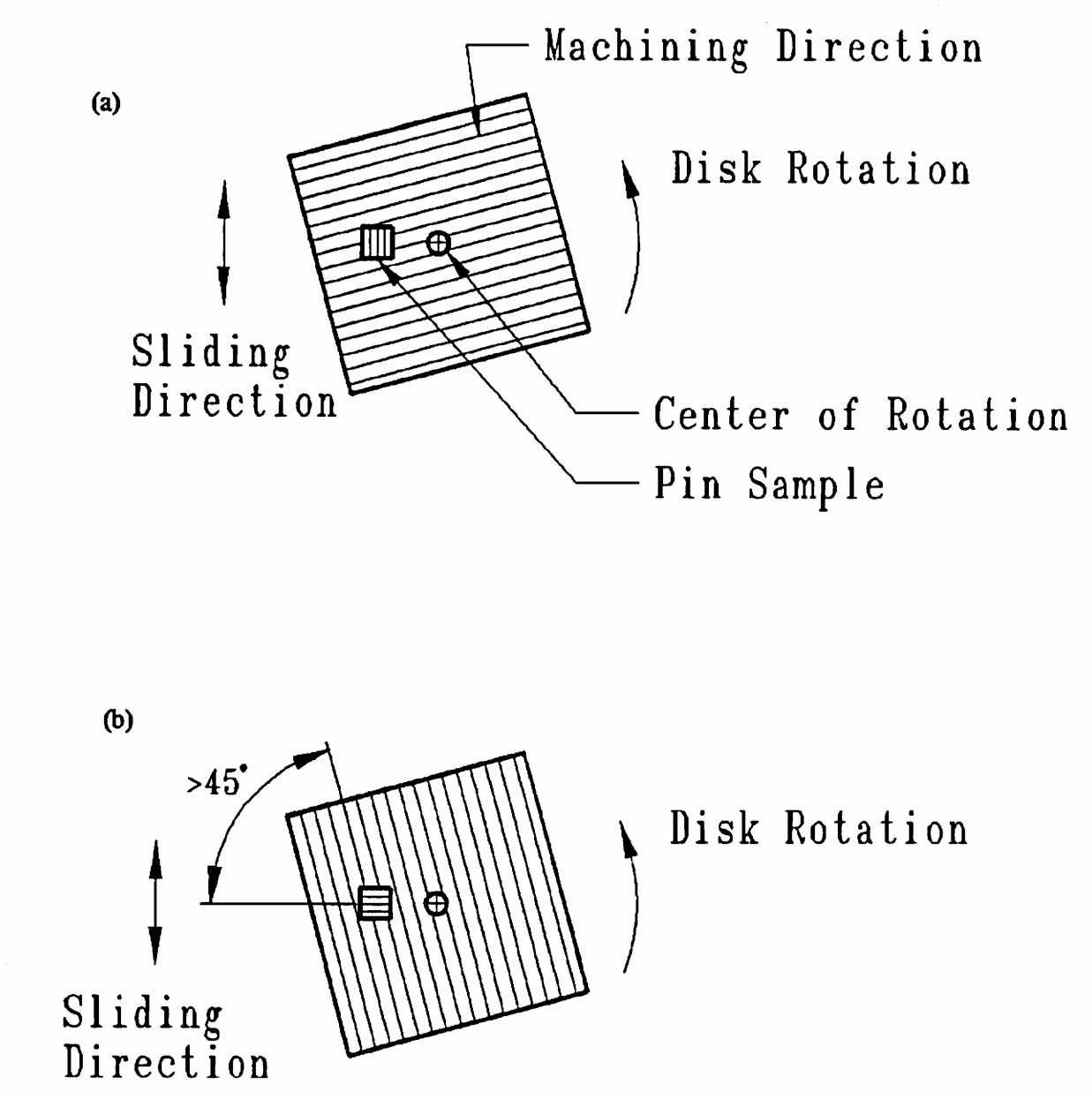

Figure 5.7 - Sample orientation (a) Pin machined direction parallel to sliding direction. (b) Pin machined direction perpendicular to sliding direction.

sphere will be used in a more shallow cavity to ensure self-alignment. Appendix E shows the calculation for the depth of the cavity necessary for a given sphere to ensure the pin does not slip out of the spherical cavity.

5.5 Rise in Friction Force

One theory was proposed to explain why the frictional force increased gradually after the first slip. It was hypothesized that the area of contact gradually increased after the first slip. The increase in area would be caused by an increase in asperity deformation which would be indicated by the upper specimen moving downward. To examine this hypothesis the vertical displacement of the slider during the test was measured. The results showed a gradual rise of the slider after slip instead of the hypothesized fall.

To determine whether the vertical rise of the slider after sliding commenced was a function of the polymer materials or of the test apparatus, tests were done with a steel ball in contact with a steel disk, a system which would experience much less elastic or plastic deformation than the polymer-polymer system. The steel-steel system should not show any changes in the area of contact during the test and the vertical displacement should remain constant. However, the steel ball-on-steel disk system showed the same vertical displacement behavior as the polymer flat-on-polymer disk. Both showed a gradual rise of the slider as relative motion commenced. Therefore, it was concluded that the gradual rise of the slider is related to the test apparatus and not the properties

of the polymer system.

An explanation for the gradual rise in friction force was discussed in Section 5.1.3.

6.0 Summary of Results and Conclusions

The objectives of this study were to gain a better understanding of the transition from static to kinetic conditions for plastics in dry contact. What causes the friction force to change? What effect do surface parameters and normal load have on the frictional behavior?

1) The new test apparatus will yield much more information about what is happening to the friction force during the transition from static to kinetic conditions.
2) All of the ABS plastic investigated in this study exhibit stick-slip or single stick behavior for practically all loads and surface roughnesses; therefore, plastic components made with the ABS materials investigated in this study will always have the potential to slip suddenly and release energy into the system which may excite other components and produce unwanted sounds.
3) The polypropylene investigated in this study does not exhibit stick-slip or single stick behavior for practically all loads and surface roughnesses; therefore, plastic components made with this material will not have a tendency to slip suddenly and

will not produce unwanted sounds.

4) The rise in friction force immediately following slip is due to the shape of the friction-velocity curve.

5) The drop in friction force during the first slip is not a function of surface roughness over the range of R_a roughnesses from 0.12 μm to 0.99 μm. It is a function of the value of friction force at higher velocities.

6) For the loads and surface roughnesses tested in this study, the deformation losses below the surface and adhesion are the main friction mechanisms in ABS plastics.

7) The static and kinetic friction forces are controlled by the same friction mechanisms. The static friction force is the local maximum friction force and the kinetic friction force is the average friction force.

8) Differences in the frictional behavior observed between this study and the study by B. McCann are due mainly to the improvements made to the test apparatus.

9) Some of the conclusions made by Mr. McCann were confirmed in this study: The tendency for stick-slip frictional behavior decreases with increasing surface roughness. The tendency for stick-slip frictional behavior increases with increasing normal load [1].

7.0 Recommendations

1) Due to the dynamic measuring capabilities of the new test apparatus, all friction testing concerned with the transition from static to kinetic conditions should be done on the new test apparatus.

2) Due to the importance of the friction-velocity curve in determining frictional behavior, and due to the questionable nature of constructing such a curve from independent friction tests, the new test apparatus should be used to find the friction-velocity relationship during the transition from static to kinetic conditions.

3) The new test apparatus could be used to find the friction-velocity relationship at much higher velocities.

4) It appears that ABS has a propensity to produce a drop in friction force when sliding commences for the surface roughnesses and loads tested. Thus, it is not promising for current ABS materials to result in noiseless contacts. Efforts should be directed toward other material systems for instrument panel components.

5) Test other materials to determine the effect of material properties (especially elastic modulus, rubber content, morphology, etc.) on frictional behavior.

6) The computer model could be modified to simulate the real situation more closely by adding damping to the equation of motion and/or by adding another degree of freedom corresponding to the dynamics of the force transducer. (See papers by Ibrahim).

7) The contribution of the viscoelastic deformation component of friction could be found by minimizing the adhesive component of friction by running tests under lubricated conditions.

8) Obtain a more complete characterization of the ABS and Polypropylene materials and surfaces by performing material property tests (e.g. morphology, percent crystallization, molecular weight, D.S.C., W.A.X.S., S.A.X.S., etc.).

References

[1] McCann, B. P., "Frictional Vibrations in Structural Polymers," Master of Science Thesis, Virginia Polytechnic Institute and State University, May 1992.

[2] Bowden, F. P., and Tabor, D., *The Friction and Lubrication of Solids*, University Press, Oxford, (1950).

[3] Childs, T. C., "Deformation and Flow of Metals in Sliding Friction," *Fundamentals of Friction: Macroscopic and Microscopic Processes*, Kluwer Academic Publ., ed. by I. L. Singer and H. M. , 209-26 (1991).

[4] Briscoe, B. J., and Tweedale, P. J., "A View of Polymer Composite Tribology," *Proc. of Amer. Soc. Mat. Conf., Tribology of Composite Materials*, ed. by P. K. Rohatgi, P. J. Blau and C. S. Yust, 15-23 (1990).

[5] Briscoe, B. J., "Friction of Organic Polymers," *Fundamentals of Friction: Macroscopic and Microscopic Processes*, Kluwer Academic Publ., ed. by I. L. Singer and H. M. Pollock, 167-82 (1991).

[6] Pascoe, M. W., and Tabor, D., "The Friction and Deformation of Polymers," *Proc. Roy. Soc. Lond.*, A235, 210-24 (1956).

[7] Briscoe, B. J., "The friction of polymers: a short review," in *Friction and Traction*, ed. by D. Dowson, M. Godet, C. M. Taylor, and D. Berthe, Westbury House, IPC Press, Guilford, 81-93 (1981).

[8] Bueche, A. M., and Flom, D. G., "Surface Friction and Dynamic Mechanical Properties of Polymers," *Wear*, 2, 168-182 (1958/59).

[9] Briscoe, B. J., and Tabor, D., "Friction and Wear of Polymers: The Role of Mechanical Properties," *Brit. Poly. J.*, 10, 74-8 (1978).

[10] Ludema K. C., and Tabor, D., "The Friction and Viscoelastic Properties of Polymeric Solids," *Wear*, 9, 329-48 (1966).

[11] Grosch, K. A., *Proc. Roy. Soc. (London)*, A274, 21, (1963).

[12] Challen, J. M., and Oxley, P. L., "An Explanation of the Different Regimes of Friction and Wear Using Asperity Deformation Models," *Wear*, 53, 229-43 (1979).

[13] Greenwood, J. A., and Williamson J.B, "Contact of Nominally Flat Surfaces," *Proc. Roy. Soc.*, A295, 300-19 (1966).

[14] Pooley, C. M., and Tabor, D., "Friction and Molecular Structure: the Behaviour of Some Thermoplastics," *Proc. Roy. Soc. Lond.*, 329, 251-74 (1972).

[15] Bahudar, S., and Ludema, K. C., "The Viscoelastic Nature of the Sliding Friction of Polyethylene, Polypropylene and Copolymers," *Wear*, 18, 109-28 (1971).

[16] Callear, J. E., and Shortall, J. B., "The Effect of Microstructure and Crystallininty on the Tensile Properties and Fracture Behavior of Injection-moulded Polytetramethylene Terephalate," *J. of Materials Science*, v. 12, 141-52 (1977)

[17] Briscoe, B. J., and Tabor, D., "Shear Properties of Thin Polymeric Films," *J. Adhesion*, 9, 145-155 (1978).

[18] Briscoe, B. J., "Friction and Wear of Organic Solids and the Adhesion Model of Friction," *Phil. Mag. A*, 43, no. 3, 511-27 (1981).

[19] Amuzu, J. K., Briscoe, B. J., and Tabor, D., "Friction and Shear Strength of Polymers," *Trans. Amer. Soc. Lub. Engrs.*, 20, n. 4, 354-7 (1977).

[20] Briscoe, B. J., and Smith, A. C., "Polymer Friction and Polymer Yield: a Comparison," *Polymer*, 22, 1587-9 (1981).

[21] Voorhes, W. G., "Investigation of Stick-Slip in Simulated Slideways," *J. Amer. Soc. Lubrication Eng.*, 18th ASLE Annual meeting, April 30-May 2, 457-62 (1963).

[22] Ibrahim, R. A., "Friction-Induced Vibration, Chatter, Squeal, and Chaos: Part I - Mechanics of Friction," *Friction-Induced Vibration, Chatter, Squeal, and Chaos*, Ed. by R. A. Ibrahim and A. Soom, *ASME*, DE- v.49, 107-21 (1992).

[23] Ibrahim, R. A., "Friction-Induced Vibration, Chatter, Squeal, and Chaos: Part II - Dynamics and Modeling," *Friction-Induced Vibration, Chatter, Squeal, and Chaos*, Ed. by R. A. Ibrahim and A. Soom, *ASME*, DE- v.49, 123-38 (1992).

[24] Rorrer, R. A., "Frictional Oscillations in Elastomeric Sliding," PhD Dissertation, Virginia Polytechnic Institute and State University, October 1991.

[25] Rabinowicz, E., *Friction and Wear of Materials*, John Wiley and Sons, NY, Sect. 4.2, 1965.

[26] Benabdallah, H., "The Influence of Contact Pressure and Roughness on the Shear Strength During Friction of Some Thermoplastics," *Annual Tech. Conf., Publ. by Soc. of Plastics Eng.*, v. 37, 689-91 (1991).

[27] Wyzgoski, M. G., "Effects of Oven Aging on ABS, Poly(Acrylonitrile-Butadiene-Styrene)," *Polymer Eng. and Sci.*, 16, no. 4, 265-9 (1976).

[28] Rudin, A., *The Elements of Polymer Science and Engineering*, Academic Press, N.Y., 1982.

[29] Moore, G. R., and Kline, D. E., *Properties and Processing of Polymers for Engineers*, Prentice Hall, 1984.

[30] Simkins, T. E., "The Mutuality of Static and Kinetic Friction," *J. ASLE, Lubrication Eng.*, 26-31 (1966).

Appendix A - Intermittent Gears.

Figure A.1 is an assembly drawing of the intermittent gear system used to modify the existing apparatus. Figure A.2 is a detailed drawing of the intermittent gears themselves. There are only two teeth on each gear. Figure A.3 is a drawing of the bearing housing and Figure A.4 shows the machining modifications made to the existing gears and shaft.

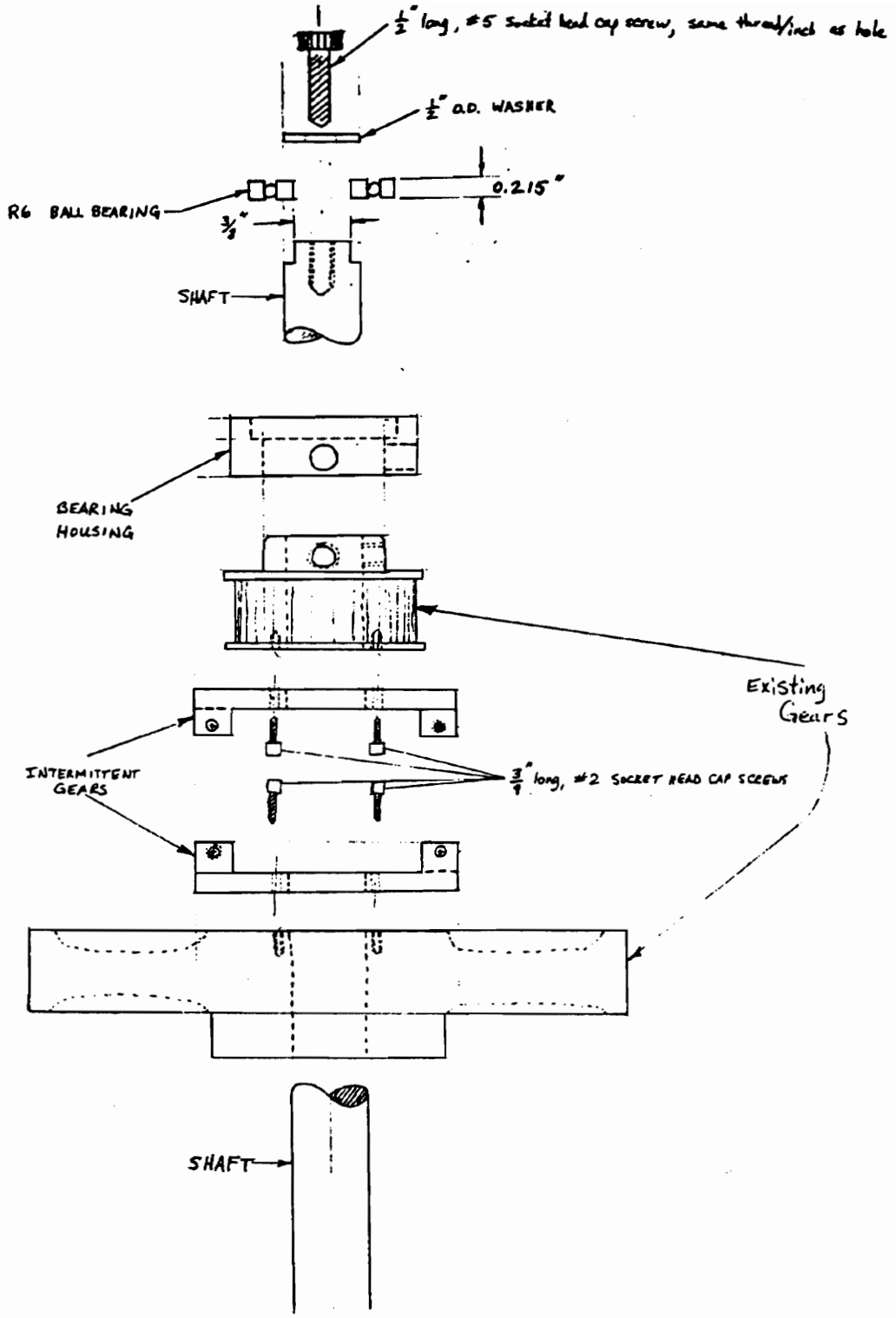

Figure A.1 - Assembly drawing for intermittent gear system.

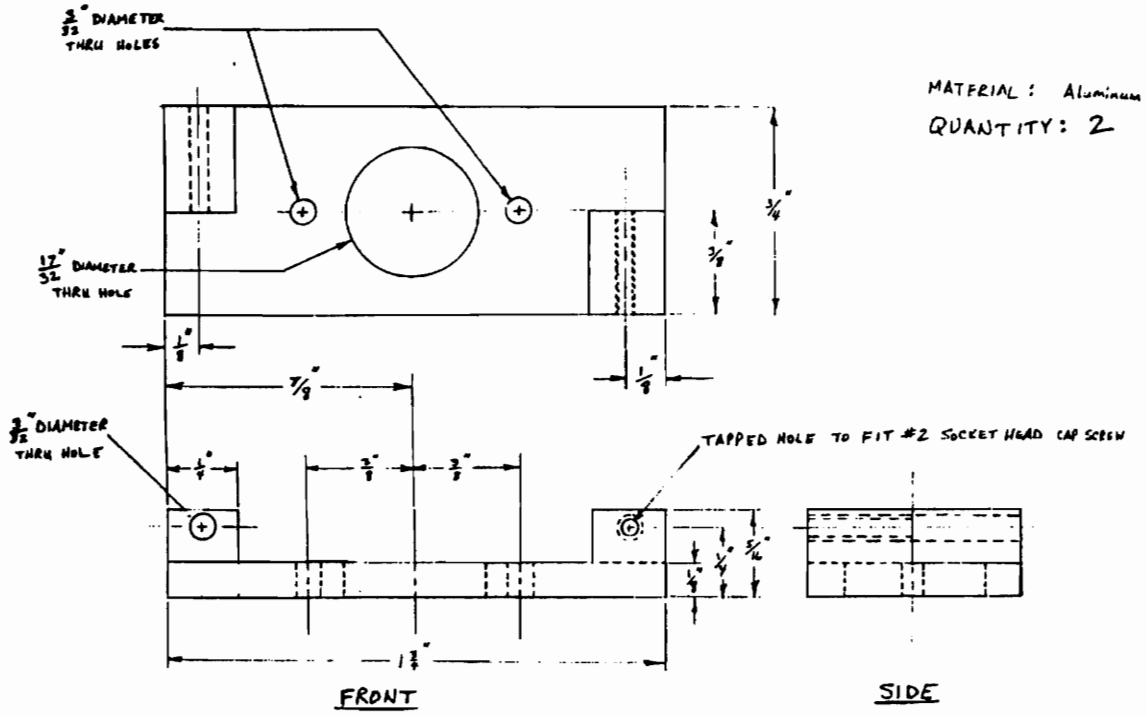

Figure A.2 - Detailed drawing of intermittent gears.

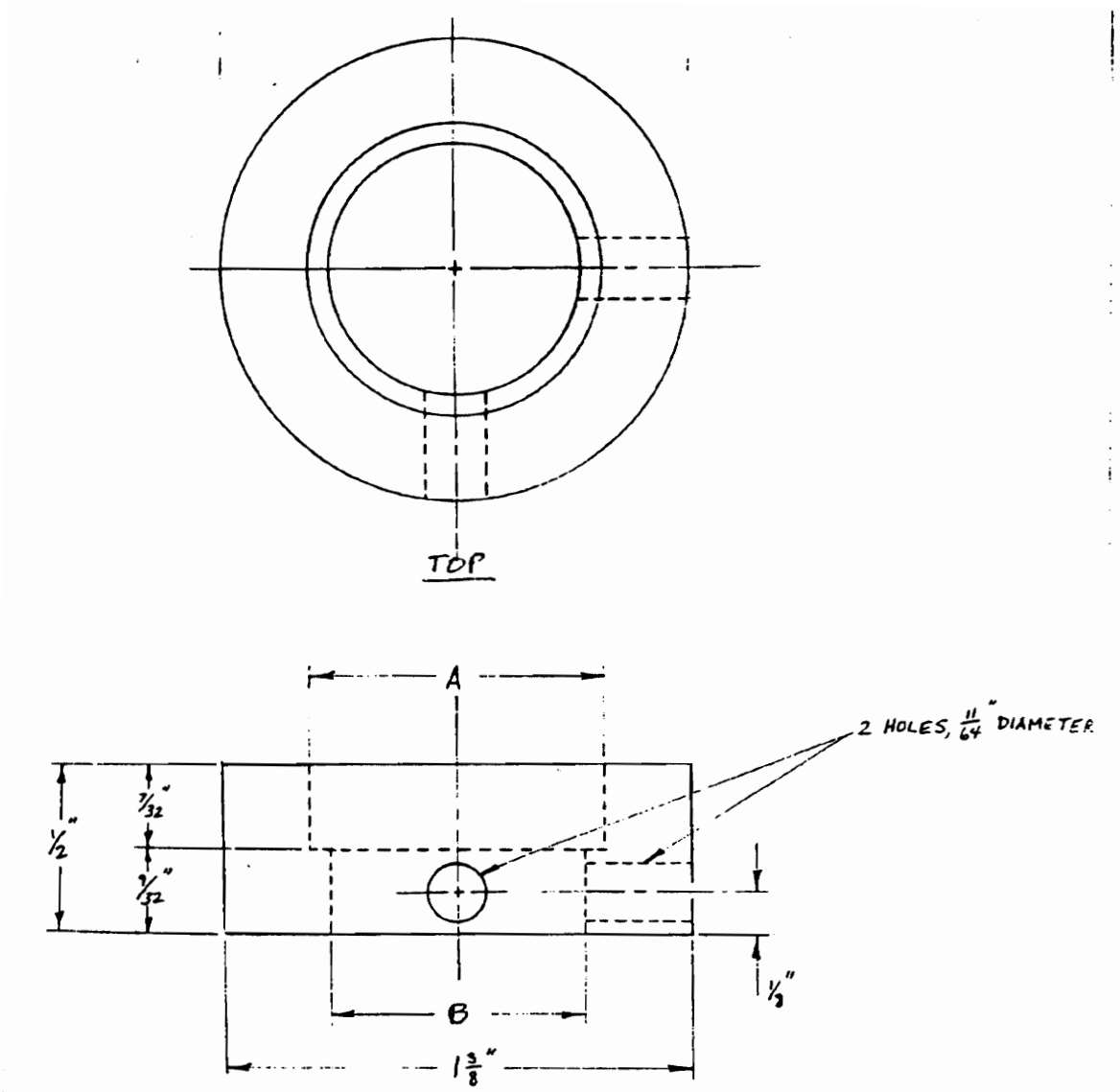

Figure A.3 - Detailed drawing of bearing housing.

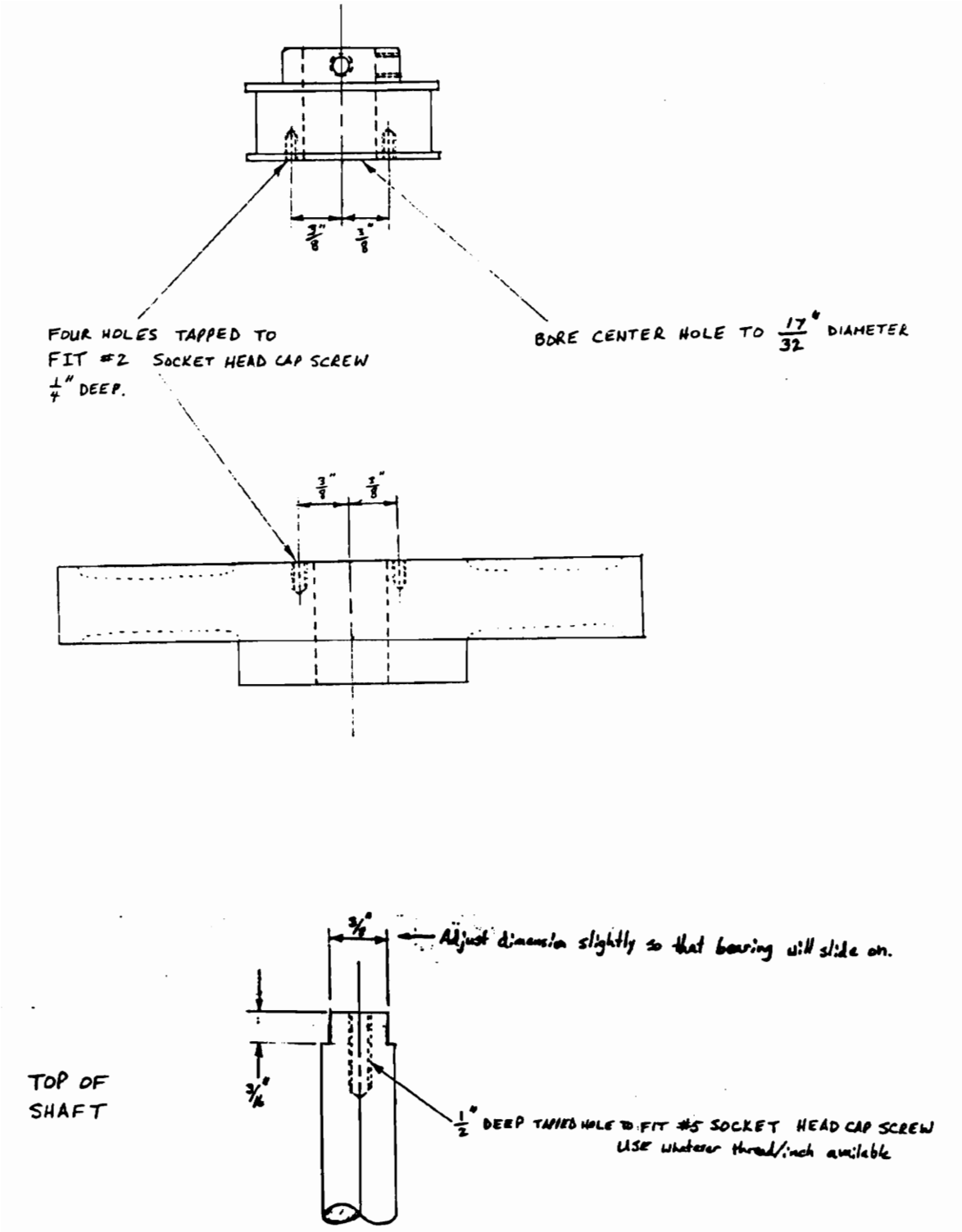

Figure A.4 - Modifications made to the existing gears and shaft.

Appendix B - Surface Parameter Computer Program.

The following is a Fortran program used to calculate surface roughness parameters. The program was written to accommodate data which has been taken with Global Lab and the Talysurf 4 profilometer. The program asks the user to input the data file name and the vertical magnification factor used on the Talysurf. The program prints the output to the screen and to a file. The following surface roughness parameters are calculated: Profile-- mean, R_a roughness, RMS roughness, data minimum, data maximum, data range, skewness, and kurtosis; Slope-- mean, RMS average, data minimum, data maximum, data range, skewness, and kurtosis; Curvature-- mean, RMS average, data minimum, data maximum, data range, skewness, and kurtosis.

```
C234567890123456789012345678901234567890123456789012345678901234567890123456789012
C  SURFACE ANALYSIS PROGRAM EDITED BY R. MOLIQUE 4/15/93
C
C  This program calculates surface characteristics using data that has
C  been acquired using the Talysurfer (J setting, x20 in horizontal;
C  if these settings are changed then the X coord. in this program
C  should be changed) and Global Lab (10000 points).
C  The data file must be changed to an ASCII file (which can be done
C  in Gobal Lab) before running this program.
C
      DIMENSION X(10000),Y(10000),Y1(10000),A(10000),A1(10000),AX(10000)
     $,AS1(10000)
      REAL KRT,KRTA,KRTAS,MF
      INTEGER PERIOD
      CHARACTER*24 DATA,DATOUT
      WRITE(*,100)
  100 FORMAT(/,' SURFACE ANALYSIS',/,' ENTER COMPLETE DATA FILE NAME',/)
C
C  The data file should be in the same directory as the compiler
C
      READ(*,110) DATA
  110 FORMAT(A24)
      WRITE(*,*)' PLEASE WAIT'
      OPEN(3,FILE=DATA)
      PERIOD=INDEX(DATA,'.')
      DATOUT='O'//DATA(:PERIOD)//'DAT'
```

```
      OPEN(4,FILE=DATOUT)
      N=10000
      READ(3,*)(Y(I),I=1,N)
      WRITE(*,*)' DO YOU WANT TO SEE THE DATA, 1-YES, 2-NO'
C      SKIP=2
      READ(*,*)SKIP
C
C  The Multiplication Factor is needed to convert the mV to microns.
C
    1 WRITE(*,*)' TYPE THE MAGNIFICATION FACTOR IN THE VERTICAL'
C     1 MULT=5000
      READ(*,*)MULT
        MF=1.0/(MULT*38.52E-6)
      WRITE(*,*)' PLEASE WAIT'
      IF(SKIP.EQ.1) THEN
        WRITE(*,*)' X (uM)          Y (uM)'
        DO 10 I=1,N
        X(I)=(I-1)*0.305
        Y(I)=Y(I)*MF
        WRITE(*,120) X(I),Y(I)
  120   FORMAT(E9.4,E20.6)
   10   CONTINUE
      ELSE
        DO 15 I=1,N
        X(I)=(I-1)*0.305
        Y(I)=Y(I)*MF
   15   CONTINUE
      ENDIF
      PI=3.1415927
      DX=X(3)-X(2)
      P=0
      AP=0
      ASP=0
      DO 20 I=1,N
      IF(I.EQ.1) THEN
         A(I)=(-Y(I+2)+4*Y(I))/(2*DX)
         AX(I)=(-Y(I+3)+4*Y(I+2)-5*Y(I+1)+2*Y(I))/(SQRT(A(I)**2+1)*DX**2
     $)
      ELSEIF(I.EQ.N) THEN
         A(I)=(3*Y(I)-4*Y(I-1)+Y(I-2))/(2*DX)
         AX(I)=(2*Y(I)-5*Y(I-1)+4*Y(I-2)-Y(I-3))/(SQRT(A(I)**2+1)*DX**2)
      ELSE
         A(I)=(Y(I+1)-Y(I-1))/(2*DX)
         AX(I)=(Y(I+1)-2*Y(I)+Y(I-1))/(SQRT(A(I)**2+1)*DX**2)
      ENDIF
        A(I)=ATAN(A(I))*(180/PI)
        P=P+Y(I)
        AP=AP+A(I)
        ASP=ASP+AX(I)
   20 CONTINUE
      YM=P/N
      AM=AP/N
      ASM=ASP/N
      R=0
      R1=0
      R2=0
      R3=0
      R4=0
```

```
      AR=0
      AR1=0
      AR2=0
      AR3=0
      AR4=0
      ASR=0
      ASR1=0
      ASR2=0
      ASR3=0
      ASR4=0
      DO 30 I=1,N
        Y1(I)=Y(I)-YM
        A1(I)=A(I)-AM
        AS1(I)=AX(I)-ASM
        R=R+Y1(I)
        AR=AR+A1(I)
        ASR=ASR+AS1(I)
        R1=R1+ABS(Y1(I))
        AR1=AR1+ABS(A1(I))
        ASR1=ASR1+ABS(AS1(I))
        R2=R2+Y1(I)**2
        AR2=AR2+A1(I)**2
        ASR2=ASR2+AS1(I)**2
        R3=R3+Y1(I)**3
        AR3=AR3+A1(I)**3
        ASR3=ASR3+AS1(I)**3
        R4=R4+Y1(I)**4
        AR4=AR4+A1(I)**4
        ASR4=ASR4+AS1(I)**4
   30 CONTINUE
      RA=R1/N
      RMS2=R2/N
      RMSA2=AR2/N
      RMSAS2=ASR2/N
      RMS=SQRT(RMS2)
      RMSA=SQRT(RMSA2)
      RMSAS=SQRT(RMSAS2)
      RMS3=RMS2*RMS
      RMSA3=RMSA2*RMSA
      RMSAS3=RMSAS2*RMSAS
      RMS4=RMS3*RMS
      RMSA4=RMSA3*RMSA
      RMSAS4=RMSAS3*RMSAS
      SKW=R3/(N*RMS3)
      SKWA=AR3/(N*RMSA3)
      SKWAS=ASR3/(N*RMSAS3)
      KRT=R4/(N*RMS4)
      KRTA=AR4/(N*RMSA4)
      KRTAS=ASR4/(N*RMSAS4)
      YMAX=Y1(1)
      YMIN=Y1(1)
      AMAX=A1(1)
      AMIN=A1(1)
      ASMAX=AS1(1)
      ASMIN=AS1(1)
      DO 40 I=2,N
        IF(Y1(I).GT.YMAX) YMAX=Y1(I)
        IF(Y1(I).LT.YMIN) YMIN=Y1(I)
```

```
      IF(A1(I).GT.AMAX) AMAX=A1(I)
      IF(A1(I).LT.AMIN) AMIN=A1(I)
      IF(AS1(I).GT.ASMAX) ASMAX=AS1(I)
      IF(AS1(I).LT.ASMIN) ASMIN=AS1(I)
 40 CONTINUE
    PTV=ABS(YMAX-YMIN)
    PTVA=ABS(AMAX-AMIN)
    PTVAS=ABS(ASMAX-ASMIN)
    WRITE(*,*)
    WRITE(*,*)' DESCRIPTIVE STATISTICS'
    WRITE(*,*)' ----------------------'
    WRITE(*,*)'                    PROFILE         SLOPE         CURVATURE
   $'
    WRITE(*,*)'                   (microns)      (degrees)      (microns-1
   $)'
    WRITE(*,*)'                  ----------     ----------     ----------
   $-'
    WRITE(4,129)YM,AM,ASM,RA,RMS,RMSA,RMSAS,YMIN,AMIN,ASMIN,YMAX,AMAX,
   $ASMAX,PTV,PTVA,PTVAS,SKW,SKWA,SKWAS,KRT,KRTA,KRTAS
129 FORMAT(1X,3(2X,F11.4),/,1X,2X,F11.4,6(/,1X,3(2X,F11.4)))
    WRITE(*,130)YM,AM,ASM
130 FORMAT('MEAN =',5X,3(4X,F11.4))
    WRITE(*,140)RA
140 FORMAT('AA ROUGHNESS =',1X,F11.4)
    WRITE(*,150)RMS,RMSA,RMSAS
150 FORMAT('RMS =',6X,3(4X,F11.4))
    WRITE(*,160)YMIN,AMIN,ASMIN
160 FORMAT('DATA MIN. =',3(4X,F11.4))
    WRITE(*,170)YMAX,AMAX,ASMAX
170 FORMAT('DATA MAX. =',3(4X,F11.4))
    WRITE(*,180)PTV,PTVA,PTVAS
180 FORMAT('DATA RANGE =',3X,F11.4,2(4X,F11.4))
    WRITE(*,190)SKW,SKWA,SKWAS
190 FORMAT('SKEWNESS =',1X,3(4X,F11.4))
    WRITE(*,200)KRT,KRTA,KRTAS
200 FORMAT('KURTOSIS =',1X,3(4X,F11.4))
    STOP
    END
```

Appendix C - Surface Parameter Formulas.

Figure A.5 shows a typical surface profile. Surface characterization parameters are calculated using the following equations from discrete data points defined along the profile. The mean of the profile height is found by:

$$\bar{y} = \frac{\sum_{i=1}^{N} y_i}{N} \tag{1}$$

where (x_i,y_i) is a coordinate of a point on the profile and N is the number of profile data points. The R_a (arithmetic average) roughness is found by:

$$R_a = \frac{1}{N\Delta x} \sum_{i=1}^{N} | y_i - \bar{y} | \Delta x \tag{2}$$

The RMS (root mean squared) roughness is found by:

$$RMS = \frac{1}{N\Delta x} \sum_{i=1}^{N} (y_i - \bar{y})^2 \Delta x \tag{3}$$

The data minimum and data maximum are equal to y_{min} and y_{max} respectively. The data range is equal to $y_{max} - y_{min}$. The Skewness is found by:

$$Sk = \frac{1}{RMS^3} \left[\frac{1}{N\Delta x} \sum_{i=1}^{N} (y_i - \bar{y})^3 \Delta x \right] \tag{4}$$

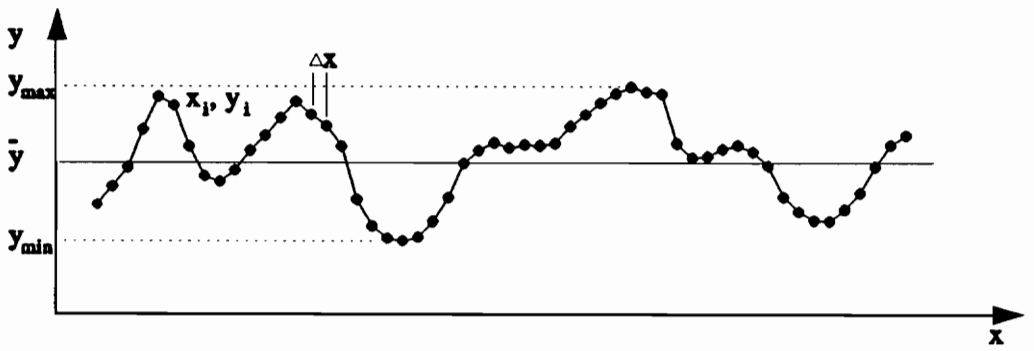

Figure A.5 - Typical surface profile.

And the Kurtosis is found by:

$$Kurt = \frac{1}{RMS^4}\left[\frac{1}{N\Delta x}\sum_{i=1}^{N}(y_i-\bar{y})^4\,\Delta x\right] \tag{5}$$

For the slope parameters, the data points are used to calculate s_1, s_2, ..., s_{N-2}; where:

$$s_i = \frac{y_{i+1}-y_{i-1}}{2\Delta x} \tag{6}$$

Then the same parameters are found using equations 3 through 5 and substituting all the y_i's for s_i's.

For the curvature parameters, the data points are used to calculate κ_1, κ_2, ..., κ_N; where:

$$\kappa_i = \frac{y_{i+1}-2y_i+y_{i-1}}{\sqrt{(s_i^2+1)\cdot\Delta x^2}} \tag{7}$$

Then the same parameters are found using equations 3 through 5 and substituting all the y_i's for κ_i's.

Appendix D - PSL Models.

The following are the block diagrams for the PSL models corresponding to the single degree-of-freedom systems shown in Figure 5.1 (a) and (b). Figure A.6 and A.7 are the block diagrams for the old and new test apparatus, respectively.

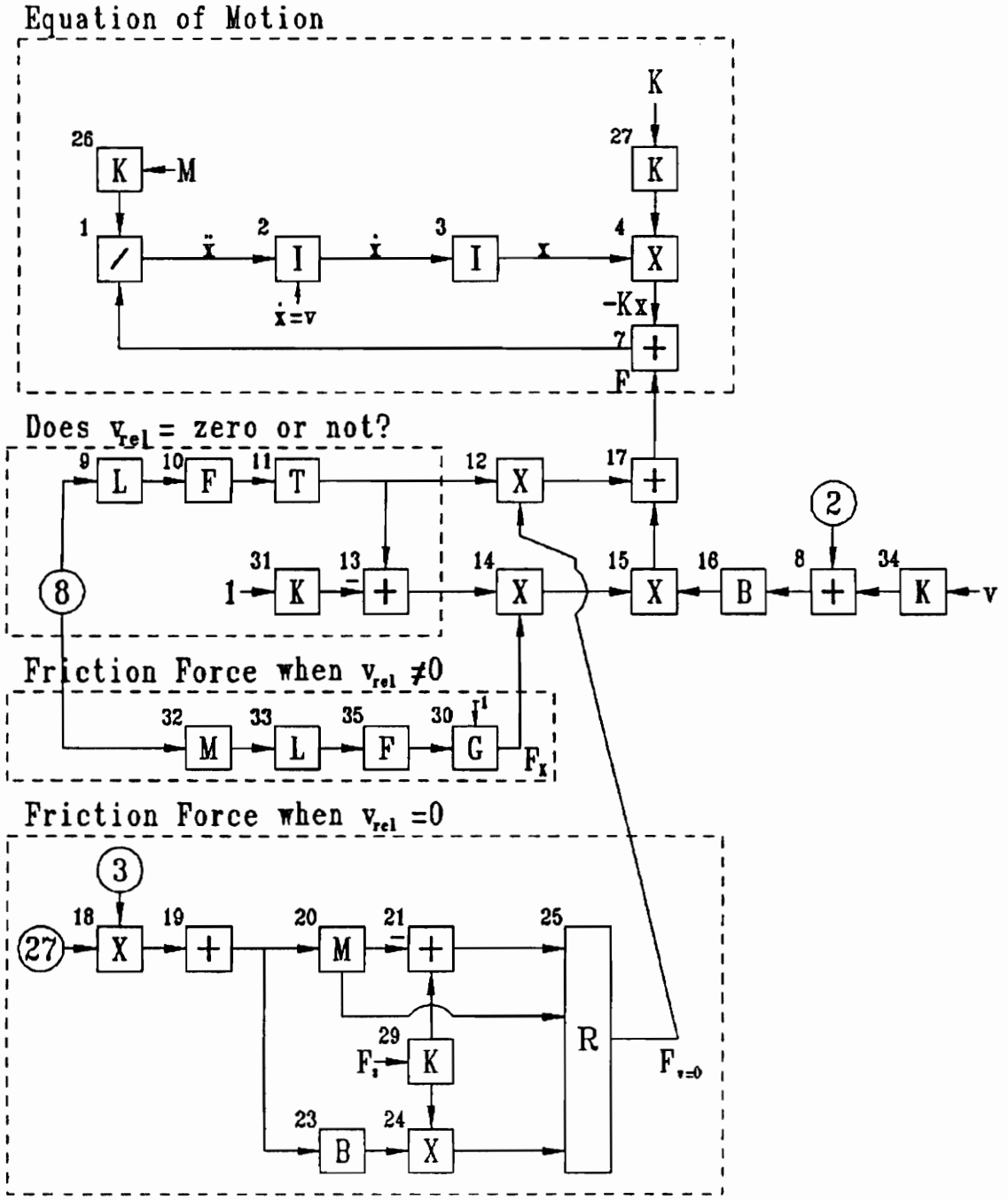

Figure A.6 - Old test apparatus model, PSL block diagram.

```
Integrator Type - Runge-Kutta, Fixed
Time - Minimum  = .0000000
Time Step       = .2000000E-04
Time - Maximum  = .3000000
```

BLK NO	TYPE	INP1	INP2	INP3	IC/Par 1	Par 2	Par 3
1	/	7	26				
2	I	1			.500000E-03		
3	I	2			.350000E-03		
4	X	3	27				
7	+	-4	17				
8	+	34	-2				
9	L	8			.250000E-05	-.250000E-05	
10	F	9			.250000E-05	-.250000E-05	
11	T	10			100.000	100.000	
12	X	11	25				
13	+	-31	11				
14	X	13	30				
15	X	14	16				
16	B	8					
17	+	12	15				
18	X	3	27				
19	+	18					
20	M	19					
21	+	-20	29				
23	B	19					
24	X	23	29				
25	R	21	19	24			
26	K				.500000		
27	K				14000.0		
29	K				6.00000		
30	G	35			-1.00000		
31	K				1.00000		
32	M	8					
33	L	32			.100000E-02	.100000E-05	
34	K				.500000E-03		
35	F	33			.100000E-02	.100000E-05	

```
Function Generator Block Number  10

Input Minimum =   -.2500000E-05
Input Maximum =    .2500000E-05

     Output ( 1) =   -1.500000
     Output ( 2) =   -1.000000
     Output ( 3) =   -.5000000
     Output ( 4) =    .0000000
     Output ( 5) =    .5000000
     Output ( 6) =   1.000000
     Output ( 7) =    .5000000
     Output ( 8) =    .0000000
     Output ( 9) =   -.5000000
     Output (10) =   -1.000000
     Output (11) =   -1.500000
```

```
Function Generator Block Number  35

Input Minimum =    .1000000E-05
Input Maximum =    .1000000E-02

     Output ( 1) =    4.400000
     Output ( 2) =    1.000000
     Output ( 3) =    3.400000
     Output ( 4) =    3.400000
     Output ( 5) =    3.400000
     Output ( 6) =    3.400000
     Output ( 7) =    3.400000
     Output ( 8) =    3.400000
     Output ( 9) =    3.400000
     Output (10) =    3.400000
     Output (11) =    4.600000
```

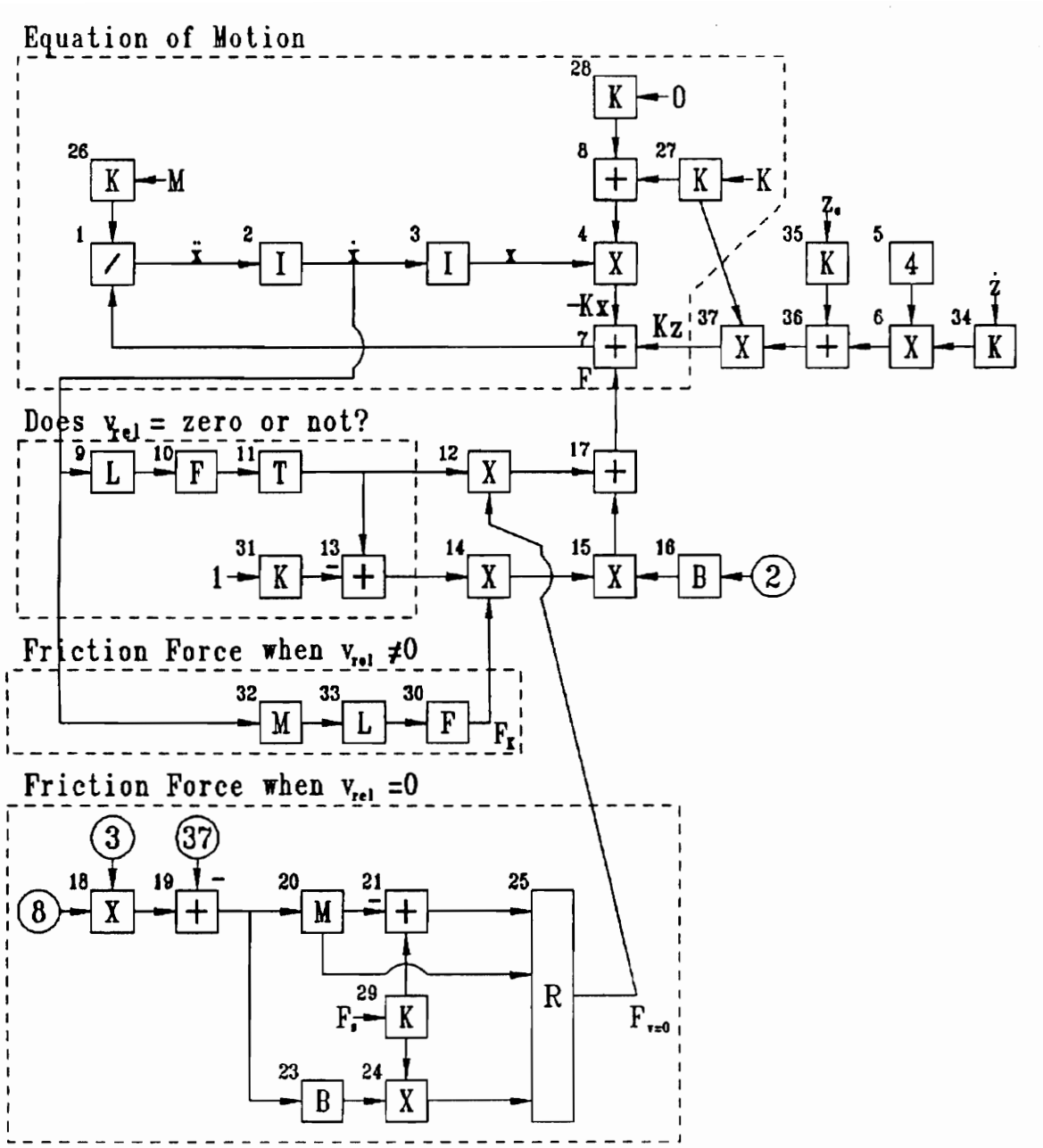

Figure A.7 - New test apparatus, PSL block diagram.

```
Integrator Type - Runge-Kutta, Fixed
Time - Minimum  = .0000000
Time Step       = .2000000E-04
Time - Maximum  = .5000000
```

BLK NO	TYPE	INP1	INP2	INP3	IC/Par 1	Par 2	Par 3
1	/	7	26				
2	I	1					
3	I	2					
4	X	3	8				
5	4						
6	X	5	34				
7	+	-4	37	17			
8	+	27	28				
9	L	2			.250000E-04	-.250000E-04	
10	F	9			.250000E-04	-.250000E-04	
11	T	10			100.000	100.000	
12	X	11	25				
13	+	-31	11				
14	X	13	30				
15	X	14	16				
16	B	2					
17	+	12	15				
18	X	3	8				
19	+	18	-37				
20	M	19					
21	+	-20	29				
23	B	19					
24	X	23	29				
25	R	21	19	24			
26	K				1.00000		
27	K				50000.0		
28	K						
29	K				7.00000		
30	F	33			.100000E-01	.100000E-04	
31	K				1.00000		
32	M	2					
33	L	32			.100000E-01	.100000E-04	
34	K				.500000E-03		
35	K						
36	+	6	35				
37	X	27	36				

```
Function Generator Block Number  10

Input Minimum =   -.2500000E-04
Input Maximum =    .2500000E-04

     Output ( 1) =   -1.500000
     Output ( 2) =   -1.000000
     Output ( 3) =   -.5000000
     Output ( 4) =    .0000000
     Output ( 5) =    .5000000
     Output ( 6) =    1.000000
     Output ( 7) =    .5000000
     Output ( 8) =    .0000000
     Output ( 9) =   -.5000000
     Output (10) =   -1.000000
     Output (11) =   -1.500000
```

```
Function Generator Block Number  30

Input Minimum =    .1000000E-04
Input Maximum =    .1000000E-01

     Output ( 1) =    7.000000
     Output ( 2) =    3.000000
     Output ( 3) =    4.000000
     Output ( 4) =    5.000000
     Output ( 5) =    5.000000
     Output ( 6) =    5.000000
     Output ( 7) =    5.000000
     Output ( 8) =    5.000000
     Output ( 9) =    5.000000
     Output (10) =    5.000000
     Output (11) =    5.000000
```

Appendix E - Pin Cavity Depth Requirements.

The following calculation is done for the design of the new test apparatus pin sample. The pin has a radius, R, and the pin sample has a spherical cavity (radius=R) drilled into the top of the sample. There is a certain cavity depth, d, required to ensure that the pin will not slip out of the cavity. In other words, the coefficient of friction between the pin sphere and the pin sample (μ_{sphere}) must be greater than the coefficient of friction between the two samples (μ_{sample}), as shown in Figure A.8.

Req'd: $\mu_{sphere} > \mu_{sample}$

Sol'n: Friction coefficient for a sphere plowing a flat:

$$\mu_{sphere} = (4/3\pi) \tan\theta$$

$$(4/3\pi) \tan\theta > \mu_{sample}$$

$$\theta > \tan^{-1} (¾\pi\ \mu_{sample})$$

and

$$\cos\theta = (R-d)/R$$

$$R-d = R \cos\theta$$

$$d = R(1-\cos\theta)$$

so,

$$d = R[1-\cos(\tan^{-1} (¾\pi\ \mu_{sample}))].$$

For example, if $\mu_{sample,\ max} = 0.5$; and R = 0.125 in; then d > 0.044 in.

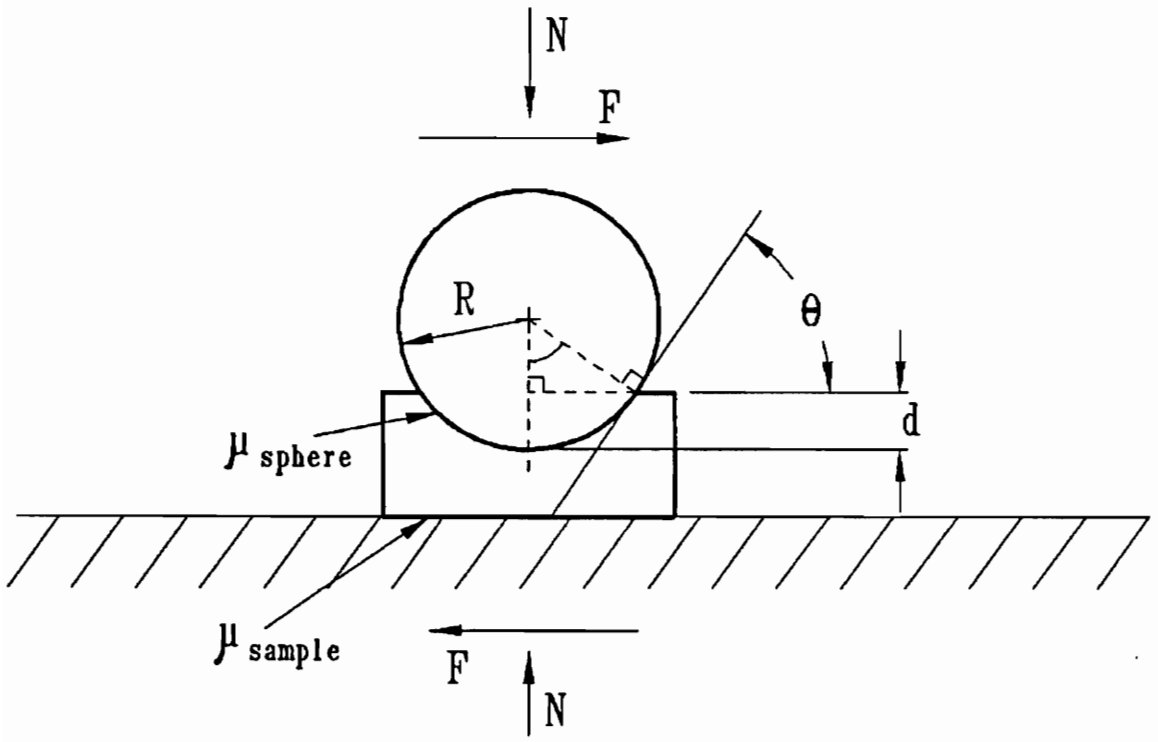

Figure A.8 - Detailed view of spherical pin and pin sample.

Appendix F - Confidence Interval Sample Calculation.

Given: A set of n data points with σ unknown.

Find: 90% confidence interval.

The values which define a 100(1-α) percent confidence interval is found by using the following equation.

$$\bar{y} \pm t_{\alpha/2} \frac{s}{\sqrt{n}}$$

where $\bar{y}$ and s are the average and standard deviation, and $t_{\alpha/2}$ is the table value for a t-distribution with n-1 degrees of freedom.

For example:

Given: n = 4; $y_1 = 1.52$, $y_2 = 2.24$, $y_3 = 1.82$, $y_4 = 1.93$.

$\bar{y} = 1.878$

$s = 0.297$

$t_{0.05,\,3} = 2.353$

Confidence Interval = (1.53, 2.23)

Conclusion: We are 90% confident that the true mean of the population lies between 1.53 and 2.23.

Vita

The author was born in Cincinnati, Ohio on August 19, 1969 to Mr. Robert Molique and Ms. Judith Molique. He received the Eagle Scout award in December 1986. Shortly thereafter he graduated as the salutatorian of the Giles High School class of 1987. He graduated Magna Cum Laude with a Bachelor of Science degree in Mechanical Engineering in May of 1992 from the Virginia Polytechnic Institute and State University. His thirst for knowledge persuaded him to pursue a Master of Science degree in Mechanical Engineering. His hunger for financial peace of mind prompted him to accept an engineering position with Kimberly-Clark Corporation upon graduation. The author will begin a new life on June 11, 1994 when he is wed to the lovely Cathy Clark.

Robert S. Molique